Simulation of hydrodynamically interacting particles confined by a spherical cavity

Christian Aponte-Rivera and Roseanna N. Zia*
Robert Frederick Smith School of Chemical and Biomolecular Engineering, Cornell University, Ithaca, New York 14850, USA
(Received 5 February 2016; published 6 June 2016)

We present a theoretical framework to model the behavior of a concentrated colloidal dispersion confined inside a spherical cavity. Prior attempts to model such behavior were limited to a single enclosed particle and attempts to enlarge such models to two or more particles have seen limited success owing to the challenges of accurately modeling many-body and singular hydrodynamic interactions. To overcome these difficulties, we have developed a set of hydrodynamic mobility functions that couple particle motion with hydrodynamic traction moments that, when inverted and combined with near-field resistance functions, form a complete coupling tensor that accurately captures both the far-field and near-field physics and is valid for an arbitrary number of spherical particles enclosed by a spherical cavity of arbitrary relative size a/R, where a and R are the particle and cavity size, respectively. This framework is then utilized to study the effect of spherical confinement on the self- and entrained motion of the colloids, for a range of particle-to-cavity size ratios. The self-motion of a finite-size enclosed particle is studied first, recovering prior results published in the literature: The hydrodynamic mobility of the particle is greatest at the center of the cavity and decays as $(a/R)/(1-y^2)$, where y is the particle distance to the cavity center. Near the cavity wall, the no-slip surfaces couple strongly and mobility along the cavity radius vanishes as $\xi \equiv R-(a+y)$, where y is center-to-center distance from particle to cavity. Corresponding motion transverse to the cavity radius vanishes as $[\ln(1/\xi)]^{-1}$. The effect of confinement on entrainment of a particle in the flow created by the motion of others is also studied, where we find that confinement exerts a qualitative effect on the strength and anisotropy of entrainment of a passive particle dragged by the flow of a forced particle. As expected, entrainment strength decays with increased distance from the forced particle. Surprisingly, however, there is a separation beyond which entrainment changes sign. For some configurations, the passive particle is dragged along with the forced particle, and at others, it is driven in the opposite direction, consistent with observations of recirculating flow and reverse particle migration in eukaryotic cells. The mobility functions presented here can be utilized to model the motion of any number of enclosed particles, making them ideal for use in dynamic simulation.

DOI: 10.1103/PhysRevFluids.1.023301

I. INTRODUCTION

Diffusion, active transport, and rheological behavior in concentrated, three-dimensionally-microconfined suspensions are emergent areas of research, driven by burgeoning interest in the mechanical behavior of biological and other microscopically small soft-matter systems. An important example is the mechanical motion of particles within eukaryotic cells, shown to play a central role in cell division [1–5], metabolism [6], and growth [1,2]. Despite this growing interest, little predictive theory and few models of this behavior exist. An important element in the construction of such models is the accurate representation of the physical forces between the microstructural constituents and the influence exerted by system boundaries on such interactions. Particle-particle

*zia@cbe.cornell.edu

and particle-boundary interactions can include electrostatic, entropic, and hydrodynamic forces, among others. While numerous models, both analytical and computational, successfully describe microstructural evolution and its connection to macroscopic flow for unbound suspensions, the study of suspensions perturbed by a finite boundary lags behind. Recent studies of planar wall and channel confinement have demonstrated that suspension structure, particle-scale dynamics, and rheology are influenced not only by interactions between particles themselves, but also by interactions between particles and confining boundaries, thus demonstrating the need for careful modeling of such interactions. However, a primary challenge in the development of predictive models is the accurate and efficient representation of many-body hydrodynamic interactions and the influence exerted on such interactions by boundaries. Numerous approaches have been developed to model the microstructural evolution of suspensions of hydrodynamically interacting particles and to connect this evolution to macroscopic flow behavior, ranging from pair theory for dilute suspensions to computational approaches for concentrated suspensions, and for systems spanning an infinite extent to those confined by finite boundaries.

Theoretical models of the dynamics of unbound suspensions have provided many important insights into the connection between structural evolution, particle-scale dynamics, and material and flow properties. Among these are the well-known non-Newtonian rheological behaviors of flow thinning [7–11] and flow thickening [8,10,12–14], flow-induced diffusion [15–19], and normal stress differences [20–24]. Some of these non-Newtonian rheological behaviors can be explained at the level of two-body interactions, showing that dilute Smoluchowski theory captures many important physical behaviors. However, many biophysical systems are crowded, with particle volume fractions well beyond the regime of validity of most pair theory, driving the need to model many-body interactions. In some cases, dilute theory can be scaled up to model behavior of concentrated suspensions, but the study of the effects of crowding and jamming on material behavior have made clear the qualitative effects exerted by three-body and higher-order interactions.

Modeling of moderate- or high-volume fractions requires accounting for three-body and higher-order interactions owing to the long-range nature of hydrodynamic interactions, characterized by fluid velocity disturbances that decay as $1/r$ (where r is the distance from a moving particle), which are not amenable to approximation via simple pairwise addition. The singular behavior of lubrication forces, as a particle comes near contact with another particle or to a boundary, further complicates the analysis. Approaches to modeling concentrated suspensions include mean-field approximations, which are useful for linear-response behavior [25–28] or, for dynamical behavior, the use of computational approaches such as dissipative particle dynamics [29], lattice Boltzmann methods [30], or Stokesian dynamics [31]. Zia *et al.* [28] recently developed a set of concentrated hydrodynamic functions to model pair interactions in concentrated systems, paving the way for analytical Smoluchowski analysis of concentrated suspensions, but application to nonequilibrium systems has not yet been demonstrated [28]. Structural evolution is also studied experimentally by direct imaging [32–35] and scattering techniques [36–40] and is related to rheology via statistical mechanics theory [33,41] and phenomenological models [42,43]. Missing in all of these models, however, is the effect of confining boundaries as would arise in, e.g., channel flow, injection, or transport in cells.

The presence of even a single confining boundary, a nearby wall, exerts a pronounced influence on hydrodynamic interactions between particles and in turn on suspension dynamics and flow properties. The effects of wall confinement on diffusion and rheology have been studied for systems that range from a point particle in the presence of a single wall [44] to finite-size particles in the presence of a single no-slip wall [45–47] as well as a flat [48,49] or deformable [50,51] fluid-fluid interface. Recent studies have focused on both a single particle [52] and concentrated suspensions [53,54] between parallel walls and single particles under the influence of charge [55] and electric fields [56]. By revealing qualitative changes to particle and flow dynamics, the study of one- and two-dimensional confinement sets an important foundation for understanding the effects of confining boundaries and elucidates the microstructural origin of some confinement-induced behaviors such as anisotropic diffusion in concentrated suspensions [54,57].

Growing interest in mechanical transport of particles in fully confined, microscale systems, however, demands new models that account for fully three-dimensional (3D) confinement, where effects such as flow recirculation and a finite range of accessible configurations influence deterministic and stochastic processes. For example, in the crowded, watery compartments of eukaryotic cells, particles undergo a variety of mechanical transport processes including passive diffusion of enzymes, metabolites, and organelles as well as active towing by motor proteins and collective motion [2–4,6,58–67]. The connection of mechanical intracellular transport to cell function and disease is recognized, but not well understood, leaving open questions such as the underlying origins of anomalous diffusion, how active motion stirs the cell interior and alters diffusion, and how intracellular trafficking impacts the motion of tracer particles used for microrheological measurements [1–6,63,65,67–79].

Experimental studies of diffusion of confined colloids suggest that careful modeling and analysis of transport can provide answers to these questions. In a study of the short-time self-diffusivity of a particle inside a spherical droplet, Cervantes-Martínez *et al.* [80] found that the presence of the boundary leads to hindered anisotropic diffusion. However, particle motion deformed the surface of the droplet, making it difficult to decouple the role of boundary deformation from that of hydrodynamic interactions with the boundary, leaving the origins of anisotropy murky. Hunter *et al.* [34] successfully decoupled these effects by creating a high-surface-tension cavity and, utilizing particle tracking microscopy, measured particle motion in a concentrated, confined colloidal suspension. They showed that confinement suppresses the mean-square displacement of enclosed particles, as compared to an unbound system at equal volume fraction. Boundary-induced anisotropy of the mean-square displacement, wherein different values are obtained when the displacement is projected along and perpendicular to the line of centers between the particle and the cavity, was also observed. The authors hypothesized that these qualitative confinement-induced changes arose due to boundary-induced gradients in the hydrodynamic mobility. However, this awaits confirmation by physical measurements, which can be challenging owing to the need for detailed information about positions of moving particles, pointing toward the need for dynamic simulation, where such information is readily obtained and motion easily visualized.

Computational modeling, where precise measurement of particle positions and trajectories is possible, provides an important complement to experiments and plays an important role in the development of predictive theory. Previous attempts to simulate 3D confined biophysical systems reveal a qualitative influence on mechanical transport. For example, Kozlowski *et al.* [81] utilized Brownian dynamics simulations and experiments to explore the impact on the migration of intracellular structures during cell division exerted by steric interactions between microtubules crisscrossing the cell. Interactions between the confining boundary and microtubules were shown to play an important role in structural migration. While the simulations recovered experimentally observed structural oscillation, the period and phase angle critical to system evolution were severely underpredicted, a limitation the authors attributed to the neglect of hydrodynamic interactions. Subsequent attempts to account for hydrodynamic interactions include the numerical study of Shinar *et al.* [82], who utilized a boundary-integral technique to model hydrodynamic coupling between a single noncolloidal particle and an enclosing cavity, in an effort to model the motion of a cell nucleus dragged by microtubules through the intracellular fluid. The authors showed that the enclosing cavity increases the hydrodynamic drag force on the nucleus (compared to unbound Stokes drag), but were unable to extend their model to more than a single finite-size particle, leading to an obvious limitation for the study of the crowded cell interior. While such experimental and numerical studies indicate that 3D confinement gives rise to novel transport behavior relevant to biological function, no predictive theory or computational model thus far can account for the combined effects of lubrication and many-body hydrodynamic interactions between two or more enclosed particles.

The most basic approach to constructing a model for the motion of many particles in a fluid-filled cavity is to directly solve the Navier-Stokes equations at all points in the enclosed suspending fluid, subject to appropriate boundary conditions, e.g., no slip and no flux through a hard enclosure. Numerous solutions utilizing this approach have been put forth, both analytical and numerical, for a

variety of systems and boundary conditions. The electrophoretic motion of a particle in a fluid-filled cavity has been studied theoretically for a single charged particle with both thin and thick Debye layers in an uncharged cavity [83–89] as well as a single particle with polarized Debye layers [90–93] or a charged particle in a charged cavity [87,94,95]. The motion of a soft particle [96,97], a particle with slip boundary conditions [96–100], and the motion of a diffusiophoretic particle [101] have also been studied. Underlying all of these single-enclosed-particle problems is a pair-level hydrodynamic problem, i.e., there are two interacting surfaces: the particle and the cavity. Methods to solve the momentum equations in these single-enclosed particle problems include asymptotic and numerical solution via finite-element, collocation, and pseudospectral methods, for example. While successful at the level of a single enclosed particle, extension to an arbitrary number of particles at arbitrary volume fractions renders this approach intractable as the divergent forces near contact demand prohibitively high computational cost associated with surface discretization. While successful at the level of a single enclosed particle, extension to even a second enclosed particle requires modeling fluid motion near three surfaces simultaneously, rendering this approach intractable as the divergent forces near contact demand prohibitively high computational cost associated with surface discretization.

The common theme in these approaches is that fluid motion is determined first and, from it, particle motion, leading to the unavoidable problem of prohibitive computational expense when treating singular interactions near contact. Recent approximations have neglected lubrication interactions entirely [102], but such approaches lead to dramatic errors such as overlapping of particles, requiring use of repulsive potentials (which bring their own difficulties), and underprediction of or no Brownian drift.

An alternative approach is to bypass determination of detailed fluid motion and to focus instead on the development of hydrodynamic functions coupling particle motion to applied forces. Early attempts to utilize this approach recognized that a single finite-size particle inside a spherical cavity constitutes a pair problem, that is, a hydrodynamics problem between a pair of surfaces, a perspective well developed in the analysis of unbound particle pairs [7,103–107]. Cunningham [108] studied the motion of a finite-size particle located precisely at the center of a fluid-filled cavity and obtained the change in hydrodynamic drag arising from the presence of the confining boundary. However, his single-multipole expansion approach requires concentric geometry and does not permit analysis at any other position of the particle within the cavity. O'Neill and Majumdar [109,110] and Jones [111] overcame this limitation by combining bispherical coordinates with a series expansion in spherical harmonics to obtain recursive relations for the hydrodynamic resistance functions coupling translational and rotational motion to the hydrodynamic force and torque acting over the surface of a finite-size particle, at an arbitrary position in the cavity. The resultant recursive relations were then solved numerically. The authors found that single-particle motion inside a spherical cavity is hindered, i.e., the hydrodynamic drag is greater than unbound Stokes drag, as evidenced by an increase in the force-to-translational motion component of the hydrodynamic resistance tensor. Although this series-expansion approach can be utilized to determine the hydrodynamic coupling between a pair of no-slip surfaces, it becomes intractable beyond the pair limit, owing to the difficulty of constructing coordinate systems where the boundary conditions over an arbitrary number of surfaces can be satisfied simultaneously. Ultimately such approaches that focus on eigenfunction expansions restrict the analysis to a single enclosed particle.

Interactions between two or more hydrodynamically interacting particles in an unbound suspension have been successfully modeled utilizing a Green's function for the unbound domain. It is then weighted by the hydrodynamic force moments exerted on the fluid by many different particles, whence Faxén formulas can be applied to determine particle motion. Computational approaches can then be employed to solve a particle displacement equation to evolve the particle positions over time, given their hydrodynamic, interparticle, and entropic interactions. Techniques such as Stokesian dynamics [31] are well known and have been utilized to solve many important problems for unbound suspensions [21,112–114] and have been recently extended to planar-wall confined suspensions [53,54] utilizing the Green's-function approach. Extension of these ideas to spherically confined suspensions has proven challenging, however.

The first Green's functions for 3D confinement began with the simplest model, a single point particle inside a solvent-filled, no-slip spherical cavity, due to Oseen [115]. This theoretical framework was subsequently utilized to model the sedimentation of a noncolloidal particle of finite size within a cavity [116], but again bars generalization beyond a single particle. Maul and Kim sought a more generalizable method [117,118] aimed toward adapting Oseen's Green's function so as to express it in terms of the Green's function for an unbound point particle, the Stokeslet. Here the idea was to make the Green's function more amenable to solutions via collocation methods, which aim to solve Ladyzhenskaya's integral representation [119] on a mesh. However, the resulting line integrals proved no less difficult to solve than direct application of Oseen's solution: The detailed fluid flow must be obtained and familiar problems of divergent forces at contact render this approach nearly intractable beyond the limit of a single confined particle. Beenakker and Mazur [120] used a Fourier-space multipole expansion method, also known as the method of induced forces, in an attempt to determine translational and rotational motion of two particles inside a spherical cavity. However, the mobility functions developed are only valid for two confined particles found far from each other as well as far from the cavity and does not account for divergent lubrication interactions near contact, limiting their application. Ultimately then, the primary objective of obtaining the Green's function is to bypass fluid motion and focus exclusively on particle motion, typically via Faxén formulas.

Felderhof and Sellier [121] applied the leading-order term of the Faxén formulas for translational and rotational motion to Oseen's Green's function in an attempt to obtain analytical expressions for the hydrodynamic coupling tensors, previously derived via a series expansion in bispherical coordinates [109–111]. The authors approximated hydrodynamic functions that couple force and torque to translation and rotation of a single point particle within the cavity. However, the no-size approximation effectively permits fluid flux through particle surfaces, leading to several errors, most principally a failure to capture torque-to-translational coupling, which in turn leads to a failure to recover trajectory reversal near the cavity wall previously predicted by O'Neill and Majumdar [109]. While their attempt to extend Oseen's Green's function to account for rotation advanced the theory, it also made clear that the effect of finite size must be included in any predictive theory or model. Together these studies show the importance of accounting for hydrodynamic interactions, as well as accounting for finite particle size and finite enclosure size, in the analysis of confined suspensions, yet none of the methods above can be generalized directly to arbitrary volume fractions and particle-to-cavity size ratio inside this spherically confined geometry. Because many systems of emergent interest, such as the cell interior, are crowded environments influenced by all of these effects, it is essential to develop alternative theoretical frameworks and computational models that can faithfully account for many-body interactions between many particles of finite size and the confining boundary.

In this work we present a theoretical model for the prediction of the motion of an arbitrary number of finite-size particles suspended in a solvent-filled cavity. Utilizing a Green's-function approach, we derive a set of mobility functions that rigorously model the many-body far-field and near-field interactions and faithfully capture the physics of a suspension of hydrodynamically interacting particles confined by a spherical cavity. This theory is valid for systems ranging from dilute to near-maximum volume fraction and for arbitrary particle-to-cavity size ratios. The dual focus of the present work is to first validate the model utilizing the well-characterized case of a single enclosed particle and then to study the motion of a pair of enclosed particles. For the former, we successfully recover prior results reported in the literature, but now with a model that can be extended to not just two but an arbitrary number of particles of arbitrary size relative to their enclosing cavity. In the present work we demonstrate and validate the model via the study of self-mobility and entrained mobility for a pair of enclosed particles, leaving the simulation of many particles for future studies of rheology and diffusion.

This article is organized as follows. In Sec. II we give a brief review of the low-Reynolds-number hydrodynamics theory, highlighting features of this method relevant to the present study. In Sec. III a model is developed for simulating hydrodynamically interacting particles inside a spherical boundary

utilizing a Stokesian dynamics [31] approach. We first develop a far-field mobility matrix coupling forces to particle motion that accounts for finite particle size. We then combine this far-field coupling with analytical theory for near-field interactions. The corresponding results for pair entrainment are given in Sec. IV B. Higher-order couplings are presented in Sec. IV C, where hydrodynamic torque couplings for self-motion and entrained motion are found to produce translational motion that leads to trajectory reversal in the former case and doublet rotation in the latter. Section IV D is devoted to the topic of finite-size effects. Results for many particles over a range of volume fractions and particle-to-cavity size ratios are treated separately elsewhere [122]. The study is concluded with a discussion in Sec. V.

II. BRIEF OVERVIEW OF MANY-BODY LOW-Re HYDRODYNAMICS

In this section we present a brief review of the fundamentals of low-Reynolds-number hydrodynamics for unbound suspensions, with a focus on the representation of many-body interactions. Although formulation of the problem begins with expressions for detailed fluid motion, solution of such expressions is bypassed utilizing well-known techniques that combine Taylor expansions and Faxén formulas. We consider a suspension of N particles of size a immersed in an incompressible Newtonian fluid of density ρ and viscosity η. Particle motion of characteristic speed U sets the fluid into motion; because the particles are small, the Reynolds number $\mathrm{Re} = \rho U A/\eta \ll 1$. Thus the importance of inertial forces in the fluid compared to viscous forces is negligible and the Navier-Stokes equations governing fluid motion become the Stokes equations.

In Stokes flow, fluid-surface interactions can be treated via the approach of Ladyzhenskaya [119] whereby the so-called integral representation gives the fluid disturbance velocity field $\boldsymbol{u}'(\boldsymbol{x}) = \boldsymbol{u}(\boldsymbol{x}) - \boldsymbol{u}^{\infty}(\boldsymbol{x})$, where $\boldsymbol{u}(\boldsymbol{x})$ is the velocity at any field point $\boldsymbol{x}$ in the suspension, including that due to forces exerted by particles on the fluid, where $\boldsymbol{u}^{\infty}(\boldsymbol{x})$ is any far-field imposed flow. The force density over the surface points $\boldsymbol{y}$ of a particle is given by the Cauchy relation $\boldsymbol{f}(\boldsymbol{y}) = \boldsymbol{n}\cdot\boldsymbol{\sigma}$, where $\boldsymbol{n}$ is the unit surface normal pointing outward from the particle surface and $\boldsymbol{\sigma}$ is the stress exerted on the particle surface by the fluid. The fluid disturbance due to the force propagates from all $\boldsymbol{y}$ throughout the fluid, i.e., to all field points $\boldsymbol{x}$, as set by the Green's-function propagator $\boldsymbol{G}(\boldsymbol{x},\boldsymbol{y})$ corresponding to the physical domain. The fluid disturbance velocity $\boldsymbol{u}'(\boldsymbol{x})$ arising from forcing of a particle α is thus a sum over all points on its surface S_α:

$$\boldsymbol{u}'(\boldsymbol{x}) = -\left[\int_{S_\alpha} \boldsymbol{f}(\boldsymbol{y})\cdot\boldsymbol{G}(\boldsymbol{x},\boldsymbol{y})dS_y + \int_{S_\infty} \boldsymbol{f}(\boldsymbol{y})\cdot\boldsymbol{G}(\boldsymbol{x},\boldsymbol{y})dS_y\right], \tag{1}$$

where the second integral, over the surface at infinity, acts to conserve mass. In an unbound suspension of hard spheres, the Green's function $\boldsymbol{G}$ is the well-known Stokeslet [115]

$$\boldsymbol{J}(\boldsymbol{x},\boldsymbol{y}) = \frac{1}{8\pi\eta a}\left(\frac{\boldsymbol{I}}{|\boldsymbol{x}-\boldsymbol{y}|} + \frac{(\boldsymbol{x}-\boldsymbol{y})(\boldsymbol{x}-\boldsymbol{y})}{|\boldsymbol{x}-\boldsymbol{y}|}\right), \tag{2}$$

which decays as $1/r$, where $r = |\boldsymbol{x}-\boldsymbol{y}|$. A simple scaling argument shows that the second integral in (1) decays with increasing distance from the surface of the forced particle and vanishes as the surface S_∞ grows infinitely far away [106], yielding

$$\boldsymbol{u}'(\boldsymbol{x}) = -\int_{S_\alpha} \boldsymbol{f}(\boldsymbol{y})\cdot\boldsymbol{G}(\boldsymbol{x},\boldsymbol{y})dS_y. \tag{3}$$

Direct solution by numerical methods is possible but leads to divergent contact forces, as discussed in Sec. I. This difficulty is bypassed by moving the Green's function out of the surface integral via a Taylor expansion of $\boldsymbol{G}$ about the center of particle α. The resulting expansion, often referred to as a multipole expansion, comprises a series of moments of the hydrodynamic surface traction $\hat{\boldsymbol{r}}\cdot\boldsymbol{\sigma}$, where $\boldsymbol{\sigma}$ is the fluid stress and $\hat{\boldsymbol{r}} = (\boldsymbol{y}-\boldsymbol{y}_\alpha)/|\boldsymbol{y}-\boldsymbol{y}_\alpha|$ is the unit normal pointing outward from the surface of the particle, with $\boldsymbol{y}_\alpha$ the location of the center of particle α. Insertion of the Taylor

expansion into (3) gives

$$\boldsymbol{u}'(\boldsymbol{x}) = -\left(1+\frac{a_\alpha}{6}\nabla_y^2\right)\boldsymbol{G}(\boldsymbol{x},\boldsymbol{y})\Big|_{\boldsymbol{y}=\boldsymbol{x}_\alpha}\cdot\boldsymbol{F}_\alpha^H - \frac{1}{2}\nabla_y\times\boldsymbol{G}(\boldsymbol{x},\boldsymbol{y})\Big|_{\boldsymbol{y}=\boldsymbol{x}_\alpha}\cdot\boldsymbol{L}_\alpha^H - \left(1+\frac{a_\alpha}{10}\nabla_y^2\right)\boldsymbol{K}(\boldsymbol{x},\boldsymbol{y})\Big|_{\boldsymbol{y}=\boldsymbol{x}_\alpha}:\boldsymbol{S}_\alpha^H+\cdots, \tag{4}$$

where the hydrodynamic force $\boldsymbol{F}^H$, torque $\boldsymbol{L}^H$, and stresslet $\boldsymbol{S}^H$ are the zeroth moment and the antisymmetric and symmetric parts of the first moment of the hydrodynamic surface traction, respectively. In addition, irreducible second and third moments of the traction are included in $\boldsymbol{G}$ and $\boldsymbol{K}$, where the couplet $\boldsymbol{K}$ is given by

$$\boldsymbol{K}(\boldsymbol{x},\boldsymbol{y}) = \nabla_y\boldsymbol{G}(\boldsymbol{x},\boldsymbol{y}) + [\nabla_y\boldsymbol{G}(\boldsymbol{x},\boldsymbol{y})]^T. \tag{5}$$

Physically, the motion of a particle α sets the fluid into motion with a velocity $\boldsymbol{u}'(\boldsymbol{x})$ relative to the imposed flow, which in turn entrains other particles β. The corresponding motion of particles β can be determined, to leading order, via Faxén formulas. The Faxén formulas for translational, rotational, and straining motion $\boldsymbol{U}_\beta$, $\boldsymbol{\Omega}_\beta$, and $\boldsymbol{E}_\beta$, respectively, of a particle β in any disturbance flow field $\boldsymbol{u}'(\boldsymbol{x})$ are

$$\boldsymbol{U}_\beta - \boldsymbol{u}^\infty(\boldsymbol{x}_\beta) = \frac{\boldsymbol{F}_\beta}{6\pi\eta a_\beta} + \left(1+\frac{a_\beta^2}{6}\nabla_x^2\right)\boldsymbol{u}'(\boldsymbol{x})\Big|_{\boldsymbol{x}_\beta}, \tag{6}$$

$$\boldsymbol{\Omega}_\beta - \boldsymbol{\omega}^\infty(\boldsymbol{x}_\beta) = \frac{\boldsymbol{L}_\beta}{8\pi\eta a_\beta^3} + \frac{1}{2}\nabla_x^2\times\boldsymbol{u}'(\boldsymbol{x})\Big|_{\boldsymbol{x}_\beta}, \tag{7}$$

$$-\boldsymbol{E}^\infty = \frac{\boldsymbol{S}_\beta}{\frac{20}{3}\pi\eta a_\beta^3} + \left(1+\frac{a_\beta^2}{10}\nabla_x^2\right)\boldsymbol{E}'(\boldsymbol{x})\Big|_{\boldsymbol{x}_\beta}, \tag{8}$$

where $\boldsymbol{E}'(\boldsymbol{x})$ is the disturbance rate of strain

$$\boldsymbol{E}'(\boldsymbol{x}) = \tfrac{1}{2}\{\nabla_x\boldsymbol{u}'(\boldsymbol{x}) + [\nabla_x\boldsymbol{u}'(\boldsymbol{x})]^T\}. \tag{9}$$

Because all N particles interact, the leading-order disturbance flow $\boldsymbol{u}'(\boldsymbol{x})$ is a sum given by

$$\boldsymbol{u}'(\boldsymbol{x}) = \sum_{\alpha=1}^{N}\Bigg[-\left(1+\frac{a_\alpha}{6}\nabla_y^2\right)\boldsymbol{G}(\boldsymbol{x},\boldsymbol{y})\Big|_{\boldsymbol{y}=\boldsymbol{x}_\alpha}\cdot\boldsymbol{F}_\alpha^H - \frac{1}{2}\nabla_y\times\boldsymbol{G}(\boldsymbol{x},\boldsymbol{y})\Big|_{\boldsymbol{y}=\boldsymbol{x}_\alpha}\cdot\boldsymbol{L}_\alpha^H - \left(1+\frac{a_\alpha}{10}\nabla_y^2\right)\boldsymbol{K}(\boldsymbol{x},\boldsymbol{y})\Big|_{\boldsymbol{y}=\boldsymbol{x}_\alpha}:\boldsymbol{S}_\alpha^H+\cdots\Bigg]. \tag{10}$$

Insertion of Eq. (10) into Eqs. (6)–(8) yields a set of linear relations between particle motion and hydrodynamic force, torque, stresslet, and higher-order moments:

$$\begin{pmatrix}\boldsymbol{U}-\boldsymbol{u}^\infty\\ \boldsymbol{\Omega}-\boldsymbol{\omega}^\infty\\ -\boldsymbol{E}^\infty\\ \vdots\end{pmatrix} = -\mathcal{M}\cdot\begin{pmatrix}\boldsymbol{F}^H\\ \boldsymbol{L}^H\\ \boldsymbol{S}^H\\ \vdots\end{pmatrix}, \tag{11}$$

where the pairwise couplings between motion and moments form the grand mobility matrix $\mathcal{M}$,

$$\mathcal{M} = \begin{pmatrix} \boldsymbol{M}^{UF} & \boldsymbol{M}^{UL} & \boldsymbol{M}^{US} & \cdots \\ \boldsymbol{M}^{\Omega F} & \boldsymbol{M}^{\Omega L} & \boldsymbol{M}^{\Omega S} & \cdots \\ \boldsymbol{M}^{EF} & \boldsymbol{M}^{EL} & \boldsymbol{M}^{ES} & \cdots \\ \vdots & \vdots & \vdots & \ddots \end{pmatrix}. \tag{12}$$

Each element of the grand mobility matrix comprises submatrices that couple the motion of each particle to the traction moments of all other particles. For example, for two particles α and β, the velocity-force coupling is

$$\boldsymbol{M}^{UF} = \begin{pmatrix} \boldsymbol{M}^{UF}_{\alpha\alpha} & \boldsymbol{M}^{UF}_{\alpha\beta} \\ \boldsymbol{M}^{UF}_{\beta\alpha} & \boldsymbol{M}^{UF}_{\beta\beta} \end{pmatrix}, \tag{13}$$

where each submatrix is itself a second-rank tensor coupling particles to one another. So-called self-mobility tensors ($\alpha\alpha$ and $\beta\beta$) characterize the motion of a particle in response to a hydrodynamic force on its own surface. In contrast, pair-mobility tensors ($\alpha\beta$ and $\beta\alpha$) characterize the entrainment of one particle by the motion of another. The grand mobility matrix depends only on geometry; for an unbound domain, it is set entirely by particle size, shape, and microstructural configuration. The minimum dissipation theorem demands a symmetric and positive-definite grand mobility matrix; this must be ensured in any model for hydrodynamically interacting colloidal particles based on this representation.

In many suspension mechanics problems, the forces acting on particles are known (e.g., gravity, electric fields, and magnetic fields) and particle motion is sought. Equation (13) appears ready to solve this problem, but two issues remain. First is a practical problem: One must solve an infinite hierarchy of equations, relating motion to an infinitude of hydrodynamic moments. More fundamentally, the mobility matrix in Eq. (13) is a strictly pairwise formulation of the interaction between the particles and further accounts only for the first reflection of hydrodynamic interactions, that is, the entrainment of particle β by particle α in turn creates a new disturbance flow that is not captured by summing the disturbance flow of individual particles via this integral formulation approach. Durlofsky *et al.* [123] showed that inverting the mobility matrix, however, automatically couples all (infinitely many) reflections between all particles, similar in ethos to a geometric series expansion, thus accomplishing the task of transforming the pair-level problem into a full many-body hydrodynamic coupling. The inverse of the grand mobility matrix is the grand resistance matrix $\mathcal{M}^{-1} = \mathcal{R}$,

$$\begin{pmatrix} \boldsymbol{R}^{UF} & \boldsymbol{R}^{UL} & \boldsymbol{R}^{US} & \cdots \\ \boldsymbol{R}^{\Omega F} & \boldsymbol{R}^{\Omega L} & \boldsymbol{R}^{\Omega S} & \cdots \\ \boldsymbol{R}^{EF} & \boldsymbol{R}^{EL} & \boldsymbol{R}^{ES} & \cdots \\ \vdots & \vdots & \vdots & \end{pmatrix} = \begin{pmatrix} \boldsymbol{M}^{UF} & \boldsymbol{M}^{UL} & \boldsymbol{M}^{US} & \cdots \\ \boldsymbol{M}^{\Omega F} & \boldsymbol{M}^{\Omega L} & \boldsymbol{M}^{\Omega S} & \cdots \\ \boldsymbol{M}^{EF} & \boldsymbol{M}^{EL} & \boldsymbol{M}^{ES} & \cdots \\ \vdots & \vdots & \vdots & \ddots \end{pmatrix}^{-1}, \tag{14}$$

giving the full many-body coupling between hydrodynamic traction moments and particle motion.

The practical problem of an infinite hierarchy of equations is solved in a correspondingly practical way: The mobility matrix is simply truncated to a finite number of moments. The physical consequence of such an approximation is the omission of near-field interactions between particles and thus it gives a far-field grand mobility tensor, denoted by $\mathcal{M}_{ff}$. The task of accounting for near-field interactions is easily and rigorously carried at by simply reintroducing the omitted interactions by linear superposition of the analytical, exact pairwise resistance functions, a technique central to the Stokesian dynamics approach pioneered by Brady and Bossis [31]. The resulting matrix forms a complete many-body near- and far-field hydrodynamic coupling tensor

$$\mathcal{R} = (\mathcal{M}_{ff})^{-1} + \mathcal{R}_{nf}. \tag{15}$$

Here $(\mathcal{M}_{ff})^{-1}$ is the inverse of the truncated far-field grand mobility matrix, capturing an infinite number of reflections between all particles. The near-field interactions are incorporated via a near-field two-body resistance tensor $\mathcal{R}_{nf}$. The functions that form the unbound-suspension matrices are well established and can be found in the literature [105–107]. Because the far-field coupling also counts the far-field pair interactions, the far-field pair couplings have been subtracted from $\mathcal{M}_{ff}$ to avoid double counting. Recent computational studies of confinement effects have extended these ideas to account for confinement by single [47] or parallel [52,53] walls, where the domain is still semi-infinite, i.e., only partially bound. In this study we develop the theoretical model for 3D microconfined hydrodynamically interacting particles enclosed inside a spherical no-slip boundary.

The linearity relation between particle motion and hydrodynamic force, torque, and stresslet are then expressed in terms of the grand resistance matrix $\mathcal{R}$ comprising the near-field resistance tensor and the inverse of the far-field grand mobility tensor, thus providing the complete hydrodynamic coupling:

$$\begin{pmatrix} \boldsymbol{F}^H \\ \boldsymbol{L}^H \\ \boldsymbol{S}^H \end{pmatrix} = -[\mathcal{R}_{nf} + (\mathcal{M}_{ff})^{-1}] \cdot \begin{pmatrix} \boldsymbol{U} - \boldsymbol{u}^\infty \\ \boldsymbol{\Omega} - \boldsymbol{\omega}^\infty \\ -\boldsymbol{E}^\infty \end{pmatrix}. \tag{16}$$

This expression can be decomposed line by line to obtain particle motion while retaining the reflections between all particles. For example, the first equation for the hydrodynamic force gives the velocity

$$\boldsymbol{U} = -(\mathcal{R}^{FU})^{-1} \cdot [\boldsymbol{F}^H + \mathcal{R}^{F\Omega} \cdot \boldsymbol{\Omega} - \mathcal{R}^{FE} \cdot \boldsymbol{E}^\infty] \tag{17}$$

$$\equiv -\mathcal{M}^{UF} \cdot [\boldsymbol{F}^H + \mathcal{R}^{F\Omega} \cdot \boldsymbol{\Omega} - \mathcal{R}^{FE} \cdot \boldsymbol{E}^\infty] \tag{18}$$

and the second line for the torque gives rotational motion, viz.,

$$\boldsymbol{\Omega} = -(\mathcal{R}^{L\Omega})^{-1} \cdot [\boldsymbol{L}^H + \mathcal{R}^{LU} \cdot \boldsymbol{U} - \mathcal{R}^{LE} \cdot \boldsymbol{E}^\infty] \tag{19}$$

$$\equiv -\mathcal{M}^{\Omega L} \cdot [\boldsymbol{L}^H + \mathcal{R}^{LU} \cdot \boldsymbol{U} - \mathcal{R}^{LE} \cdot \boldsymbol{E}^\infty]. \tag{20}$$

Thus, to compute the motion of particles in a hydrodynamically interacting suspension, one must compute the configuration-dependent couplings between particles $\mathcal{R}^{UF}$ and $\mathcal{R}^{\Omega L}$, along with the analogous couplings $\mathcal{R}^{UL}$, $\mathcal{R}^{\Omega F}$, $\mathcal{R}^{ES}$, $\mathcal{R}^{\Omega S}$, and $\mathcal{R}^{EF}$. The total many-body mobility $\mathcal{M}^{UF}$, $\mathcal{M}^{\Omega L}$, $\mathcal{M}^{UL}$, $\mathcal{M}^{\Omega F}$, $\mathcal{M}^{ES}$, $\mathcal{M}^{\Omega S}$, and $\mathcal{M}^{EF}$ couplings can be obtained upon blockwise inversion of the total many-body resistance coupling as shown in Eqs. (18)–(20). Henceforth this notation refers to the total many-body couplings between all particles.

III. SPHERICAL CONFINEMENT: THEORETICAL FRAMEWORK

In this section we present the framework with which to model the motion of hydrodynamically interacting particles confined inside a spherical boundary. Careful consideration is given to the development of the far-field grand mobility matrix to accurately represent the many-body hydrodynamic interactions of spherically confined particles, as well as the near-field and lubrication interactions. As in Sec. II, we consider N hard spherical particles of size a in a fluid of density ρ and viscosity η whose motion is governed by the Stokes equations, owing to a vanishingly small Reynolds number. The fluid and particles are confined to a finite domain: a hard, no-slip spherical cavity of radius R (Fig. 1). Any far-field flow $\boldsymbol{u}^\infty$ present can arise due only to external forces applied to the particles or to motion of the cavity. Ladyzhenskaya's integral representation gives the

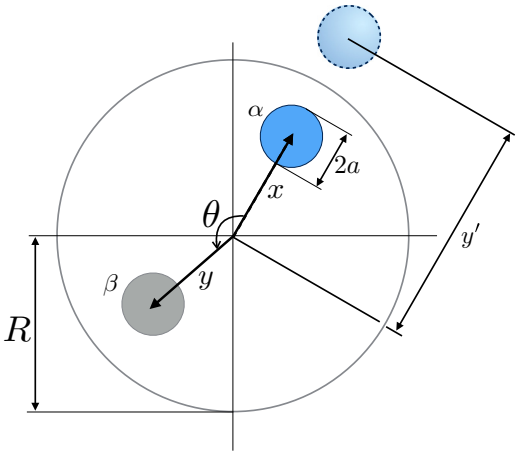

FIG. 1. Model system with an image point external to the cavity.

fluid disturbance arising from traction on the particle surfaces S_α,

$$\boldsymbol{u}'(\boldsymbol{x}) = -\int_{S_a} \boldsymbol{f}(\boldsymbol{y})\cdot\boldsymbol{G}(\boldsymbol{x},\boldsymbol{y})dS_y - \int_{S_c} \boldsymbol{f}(\boldsymbol{y})\cdot\boldsymbol{G}(\boldsymbol{x},\boldsymbol{y})dS_y, \tag{21}$$

where now the integral at infinity has become an integral over the cavity surface S_c. The second integral does not vanish, in contrast to Eq. (1), a consequence of the finite domain size. Seeking a solution in this form requires the surface traction over the surface of the cavity. To avoid this tedious calculation, an image point is utilized to modify the Green's function so as to satisfy the no-slip and no-flux boundary conditions over the cavity surface. The image point creates a perturbation that exactly satisfies the no-slip and no-flux boundary conditions at the surface of the cavity,

$$\boldsymbol{G}(\boldsymbol{x},\boldsymbol{y}) = \boldsymbol{J}(\boldsymbol{x},\boldsymbol{y}) + \boldsymbol{J}^c(\boldsymbol{x},\boldsymbol{y}), \tag{22}$$

where $\boldsymbol{J}(\boldsymbol{x},\boldsymbol{y})$ is the unbound Stokeslet and $\boldsymbol{J}^c(\boldsymbol{x},\boldsymbol{y})$ is a tensor that enforces the no-slip and no-flux conditions that define the surface of the cavity. The tensor $\boldsymbol{J}^c(\boldsymbol{x},\boldsymbol{y})$, due to Oseen, is given by the expression [115]

$$\boldsymbol{J}^c(\boldsymbol{x},\boldsymbol{y}) = -\frac{1}{8\pi\eta R}\Bigg[\frac{\boldsymbol{I}}{y|\boldsymbol{x}-\boldsymbol{y}'|} + \frac{(\boldsymbol{x}-\boldsymbol{y}')(\boldsymbol{x}-\boldsymbol{y}')}{y^3|\boldsymbol{x}-\boldsymbol{y}'|^3} + \frac{y^2-1}{y}\Bigg(\frac{\boldsymbol{y}\boldsymbol{y}}{y^4|\boldsymbol{x}-\boldsymbol{y}'|}$$

$$-\frac{\boldsymbol{y}(\boldsymbol{x}-\boldsymbol{y}')+(\boldsymbol{x}-\boldsymbol{y}')\boldsymbol{y}}{y^4|\boldsymbol{x}-\boldsymbol{y}'|^3} + \frac{2\boldsymbol{y}\boldsymbol{y}\boldsymbol{y}\cdot(\boldsymbol{x}-\boldsymbol{y}')}{y^6|\boldsymbol{x}-\boldsymbol{y}'|^3}\Bigg) + (x^2-1)\nabla_{\boldsymbol{x}}\boldsymbol{\varphi}\Bigg], \tag{23}$$

where

$$\boldsymbol{\varphi} = \frac{y^2-1}{2y^3}\Bigg(\frac{3\boldsymbol{y}}{y} + \frac{\boldsymbol{x}-\boldsymbol{y}'}{|\boldsymbol{x}-\boldsymbol{y}'|^3} + 2\boldsymbol{y}\boldsymbol{y}'\cdot\nabla_{\boldsymbol{x}}\frac{1}{|\boldsymbol{x}-\boldsymbol{y}'|} + \frac{3x\left[x-(1-y|\boldsymbol{x}-\boldsymbol{y}'|)\frac{\boldsymbol{x}\cdot\boldsymbol{y}}{xy^2}\right]}{|\boldsymbol{x}-\boldsymbol{y}'|}\frac{\boldsymbol{x}-\boldsymbol{x}\cdot\boldsymbol{y}'\boldsymbol{y}}{(xy')^2-(\boldsymbol{x}\cdot\boldsymbol{y}')^2}\Bigg). \tag{24}$$

Here $\boldsymbol{y}' = \boldsymbol{y}/y^2$ is the position of the image point outside a spherical boundary and all lengths have been made dimensionless on the radius R of the cavity. We note that the expression for $\boldsymbol{J}^c(\boldsymbol{x},\boldsymbol{y})$ differs from the corresponding expression in the study of an infinitesimal point of Felderhof and Sellier [121], owing to a typographical error in that publication. As written, Eq. (23) appears to diverge at the point $y = 0$, suggesting that even a weak disturbance at the center of the cavity produces infinitely strong flows. Fortunately, this is a mathematically removable singularity. Straightforward

algebraic manipulation removes the singularity to show that the Green's function is mathematically entire. Similarly, although at first glance some components of the mobility tensors (derived in the Appendix) appear to diverge for the values $\hat{\boldsymbol{x}}\cdot\hat{\boldsymbol{y}}=1, \hat{\boldsymbol{x}}\cdot\hat{\boldsymbol{y}}=-1, \boldsymbol{x}=0$, and $\boldsymbol{y}=0$, the singularities can be removed upon taking the appropriate limits at those values.

As in Sec. II, the disturbance flow $\boldsymbol{u}'(\boldsymbol{x})$ given by (21) accounts for the motion of all particles, where now Eq. (22) is utilized for the Green's function to give

$$\boldsymbol{u}'(\boldsymbol{x}) = -\sum_{\alpha=1}^{N}\int_{S_\alpha} \boldsymbol{f}(\boldsymbol{y})\cdot[\boldsymbol{J}(\boldsymbol{x},\boldsymbol{y})+\boldsymbol{J}^c(\boldsymbol{x},\boldsymbol{y})]dS_y. \tag{25}$$

Now the integral over the cavity surface has been replaced by the no-slip and no-flux condition satisfied by the Green's function, i.e., $\boldsymbol{J}(\boldsymbol{x},\boldsymbol{y})+\boldsymbol{J}^c(\boldsymbol{x},\boldsymbol{y})=0$ at $y=R$. A Taylor expansion of $\boldsymbol{J}(\boldsymbol{x},\boldsymbol{y})$ and $\boldsymbol{J}^c(\boldsymbol{x},\boldsymbol{y})$ for a given particle α about its center $\boldsymbol{y}$ yields a sum of moments of the hydrodynamic surface traction exerted on particle α. Upon integration these again become the hydrodynamic force, torque, stresslet, etc., projected through the Stokeslet, rotlet, and couplet analogs:

$$\begin{aligned}\boldsymbol{u}'(\boldsymbol{x}) = &-\left(1+\frac{a_\alpha}{6}\nabla_y^2\right)[\boldsymbol{J}(\boldsymbol{x},\boldsymbol{y})+\boldsymbol{J}^c(\boldsymbol{x},\boldsymbol{y})]\Big|_{\boldsymbol{y}=\boldsymbol{x}_\alpha}\cdot\boldsymbol{F}_\alpha^H - \frac{1}{2}\nabla_y\times[\boldsymbol{J}(\boldsymbol{x},\boldsymbol{y})+\boldsymbol{J}^c(\boldsymbol{x},\boldsymbol{y})]\Big|_{\boldsymbol{y}=\boldsymbol{x}_\alpha}\cdot\boldsymbol{L}_\alpha^H\\ &-\left(1+\frac{a_\alpha}{10}\nabla_y^2\right)\boldsymbol{K}^c(\boldsymbol{x},\boldsymbol{y})\Big|_{\boldsymbol{y}=\boldsymbol{x}_\alpha}:\boldsymbol{S}_\alpha^H+\cdots,\end{aligned} \tag{26}$$

where an irreducible second and third moment are included in $\boldsymbol{J}+\boldsymbol{J}^c$ and $\boldsymbol{K}^c$ and the couplet $\boldsymbol{K}^c$ is given by

$$\boldsymbol{K}^c(\boldsymbol{x},\boldsymbol{y}) = \nabla_y[\boldsymbol{J}(\boldsymbol{x},\boldsymbol{y})+\boldsymbol{J}^c(\boldsymbol{x},\boldsymbol{y})]+\{\nabla_y[\boldsymbol{J}(\boldsymbol{x},\boldsymbol{y})+\boldsymbol{J}^c(\boldsymbol{x},\boldsymbol{y})]\}^T. \tag{27}$$

As in Sec. II, insertion of (26) into the Faxén formulas yields a set of linear relations between particle motion and hydrodynamic force, torque, stresslet, and higher-order moments, all coupled by a grand mobility tensor $\mathcal{M}$. The tensor is truncated as discussed in Sec. II to the level of the stresslet (taking care to retain the irreducible quadrupoles and octupole that capture finite particle size), to give a far-field mobility matrix for the spherical domain $\mathcal{M}_{ff}$, which upon inversion couples all particles to one another and to the cavity. Finally, to complete the theoretical framework, near-field and lubrication interactions are accounted for in a pairwise fashion (cf. Sec. II) and the sum couples all near- and far-field many-body particle-particle and particle-cavity interactions, expressed compactly as

$$\mathcal{R} = (\mathcal{M}_{ff})^{-1}+\mathcal{R}_{nf}. \tag{28}$$

For convenience, the near-field particle-particle and particle-cavity interaction tensor $\mathcal{R}_{nf}$ is split into two contributions. Because near-field particle-particle interactions can be accounted for pairwise, they are given by the unbound resistance functions, which we denote by $\mathcal{R}_{nf,\mathrm{unbound}}$; the near-field particle-cavity interactions are given by the pairwise resistance tensor $\mathcal{R}_{nf,c}$. As discussed in Sec. II, the former are well established and can be found in the literature [105–107]. For the latter, the submatrices that correspond to particle-cavity interactions $\mathcal{R}_{nf,c}^{FU}$, $\mathcal{R}_{nf,c}^{F\Omega}$, $\mathcal{R}_{nf,c}^{LU}$, and $\mathcal{R}_{nf,c}^{F\Omega}$ were determined by O'Neill and Majumdar [109] for couplings perpendicular to the line of center of the particle and the cavity and by Jones [111] for motion along the line of centers. When combined as shown in Eq. (28), these couplings form a grand resistance matrix that accounts for all many-body particle-particle and particle-cavity hydrodynamic interactions over all separations and particle concentrations. This coupling depends only on the geometry of the suspension, which now comprises particle and cavity size and shape, as well as spatial arrangement of particles relative to one another and to the confining spherical boundary. With it, particle motion can be deduced from hydrodynamic force and torque without requiring knowledge of the hydrodynamic traction over the cavity. Any motion of the enclosure can be incorporated in a straightforward manner by introducing

the corresponding far-field flow $\boldsymbol{u}^{\infty}(\boldsymbol{x})$. The functions that represent the components of the far-field grand mobility matrix are presented and evaluated next.

IV. RESULTS

We begin by presenting the components of the far-field grand mobility matrix developed in the present work. Its inverse is then combined with the near-field grand resistance tensor as described in Sec. III. Blockwise inversion of the resulting many-body resistance tensor preserves all couplings and permits solution and examination of the velocity-force, velocity-torque, rotation-force, and rotation-torque relationships. The translational motion of a single particle to which an external force is applied and the entrainment of a second, passive particle in the flow of a forced particle are then studied in Secs. IV A and IV B, respectively. Higher-order couplings are then studied in Sec. IV C. The effects of point-particle approximations are discussed in Sec. IV D.

A. Single particle inside a spherical cavity: Force-to-translation coupling

The simplest coupling of particle motion to hydrodynamic traction is that between velocity $\boldsymbol{U}$ and hydrodynamic force $\boldsymbol{F}^{H}$. For an isolated sphere alone in a solvent, $\boldsymbol{U} = -\boldsymbol{M}^{UF} \cdot \boldsymbol{F}^{H}$, where $\boldsymbol{M}^{UF} = (1/6\pi\eta a)\boldsymbol{I}$. If the particle is then placed inside a solvent-filled cavity, one expects motion slower than its unbound Stokes velocity, owing to hydrodynamic coupling to the no-slip surface of the cavity, in some sense similar to coupling between an unbound pair. The correction to unbound mobility that accounts for the presence of the cavity was derived in the present study via the method described in Sec. III. To reveal the strength of hydrodynamic coupling along and transverse to the line of centers $\hat{\boldsymbol{y}}$ between a particle and the cavity, the tensor is projected onto the two corresponding orthogonal subspaces $\hat{\boldsymbol{y}}\hat{\boldsymbol{y}}$ and $\boldsymbol{I} - \hat{\boldsymbol{y}}\hat{\boldsymbol{y}}$, respectively. Projection onto the subspace $\hat{\boldsymbol{y}}\hat{\boldsymbol{y}}$ yields

$$6\pi\eta a M^{UF,\parallel}_{ff,\alpha\alpha} = 1 + \left(\frac{a}{R}\right)\left[-\frac{9}{4(1-y^2)}\right] + \left(\frac{a}{R}\right)^3\left[\frac{3y^2+5}{2(1-y^2)^3}\right] + \left(\frac{a}{R}\right)^5\left[-\frac{y^4+10y^2+5}{4(1-y^2)^5}\right]. \tag{29}$$

The term proportional to a/R corresponds to the motion of an infinitesimal point inside a spherical cavity and has been previously reported [121]. In this work we account for the finite size of particles, which requires the terms of order $(a/R)^3$ and $(a/R)^5$ in Eq. (29) that arise from the irreducible components of the second and third moments of the hydrodynamic surface traction. While the computation is tedious, terms to this order are necessary to ensure that the grand mobility matrix is positive-definite. As expected, in the limit $a/R \to 0$, the unbound solution is recovered, giving the Stokes drag on a single hard particle. A similar projection in the perpendicular direction gives

$$6\pi\eta a M^{UF,\perp}_{ff,\alpha\alpha} = 1 - \left(\frac{a}{R}\right)\left[\frac{9(y^4-3y^2+4)}{16(1-y^2)}\right] + \left(\frac{a}{R}\right)^3\left[-\frac{3y^6-12y^4+21y^2-20}{8(1-y^2)^3}\right]$$

$$+ \left(\frac{a}{R}\right)^5\left[-\frac{y^8-5y^6+11y^4+5y^2+20}{16(1-y^2)^5}\right]. \tag{30}$$

Combined, (29) and (30) give the far-field velocity-force self-mobility of a sphere within a suspension of an arbitrary number of particles, confined by a hard spherical cavity. Analogous expressions for the remaining couplings (force, torque, velocity, rotation, straining, and stresslet) derived in the present study are shown in the Appendix. As detailed in Sec. III, all of the far-field couplings are then assembled into a far-field grand-mobility matrix, inverted, superimposed with the near-field grand resistance matrix, and solved blockwise. The resultant self-mobility couplings account for the infinite hierarchy of reflections between a finite-size particle and an arbitrary number $N-1$ of other

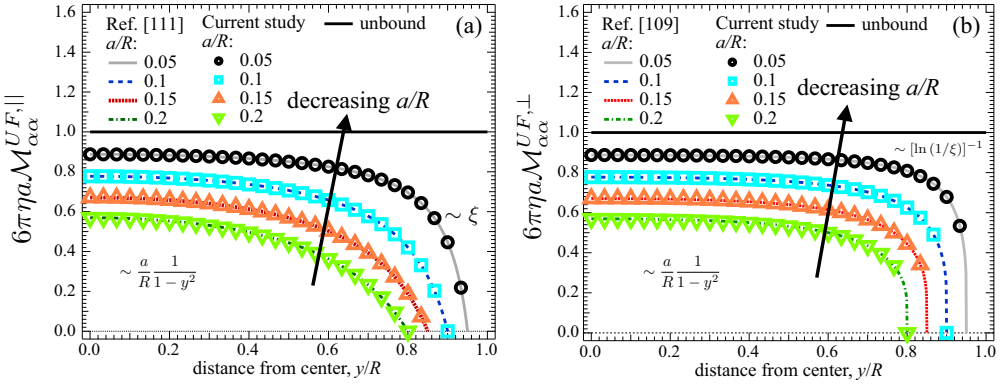

FIG. 2. Confined self-mobility plotted as a function of position in the cavity, connecting a force acting (a) along and (b) transverse to the particle-cavity line of centers to the velocity of the particle in the same direction. The scaling for the decrease in the mobility is shown when the particle is in both the far field $\sim (a/R)/(1-y^2)$ and the lubrication region, where the decrease scales with the surface-to-surface separation $\xi = 1 - a/R - y_\alpha$. Open symbols represent the mobility functions from the present study, obtained via blockwise inversion of Eq. (16) after insertion of Eqs. (A1) [which includes Eqs. (29) and (30)]–(A3) into (28). Solid lines show the bispherical series solution [109,111].

particles and with the enclosing cavity. Its elements $\mathcal{M}^{UF}_{ff,\alpha\alpha}$, $\mathcal{M}^{\Omega L}_{ff,\alpha\alpha}$, $\mathcal{M}^{UL}_{ff,\alpha\alpha}$, $\mathcal{M}^{\Omega F}_{ff,\alpha\alpha}$, $\mathcal{M}^{ES}_{ff,\alpha\alpha}$, $\mathcal{M}^{\Omega S}_{ff,\alpha\alpha}$, and $\mathcal{M}^{US}_{ff,\alpha\alpha}$ give the corresponding self-motion of a particle subjected to hydrodynamic force, torque, and stresslet as it is hindered by interactions with other particles and with the enclosing cavity (all far-field self-mobilities UF, ΩL, UL, ES, ΩS, and US derived in the present study can be found in the Appendix).

We begin with the simplest case: a single particle suspended in pure solvent enclosed by the cavity ($N = 1$). We focus first on the coupling between translational velocity and force, for which the components along and transverse to the line of centers $\mathcal{M}^{UF,\parallel}_{\alpha\alpha}$ and $\mathcal{M}^{UF,\perp}_{\alpha\alpha}$ are plotted in Figs. 2(a) and 2(b), respectively, as a function of the position of the particle relative to the cavity center. The mobility is made dimensionless by the lone single-particle mobility $1/6\pi\eta a$ and particle position is scaled on the cavity size R. Two sets of curves are shown in each plot alongside the hydrodynamic mobility of a particle in an unbound domain (solid horizontal line). The open symbols give the results obtained via the present approach (valid for an arbitrary number of confined particles). The solid and dashed curves correspond to results obtained from the method of Jones (which cannot be generalized beyond a single confined particle) [111]. Agreement between the prior theory and our theory is excellent, for all particle-to-cavity size ratios a/R and particle positions y/R studied, validating the present framework by recovering previously published results for a single confined particle. However, unlike prior models, our framework can model the motion of an arbitrary number of particles.

A comparison of the curves to the isotropic unbound mobility reveals that 3D confinement gives rise to anisotropic hindrance of partible mobility. The confined-mobility curves all lie under the unbound mobility line, showing that hydrodynamic coupling between the two no-slip surfaces hinders particle motion. Further, in contrast to the position-independent mobility for a particle in an unbound domain, the mobility of a confined particle depends on its proximity to the cavity wall. Unsurprisingly, the mobility of a particle of finite size is greater near the center of a cavity than near the cavity surface, owing to the changing proximity of their no-slip surfaces. The mobility decreases monotonically from its maximum at the center as it approaches the cavity surface, vanishing entirely at particle-wall contact. Finally, a comparison of Fig. 2(a) to Fig. 2(b) reveals that near the cavity wall, the mobility is anisotropic, with transverse motion decaying less rapidly than motion toward or

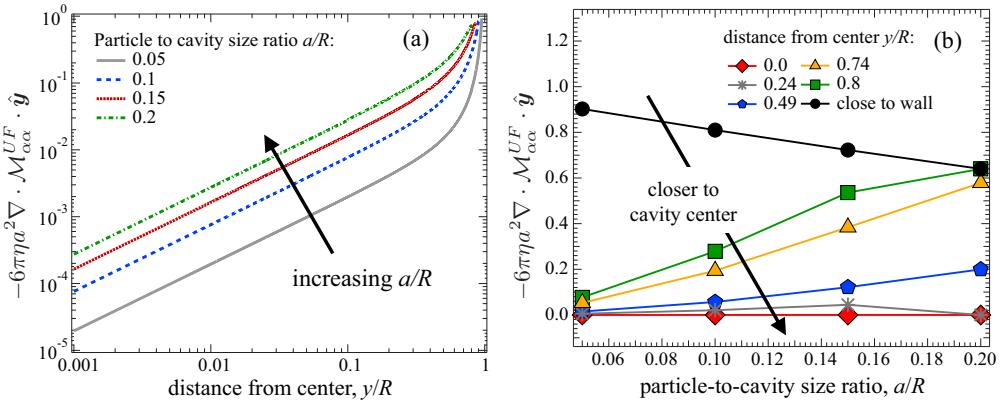

FIG. 3. Drift velocity along the particle-cavity line of centers as a function of (a) position in the cavity and (b) particle-to-cavity size ratio a/R.

away from the wall. This is consistent with near-contact mobility between a pair of spheres, where transverse lubrication interactions are weaker than longitudinal encounters.

While for all size ratios a/R the reduction in mobility becomes steeper as the particle approaches the wall, the rate of this decay depends qualitatively on the particle-to-cavity size ratio. Because the size ratio affects the slope, it changes the divergence of the mobility $\boldsymbol{\nabla} \cdot \mathcal{M}$. The physical relevance of the divergence of the mobility is best understood in the context of colloidal particles where, owing to Brownian motion, a particle will migrate from regions of low to high mobility, moving as though driven by a deterministic force, the Brownian drift. The quantity $\boldsymbol{\nabla} \cdot \mathcal{M}$ sets the corresponding drift velocity and gives the tendency of the particle to migrate toward the region of highest mobility. Because mobility is highest at the cavity center, projection of the drift velocity along the cavity radius gives the strength of the tendency of the particle to drift away from the wall and toward the center. The projection of $\boldsymbol{\nabla} \cdot \mathcal{M}$ onto a unit vector $-\hat{\boldsymbol{y}}$ pointing toward the center of the cavity is plotted in Fig. 3(a) as a function of the distance between the particle and the center of the cavity. Four curves are shown, each curve corresponding to a different particle-to-cavity size ratio. Near the wall (far right end of the horizontal axis) the drift velocity is large, indicating a strong tendency to migrate away from the wall. Near the center, the drift velocity is three orders of magnitude weaker, indicating the tendency of a lone particle to remain there. This position-dependent behavior, where the particle tends to drift away from the wall and remain near the center, is observed for all size ratios studied.

Alternatively, one can ask how the strength of the push away from the wall changes as a particle grows larger, by inspecting how the radial drift velocity changes with size ratio a/R, as shown in Fig. 3(b). The diamonds show behavior nearest the center of the cavity and the closed circles show behavior nearest the wall, with several other intervening positions shown as noted in the legend. The diamonds show that a particle at the center has zero drift velocity regardless of particle size, demonstrating that the preferred position of an isolated particle in a spherically confined domain is always at the center of the cavity. As the particle moves away from the center (stars, pentagons, triangles, and squares), the drift velocity increases, for all particle sizes, tending to push a particle back toward the center. The strength of this push at a given position increases as the confined particle grows larger, as indicated by the positive slopes, owing to the growing distance of the particle to the region of highest mobility, i.e., the center of the cavity. However, this trend reverses very near the wall (closed circles): The strength of the push decreases as the particle grows larger, as evidenced by the negative slope. This behavior can be understood by recalling that the closest a particle can come to contacting the cavity wall is the position $y_{\max} = 1 - a/R$, its maximum position. A large particle at its maximum position is thus closer to the region of highest mobility, i.e., the center of the

cavity, than a small particle at its maximum position. Because a small particle can be farther from the center of the cavity than a large particle, its maximum drift velocity is higher.

B. Hydrodynamically interacting pair: Force-to-translation coupling

In the previous section, we presented the expression derived in this study for the self-mobility $\mathcal{M}^{UF}_{\alpha\alpha}$ of a spherically confined particle in a suspension of arbitrary concentration, in response to a hydrodynamic force on its own surface [Eqs. (29) and (30)]. The simplest case of a single confined particle was studied first, toward understanding the influence exerted on particle mobility by the cavity. The motion of such a particle entrains the fluid in the cavity and in turn any nearby particles will be entrained by this flow. This coupling was captured by the many-body entrainment mobility $\mathcal{M}_{\beta\alpha}$ as discussed in Sec. III, to yield the full coupling and the motion of an arbitrary number of forced and entrained particles, as it is influenced by the cavity. Whether two, three, or many particles are enclosed in the cavity, forced or passive, their motion is given by precisely the same expressions and process. We illustrate this process here, utilizing the many-body coupling derived in the present study and, from it, present results for the motion of a pair of spherically confined particles.

The entrained mobility $\mathcal{M}^{UF}_{\beta\alpha}, \beta \neq \alpha$, is the hydrodynamic coupling that describes the entrainment of particle(s) β in the flow field produced by the motion of particle(s) α. Each particle interacts with the other and with the cavity via disturbance flows propagated by their motion. The initial disturbance propagated by particle α is, as described in Sec. II, given by the Stokeslet $\boldsymbol{J}$ plus a correction due to the hindrance of the cavity $\boldsymbol{J}^c$ defined in Eqs. (23) and (24). Thus, the strength of the entrainment of particle β is weaker than if the domain was unbound. Here $\alpha, \beta \in [1, N]$, where N is arbitrary.

The grand mobility tensor for a confined system must ultimately recover the unbound behavior in the limit $a/R \to 0$. We leverage this fact to more clearly reveal the influence of the cavity, by artificially dividing the mobility into two expressions

$$\boldsymbol{M}^{UF}_{\beta\alpha} = \left(\boldsymbol{M}^{UF}_{\beta\alpha}\right)^{\text{unbound}} + \boldsymbol{M}^{UF,c}_{\beta\alpha}, \tag{31}$$

where the motion due to unbound entrainment is $(\boldsymbol{M}^{UF}_{\beta\alpha})^{\text{unbound}}$. Making lengths dimensionless by the radius of the cavity R gives

$$6\pi\eta a(\boldsymbol{M}^{UF}_{\beta\alpha})^{\text{unbound}} : \hat{\boldsymbol{r}}\hat{\boldsymbol{r}} = \frac{a}{R}\left(\frac{3}{2}r^{-1} - r^{-3}\right)x. \tag{32}$$

The cavity contribution $\boldsymbol{M}^{UF,c}_{\beta\alpha}$, as obtained in the present study via our method, can be projected radially to yield Eq. (33),

$$\begin{aligned}
6\pi\eta a M^{UF,||,c}_{\beta\alpha} = &\left\{\left(\frac{a}{R}\right)[-3(\{6-2y^2+4bxy(-5+y^2)+(1+b^2)x^4y^2(-1+3y^2)\right.\\
&-4bx^3y(-2+b^2+5y^2)+x^2[-4+9y^2+y^4+b^2(2+19y^2-3y^4)]\}/8y^5\zeta^5\\
&-3\{4b^3x^2y^2+b^2xy[3-5y^2+x^2(-5+3y^2)]+xy[6-4y^2+3x^4y^2(-1+y^2)\\
&+x^2(-4+9y^2-3y^4)]+b[3(-1+y^2)-9x^4y^2(-1+y^2)+x^2(3-16y^2\\
&+9y^4)]\}/8(-1+b^2)xy^4\zeta^3+9b(-1+x^2)(-1+y^2)(-1+2bxy-x^2y^2)/8(-1\\
&\left.+b^2)xy^3\zeta^2)]+\left(\frac{a}{R}\right)^3(3\{4b^5x^4y^2[-1+2(-2+x^2)y^2+y^4]+b^4x^3y[2+(34\right.\\
&-7x^2)y^2+(-7-2x^2+x^4)y^4+3x^2y^6]+2b^3x^2y^2[-14+3y^2-3x^4y^2+x^2(7-2y^2\\
&+y^4)]-xy^3[2+x^8y^4+2x^2(-12+7y^2)+x^6y^2(5-2y^2+y^4)+x^4(14-6y^2\\
&+3y^4)]-b^2xy[-14+5y^2+17x^6y^4+x^2(9-12y^2+14y^4)+x^4y^2(14-38y^2\\
&+21y^4)]+b[-2+y^2+7x^8y^6+x^6y^4(33-14y^2+7y^4)+x^2(1-14y^2+15y^4)
\end{aligned}$$

$$+x^4y^2(11-50y^2+29y^4)]\}/8(-1+b^2)xy^8\zeta^7+[3b(-2+x^2+y^2)(-1+2bxy$$
$$-x^2y^2)^3]/8(-1+b^2)xy^7\zeta^6)+\left(\frac{a}{R}\right)^5\{[-10+81x^2y^2-48x^4y^4-32b^4x^4y^4$$
$$+x^6y^6-3b^2x^2y^2(21-46x^2y^2+x^4y^4)+4bxy(5-36x^2y^2+9x^4y^4)+b^3(72x^3y^3$$
$$-48x^5y^5)]/8y^9\zeta^9+[24b^3x^4y^4+b^2(3xy-42x^3y^3-17x^5y^5)-xy(10-7x^2y^2$$
$$+4x^4y^4+x^6y^6)+b(1+21x^2y^2+11x^4y^4+7x^6y^6)]/8(-1+b^2)xy^8\zeta^7$$
$$+b(-1+2bxy-x^2y^2)^3/8(-1+b^2)xy^7\zeta^6\}\Big\}\hat{\boldsymbol{y}}\hat{\boldsymbol{y}}, \tag{33}$$

where $b=\hat{\boldsymbol{x}}\cdot\hat{\boldsymbol{y}}$ and the distance of the entrained particle to the image point of the forced particle is $\zeta=y^{-1}\sqrt{1-2bxy+y^2}$. Higher-order moments of the hydrodynamic surface traction also give rise to cavity contributions corresponding to both self-mobility and pair mobility, which describes many-body entrainment of particles by disturbance flows.

Equations (29)–(33) give only force-velocity couplings; the far-field grand mobility matrix must be populated with higher-order pair-level couplings to the level of the stresslet. Higher-order couplings for the confined self- and entrained motion are provided in the Appendix up to the level of the stresslet. Following its construction, inversion of this far-field grand mobility matrix automatically captures an infinitude of reflected interactions between all particles and the cavity, giving an N-body far-field hydrodynamic coupling. That is, coupling between an arbitrary number of particles to one another and the cavity is automatically captured by this Stokesian dynamics approach.

To elucidate the effect of confinement on entrainment, we consider first the simplest case, $N=2$ enclosed particles. A second particle β is inserted into the cavity and we ask how it moves in response to a force exerted on particle α. In Fig. 4 a contour plot illustrating the complete analytical coupling, that is, including near-field and far-field interactions, is presented for the induced motion along and transverse to the line of external force, in Figs. 4(a) and 4(b), respectively. Here the force $\boldsymbol{F}$ exerted on the source particle is directed along the radius of the cavity. Each contour plot shows the plane passing through the center of the spherical cavity; the forced particle is at the center of the closed black circle, which encloses a region excluding particle centers. In Fig. 4(a), the colorized regions represent the strength and direction of entrainment, ranging from dark red for strong entrainment in the same direction as the external force to dark blue for strong entrainment in the direction antiparallel to the external force. As can be seen in Fig. 4(a), the entrainment field is axisymmetric about the external force, regardless of the position of the forced particle. In the $y=0$ contour plot, the forced particle is placed at the center of the cavity. As indicated by the dark red, orange, and yellow regions ahead of and trailing the forced particle, a second particle placed in those regions will be pushed or pulled along by the motion of the forced particle. The regions flanking the line of forcing are initially dark red, close to the forced particle, but rapidly transition to dark blue. That is, a second particle closely flanking the forced particle will travel along with it, but a short (transverse) distance away, an entrained particle will travel in the opposite direction. This trend continues when the forced particle is placed closer to the spherical cavity, i.e., for $y=0.2$, 0.4, and 0.6 as shown in Fig. 4(a). Here it can be seen that entrainment is strongest in the region nearest the forced particle. As $y\to 0.9$, the region farthest from the forced particle (green region) is only weakly disturbed; particles in this region hardly move in response to the forced particle. The region closest to the cavity wall is green, regardless of the position of the forced particle, owing to the no-slip and no-flux condition of the cavity surface.

The entrained particle will also undergo motion transverse to the applied radial force, as illustrated in Fig. 4(b). As in Fig. 4(a), the strength of entrainment varies from dark red to dark blue, but here dark red corresponds to strong entrainment in the positive y direction and dark blue to strong entrainment in the negative y direction, as noted by the axes in each image. Thus, particles placed

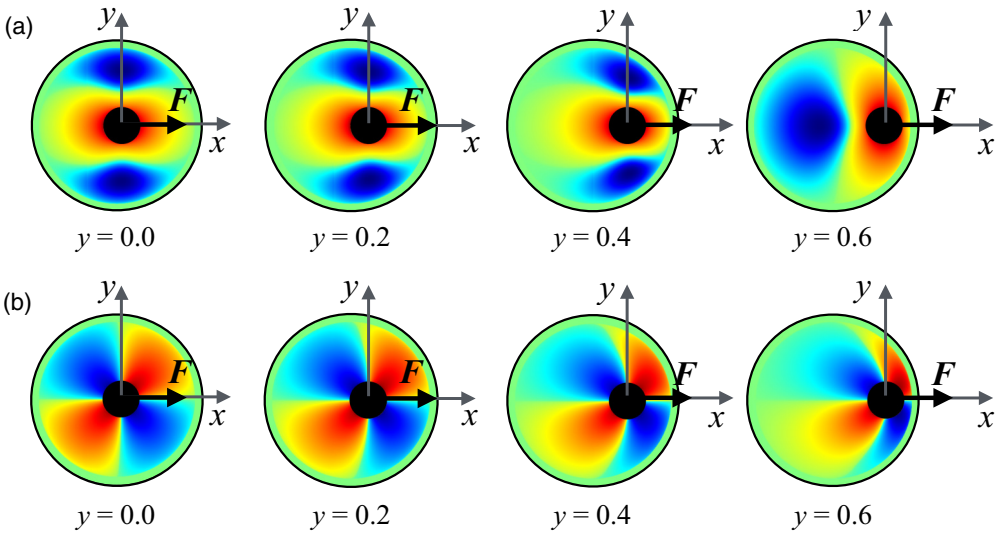

FIG. 4. Hydrodynamic entrainment of a passive finite-size particle dragged by the disturbance flow of a forced particle. The distance y of the forced particle to the center of the cavity is given below each plot; the particle-to-cavity size ratio for all of the plots is $a/R = 0.1$. Brighter colored regions (red) represent entrainment in the positive direction and dark colored regions entrainment in the opposite direction. (a) Radial entrainment on a second particle due to a radial force on the forced particle and (b) perpendicular entrainment of a second particle due to a radial force on another forced particle in the cavity.

in the red region ahead of the forced particle (upper right-hand red region) will move orthogonal to the applied force and away from its line of action; those placed in the red region trailing the forced particle (lower left-hand red region) will move orthogonally toward the line of action of the force, i.e., in the positive y direction. Blue regions indicate entrainment mirrored across the x axis.

The line of action of the applied force may also act transverse to the cavity radius (i.e., transverse to the line of centers between the cavity and the forced particle). The response of an entrained particle is shown in Fig. 5. The colorized regions in Fig. 5(a) again represent the strength and direction of entrainment, ranging from dark red for strong entrainment in the same direction as the external force (positive direction along the y axis) to dark blue for strong entrainment in the direction opposite the external force. The entrainment field in Fig. 5(a) is axisymmetric only when the forced particle is precisely at the center of the spherical cavity. As the particle moves away from the center, this symmetry is lost. The dark red, orange, and yellow regions indicate that the motion of the forced particle will push or pull a second particle particle in the same direction. The region flanking the line of forcing is red close to the forced particle; however, it quickly transitions to dark blue. The size and location of the dark blue regions flanking the forced particle, i.e., regions where a second particle will be entrained in the opposite direction, vary with the position of the forced particle. For $y = 0.2$, blue regions also flank the line of action of the applied force, but the region of reverse entrainment to the right of the external force shrinks while that to the left grows. This trend continues as the forced particle moves nearer to the wall, as shown for $y = 0.4$ and 0.6. One can envision that, as the forced particle moves toward the wall, both parallel and transverse motion of an entrained particle vanish.

The entrained particle will also undergo motion transverse to the line of action of the force, as illustrated in Fig. 5(b). Again the strength of entrainment varies from dark red to dark blue; here dark red corresponds to entrainment in the positive x direction and dark blue corresponds to entrainment in the negative x direction. In consequence, particles placed in the red region ahead of the forced particle (i.e., the upper right-hand red region) will move orthogonally to the applied force and away from its line of action; those placed in the red region trailing the forced particle (lower left-hand red

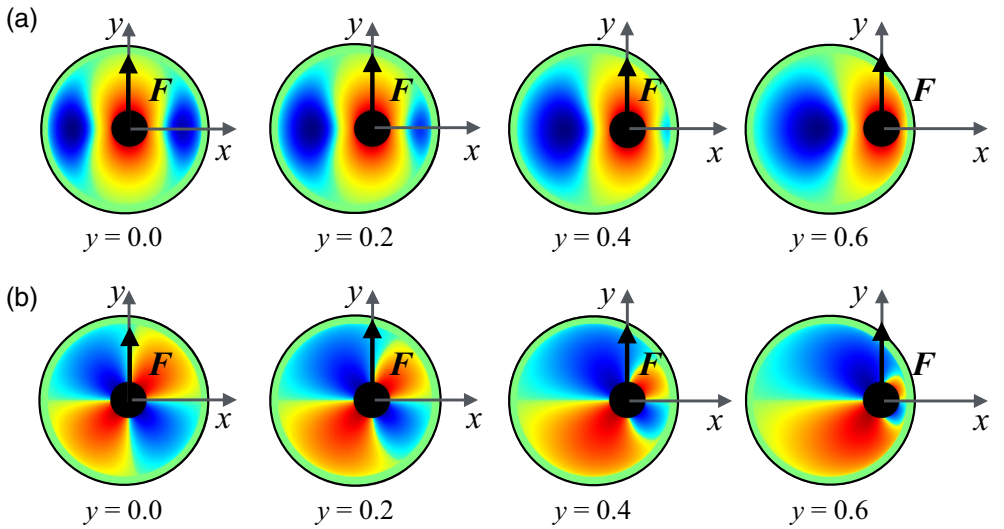

FIG. 5. Contour plots of the hydrodynamic entrainment of a second particle inside the spherical cavity due to the disturbance flow propagated by another forced particle. The distance y of the forced particle to the center of the cavity is given below each plot; the particle-to-cavity size ratio for all of the plots is $a/R = 0.1$. Brighter colored regions (red) represent entrainment in the positive direction and dark colored regions entrainment in the opposite direction. (a) Perpendicular entrainment due to a perpendicular force acting on a forced particle and (b) radial entrainment due to a perpendicular force on a forced particle.

region) will move orthogonally toward the line of action of the force, in the positive y direction. As in Fig. 4(b), blue regions indicate entrainment mirrored across the x axis.

In summary, the hydrodynamic coupling between a pair of particles interacting inside a spherical cavity shows qualitative differences from that between an unbound pair. The coupling can be resolved into contributions of entrainment in response to radial and transverse components of an externally applied force. The most intuitively obvious difference is that apparent flow recirculation (conservation of mass) creates regions in which motion of a forced particle drives motion of a second particle in the opposite direction when the force on the forced particle acts along the line of the center of the particle and the cavity. In addition, regardless of the direction of the external force, entrainment is reduced owing to the presence of no-slip surface of the cavity. We emphasize that the model presented is not restricted to a confined pair; our framework is fully applicable to an arbitrary number of particles at arbitrary volume fractions and particle-to-cavity size ratio.

C. Higher-order couplings

In Secs. IV A and IV B it was shown that the presence of a confining spherical cavity influences the hydrodynamic coupling between interacting spheres. This influence alters couplings between particle velocity, rotation, and straining motion to moments of the hydrodynamic traction: force, torque, stresslet, and higher-order moments. This infinite hierarchy of couplings is summarized compactly in Eq. (12); expressions for the individual entries in the grand mobility matrix were given in that section and in the Appendix and the coupling between particle translation and hydrodynamic force was studied. In the present section we explore another coupling, that between particle translation and hydrodynamic torque. We recall that a hydrodynamic torque on the surface of a single unbound particle produces no translation. However, proximity to a nearby surface can produce such coupling. For example, in the presence of a nearby wall, a particle subjected to a hydrodynamic torque about an axis parallel to the wall will translate along the wall. Similarly, for an unbound pair, a torque about an axis perpendicular to their line of centers will produce translation, but torque about their line

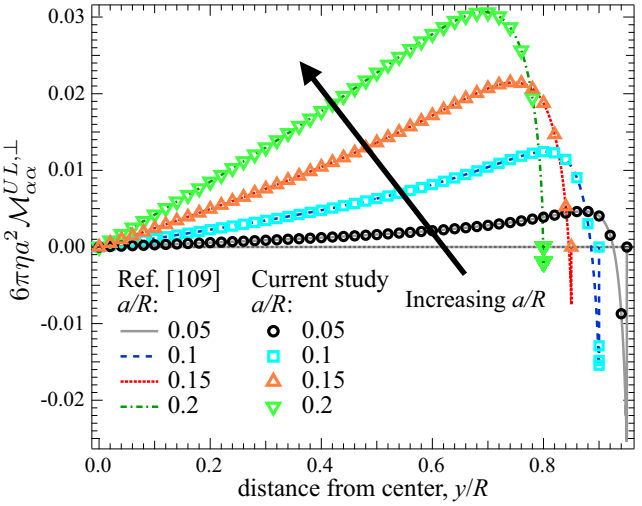

FIG. 6. Torque to translation coupling for a single particle inside a spherical cavity.

of centers produces no translation. Let us examine the analogous couplings for particles confined inside a sphere.

1. Single particle inside a spherical cavity: Torque–to–translational-motion coupling

The element of the grand mobility matrix $\mathcal{M}$ that describes torque-to-translational *self-mobility* of a particle in a spherically confined suspension $\mathcal{M}^{UL}_{\alpha\alpha}$ was derived in the present study utilizing the methods of Sec. III, where the far-field contribution is given by Eq. (A2). This expression gives the translational motion of a particle due to a hydrodynamic torque on its surface, in the presence of an arbitrary number of other particles and the confining cavity. While it is a tensor, only the antisymmetric component $\boldsymbol{\epsilon} \cdot \hat{\boldsymbol{y}}$, where $\boldsymbol{\epsilon}$ is the Levi-Cività tensor, is nonzero. This element, $\mathcal{M}^{UL,\perp}_{\alpha\alpha} = \mathcal{M}^{UL}_{\alpha\alpha} : -\frac{1}{2}\boldsymbol{\epsilon} \cdot \hat{\boldsymbol{y}}$ with the first index of $\mathcal{M}^{UL,\perp}_{\alpha\alpha}$ an inner product with the second index of $\boldsymbol{\epsilon}$ and vice versa, gives the translational motion of a particle α, along the cavity radius, due to a torque on its own surface, as influenced by other suspended particles β and the confining cavity.

To understand this coupling we study the simplest case of a single confined particle $N = 1$ plotted in Fig. 6 as a function of the distance of the particle from the center of the cavity, for a range of particle-to-cavity size ratios a/R (open symbols). The solid curves give the corresponding self-mobilities obtained via the method of O'Neill and Majumdar [109], which is limited to a single particle. Agreement between our N-body approach and the prior single-particle model is excellent.

Inspection of these plots reveals the effect of spherical confinement on the ability of a particle to translate in response to a torque. Due to the spherical symmetry of the configuration, when the particle is at the center, the torque-to-translation coupling is zero, so a particle will undergo no translational motion in response to torque. As the particle moves away from the center, it couples to the cavity, translating with a velocity $\boldsymbol{U}_\alpha = \mathcal{M}^{UL}_{\alpha\alpha} \cdot \boldsymbol{L}_\alpha$, in a direction perpendicular to both the torque and the line of centers between the particle and the cavity. With increasing proximity to the cavity surface, the particle translates faster, owing to stronger hydrodynamic coupling between the particle and the wall. This behavior is similar to the hydrodynamic coupling between a pair of unbound particles when one of the particles is acted on by a torque perpendicular to the line of centers: Outside the lubrication region, entrainment of the second particle will increase monotonically with increasing proximity. However, for a particle inside a spherical cavity, the translation of the particle reaches a maximum as it approaches the cavity surface. Beyond this point the translation of the particle reaches a stall condition near the wall, where translation ceases even with applied torque (points of intersection

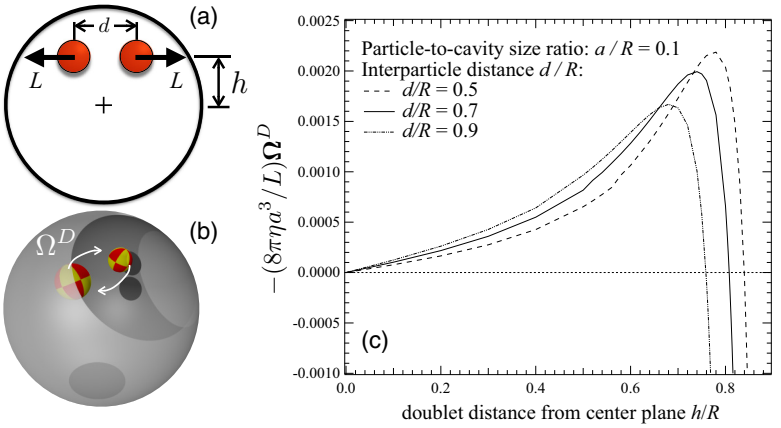

FIG. 7. (a) Model system. Two particles at a distance d from each other and at a height h from the center plane of the cavity are acted on by an external torque $\boldsymbol{L}$. (b) Simulation snapshot. Equal and opposite torques act on a pair of particles along their lines of centers, causing the particles to rotate as a doublet about an axis centered at the cavity. (c) Rate of rotation of the doublet as a function of the particles' height from the center plane of the cavity.

with the horizontal dashed line). Beyond this stall point, the direction of translation reverses and the particle translates in the opposite direction, undergoing a rolling motion over the surface of the cavity similar to the motion of a particle acted on by a torque near a planar wall. As the particle comes close to contact with the cavity surface its mobility must decrease again, eventually vanishing at the maximum position of the particle as a consequence of lubrication interactions between the no-slip surfaces. The N-body far-field expressions (found in the Appendix) utilized here for $N = 1$ are just as easily utilized to describe the self-motion in the presence of many enclosed particles.

2. *Hydrodynamically interacting pair inside the spherical cavity: Doublet rotation*

We again consider the effect of confinement on entrained translational motion, but now where such motion arises due to hydrodynamic torque, rather than hydrodynamic force. To study the motion, we implemented hydrodynamic functions developed in the present study into Stokesian dynamics: the mobility tensors coupling translation to force $\boldsymbol{M}^{UF}_{\beta\alpha}$, translation to torque $\boldsymbol{M}^{UL}_{\beta\alpha}$, and rotation to torque $\boldsymbol{M}^{\Omega L}_{\beta\alpha}$ [see Eqs. (A1)–(A3) and (A7a)–(A9f)]. To illustrate the effect of the cavity on such motion, we again start with the simplest case of a pair of particles. They are placed in the cavity at a separation $d = 0.5R, 0.7R$, and $0.9R$, with each particle equidistant from an axis passing through the center of the cavity [Fig. 7(a)]. When an external torque is applied to each particle along the line of centers of the particles and pointing in an outward direction as shown, both particles translate. In addition, they rotate together as a doublet as indicated in Fig. 7(b). No force is required to maintain a fixed separation between the pair, a consequence of the symmetry of the grand mobility matrix.

Their rate of rotation varies with the distance of the doublet from the center plane of the cavity h/R as plotted in Fig. 7(c). Three curves are shown, each corresponding to a doublet of particles at different interparticle distances. At the far left of the horizontal axis, where the pair is nearest the cavity center, the particles do not revolve about the cavity center, regardless of their center-to-center separation. Away from the center plane of the cavity, the torque-to-translation coupling emerges and they rotate as a doublet. Interestingly, the direction of doublet rotation depends on proximity to the cavity wall. As shown in Fig. 7(c), away from the wall, the doublet rotates in a clockwise sense [white arrows in Fig. 7(b)], revolving faster and faster around the cavity center for positions nearer the wall. However, a maximum is reached and it depends on their separation. Beyond this point, their revolution about the cavity center slows down, until a stall condition is reached very near the

wall where the rate of rotation becomes zero, as indicated by the horizontal dashed line in Fig. 7(c). Beyond this stall point, their revolution about the cavity center reverses and the doublet commences to rotate in the counterclockwise direction; both particles undergo a rolling motion over the surface of the cavity. This motion is analogous to the rolling motion of a single particle inside the spherical cavity described in the previous section. This interesting result highlights how the presence of the cavity can reverse rotational motion. Notably, this behavior is captured in the far-field interactions by the finite size of the particle, which was neglected in prior models.

In summary, the presence of a confining cavity couples particle translation to torque. Depending on the position of the particles, such coupling leads to a surprising reversal of motion, behavior, it turns out, similar to that observed in some biophysical systems [124]. The presence of the cavity also leads to reversals of translational motion (as shown in the previous section). Accurate modeling of such behaviors requires a treatment of both far-field and near-field hydrodynamic interactions as done in this study. The N-body far-field expressions (found in the Appendix) can be utilized to study such entrainment in a suspension of arbitrary concentration.

D. Point-particle approximation and effects of finite size

In the present study we have been careful to account for the finite particle size, but it is natural to ask what, if any, consequences would arise were we to simply model particles as infinitesimal points. In some problems, such simplifications can yield rapid insight into leading-order behavior, revealing the physics of primary interest. By way of example, the leading-order (point-particle) solution for a particle translating in (unbound) Stokes flow reveals the surprising strength of the hydrodynamic force coupling $1/r$ compared to, say, the gravitational or Coulombic coupling, which both scale as $1/r^2$. However, the no-flux condition for hard particles can be respected only by accounting for finite size, a straightforward computation for spheres. When two particles interact in an unbound fluid, neglecting finite size gives a good leading-order estimate of the strength of force-velocity coupling, but underpredicts the strength of entrainment when the particles are separated by less than several particle diameters. The consequences grow more severe when the system becomes more geometrically complex. Perhaps the most familiar example resulted in the development of the Rotne-Prager tensor: Early attempts to model the motion of polymer chains as interconnected point-particle beads led to loss of positive-definiteness of the diffusion (mobility) tensor in some configurations [125,126]. Rotne and Prager [127] addressed this situation by accounting for finite particle size in the force-translation coupling; the Rotne-Prager tensor has since been widely utilized to model hydrodynamic couplings between particles in an unbound suspension. However, its inclusion of pair-only coupling and neglect of higher-order traction moments restrict its validity to widely separated particles, e.g., dilute suspensions. In studies of concentrated suspensions, Durlofsky *et al.* [123] reported that neglect of finite-size terms, even in a mobility matrix that includes force, torque, and stresslet couplings to account for many-body interactions, results in loss of positive-definiteness for an unbound suspension. Thus, especially for concentrated suspensions, inclusion of higher-order traction moments does not guarantee that the grand mobility matrix will remain positive-definite, required to respect the energy dissipation theorem.

In the context of a spherically confined suspension, accounting for finite particle size becomes important at the level of just a single confined particle and emerges first with the force-velocity coupling. This can be seen in the study of Felderhof and Sellier [121], who, in an attempt to approximate the force-velocity coupling via a point particle, projected Oseen's Green's function along and transverse to the cavity radius. They compared this result to the corresponding components of the invert of O'Neill and Majumdar's finite-size resistance tensor and found good agreement for small particles in the latter study. However, closer interrogation of their results reveals two concerns: First, as particle size grows, the point-particle approximation severely underpredicts the hydrodynamic force. More troubling is the behavior obtained upon inversion of the point-particle coupling, shown by the dashed lines in Fig. 8(a), where the severe consequences of the approximation are clearly revealed: The force-velocity element of the resistance tensor diverges at arbitrary positions

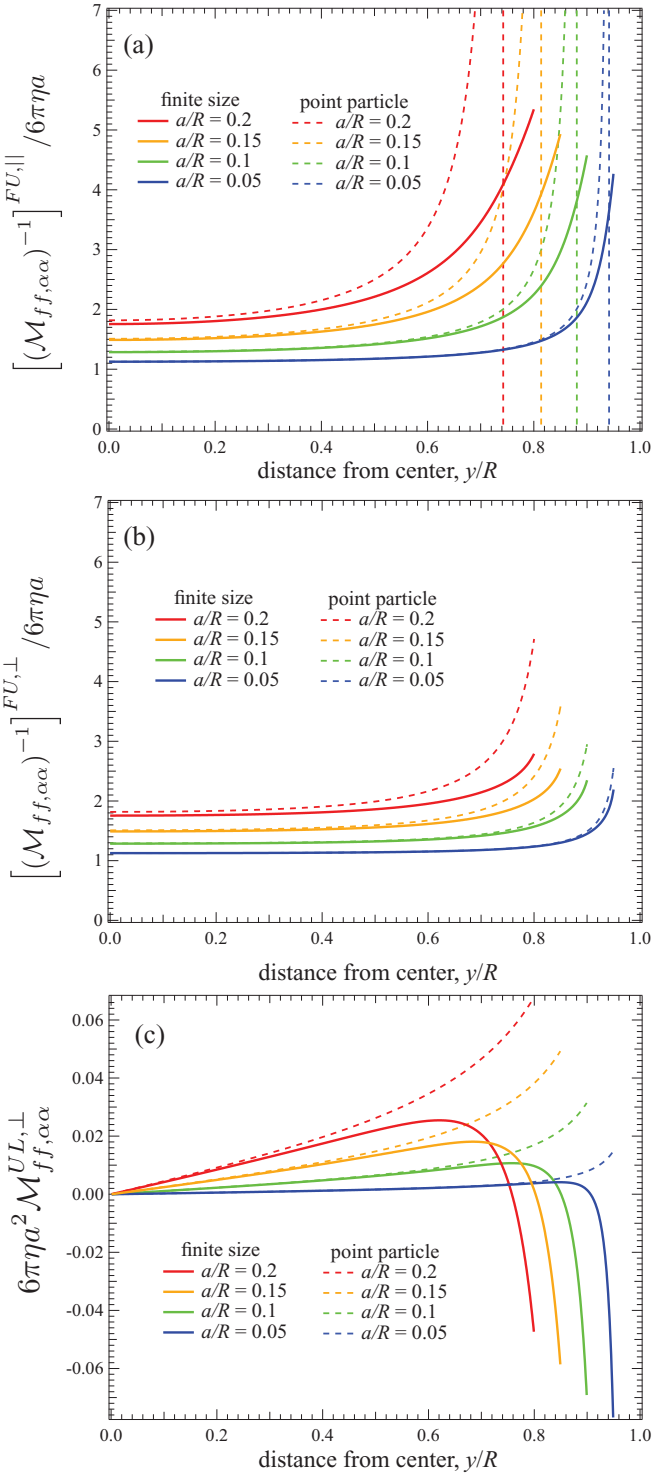

FIG. 8. Self-mobility, as developed in the present study, of a particle modeled with finite size (solid curves) and as a point particle (dashed curves). Force-velocity coupling is shown (a) along [Eq, (29)] and (b) transverse [Eq. (30)] to the cavity radius. (c) Torque-velocity coupling [Eq. (A2)].

in the cavity. Because inversion is the key step that couples reflections and many-body interactions, the regime of validity of this approach is fixed-velocity motion of a single enclosed particle.

In the present study we accounted for finite size [see Sec. III, Eq. (29)] and these results are presented as solid curves in Fig. 8(a), showing a monotonic increase of far-field resistance to a finite value, a physically reasonable result. We can utilize our result (29) to identify the source of the divergent behavior in the point-particle approximation: a pole at $y = (1/2)[4 - 9(a/R)]^{1/2}$ that can only be removed by inclusion of the finite-size terms of $O((a/R)^3)$ and $O((a/R)^5)$ in that expression. The transverse projection of the same coupling is shown in Fig. 8(b), where the effect of finite size is quantitative.

The second consequence of neglecting finite size is failure to predict reversal of particle motion in the torque-translation coupling, originally predicted by O'Neill and Majumdar [109]. Felderhof and Sellier derived a Green's function for the torque-rotation coupling of an enclosed point particle by taking the curl of Oseen's confined Stokeslet, finding a continuous increase in particle velocity with approach to the wall, as shown by the dashed lines in Fig. 8(c). They compared their result with the corresponding result from O'Neill and Majumdar, finding significant qualitative disagreement: O'Neill and Majumdar predicted a sign reversal, whereby a particle will reverse its translational motion near the wall and begin to roll along the wall. The mobility functions derived in the present work (A2) account for finite size and also find this reversal, as shown by the solid lines in Fig. 8(c). The key advantage to our method is of course its built-in ability to model two, three, or many enclosed particles.

In summary, accounting for finite particle size is essential to the accurate modeling of particle motion in a spherically confined fluid. While approximating particles as points significantly simplifies formulation of the mathematical model, it leads to qualitative errors so significant as to render the model unviable.

V. CONCLUSION

In this work we have presented a framework to model particle motion in hydrodynamically interacting colloidal suspensions subjected to 3D confinement by a spherical cavity. This framework comprises analytical expressions for the far-field grand mobility tensor coupling particles hydrodynamically to one another and to the confining cavity that, when combined with near-field couplings, is valid for an arbitrary number of particles for a wide range of particle volume fractions, from dilute to near-maximum packing fraction. We presented couplings of translation, rotation, and straining motion to force, torque, and the stresslet, giving particular attention to the force-translation, torque-rotation, and torque-translation behavior. We employed this framework to study two fundamental aspects of particle movement, self-motion and entrained motion, with a view toward its ultimate employment for many-particle systems in dynamic simulation.

The self-motion was studied first and utilized to illustrate the leading-order effects of confinement and to validate the model by recovering results reported in prior work [109,111], namely, the reduction of particle velocity by hydrodynamic coupling to the enclosing cavity. Beyond this result, we found that confinement gives rise to a drift velocity that tends to push a colloid away from the cavity wall toward the center. This push is strongest near the wall for smaller particles; once away from the wall however, larger particles experience a stronger tendency to seek the cavity center. One implication of this finding is that particles in biophysical systems may segregate spatially according to size.

We have derived the results for the motion of a pair of finite-size particles enclosed in a spherical cavity. We found that the entrainment velocity of a second particle in the flow created by another forced particle is qualitatively changed by the presence of the cavity in two ways. First, the strength of the entrainment at a distance r from the forced particle depends on the proximity of both to the cavity. Second, a reversal in motion occurs for particles located some distance transverse to the line of external forcing, consistent with recirculation flows reported in a range of cellular systems [66,67,124,128].

The study of higher-order couplings revealed several remarkable results. First, unlike a single unbound particle, a single confined particle will translate in response to a hydrodynamic torque on its surface. We find that such motion reverses in direction as a particle moves from the cavity center to the wall, resulting in a rolling motion of the particle along the cavity surface, similar to the behavior of a sphere near a planar wall. A confined pair of particles subjected to hydrodynamic torque will not only rotate individually but will also rotate as a doublet about the cavity axis. We explored the dependence of this coupling on proximity of the pair to the cavity wall, again finding a stall and reversal of motion as the pair approaches the surface.

Finally, the effect of finite size was explored, where we found that no regime of validity exists for approximating particles in spherical confinement as point particles. Such simplification results in errors ranging from spurious poles throughout the cavity domain to a failure to predict motion reversal near the cavity wall.

All functions derived give motion of particles in a suspension of N particles of equal size, where N is arbitrary. Motion in a polydisperse system can also be studied utilizing the methods presented here. In this case the differing sizes of the forced and entrained particles will lead to changes in self-, entrained, and relative motion analogous to that exhibited by unbound particle pairs; the influence of the cavity is expected to dominate when such particles are near the enclosing surface, but size-ratio effects will play a stronger role away from the cavity surface. This approach will yield an analogous set of far-field mobility functions.

The framework presented herein provides a method by which one can study a variety of crowded 3D confined systems, ranging from eukaryotic cells to suspensions confined by microcapsules, to study their transport and rheological properties in the presence of hydrodynamic interactions.

ACKNOWLEDGMENTS

This work was supported in part by an NSF BRIGE Grant No. 1342218 and by an NSF Graduate Research Fellowship Grant No. DGE-0707428. C.A.-R. thanks Yu Su in the Zia Group for assistance with Stokesian dynamics simulations.

APPENDIX: CAVITY CONTRIBUTION TO THE GRAND MOBILITY MATRIX

In this Appendix we list the contribution of the spherical cavity to all of the components of the grand mobility matrix required to carry out simulations of hydrodynamically interacting particles confined inside a spherical no-slip boundary. Note that the mobilities corresponding to the diagonal and upper blocks of the grand mobility matrix (UF, UL, US, ΩL, ΩS, and ES) are listed since the remaining terms may be obtained by an appropriate transposition.

1. Self-mobilities

The far-field self-mobilities of a particle inside a spherical cavity are listed for all the components of the grand mobility matrix (y is the magnitude of the position vector of the particle in a coordinate system whose origin lies at the center of the spherical cavity):

$$
\begin{aligned}
6\pi\eta a M^{UF,c}_{ij,\alpha\alpha} = &\left\{\left(\frac{a}{R}\right)[9/4(-1+y^2)] + \left(\frac{a}{R}\right)^3[-(3y^2+5)/2(-1+y^2)^3]\right.\\
&\left. + \left(\frac{a}{R}\right)^5[(5+10y^2+y^4)/4(-1+y^2)^5]\right\}\hat{y}_i\hat{y}_j\\
&+ \left\{\left(\frac{a}{R}\right)[9(4-3y^2+y^4)/16(-1+y^2)]\right.
\end{aligned}
$$

$$+\left(\frac{a}{R}\right)^3[(-20+21y^2-12y^4+3y^6)/8(-1+y^2)^3]$$

$$+\left(\frac{a}{R}\right)^5[(20+5y^2+11y^4-5y^6+y^8)/16(-1+y^2)^5]\Bigg\}(\delta_{ij}-\hat{y}_i\hat{y}_j), \quad \text{(A1)}$$

$$6\pi\eta a^2 M^{UL,c}_{ij,\alpha\alpha} = \left\{\left(\frac{a}{R}\right)^2[9y(-2+y^2)/16(-1+y^2)]\right.$$

$$\left.+\left(\frac{a}{R}\right)^4[3y(-10+5y^2-4y^4+y^6)/16(-1+y^2)^4]\right\}\hat{y}_s\epsilon_{ijs}, \quad \text{(A2)}$$

$$6\pi\eta a^3 M^{\Omega L,c}_{ij,\alpha\alpha} = \left\{\left(\frac{a}{R}\right)^3[3/4(-1+y^2)^3]\right\}\hat{y}_i\hat{y}_j$$

$$+\left\{\left(\frac{a}{R}\right)^3[3(4+12y^2-9y^4+3y^6)/16(-1+y^2)^3]\right\}(\delta_{ij}-\hat{y}_i\hat{y}_j), \quad \text{(A3)}$$

$$6\pi\eta a^2 M^{US,c}_{ijn,\alpha\alpha} = \left\{\left(\frac{a}{R}\right)^2[-(27y)/(8(-1+y^2)^2)]+\left(\frac{a}{R}\right)^4[9y(23+7y^2)/20(-1+y^2)^4]\right.$$

$$\left.+\left(\frac{a}{R}\right)^6\{-[9y(35+42y^2+3y^4)]/40(-1+y^2)^6\}\right\}\hat{y}_i(\delta_{jn}-\hat{y}_j\hat{y}_n)$$

$$+\left\{\left(\frac{a}{R}\right)^2[9y(-3+y^2)/16(-1+y^2)^2]\right.$$

$$+\left(\frac{a}{R}\right)^4\{-[3y(-138+59y^2-20y^4+3y^6)]/80(-1+y^2)^4\}$$

$$\left.+\left(\frac{a}{R}\right)^6\{-[3y(105+42y^2+18y^4-6y^6+y^8)]/80(-1+y^2)^6\}\right\}$$

$$\times(\delta_{ij}\hat{y}_n+\delta_{in}\hat{y}_j-2\hat{y}_i\hat{y}_j\hat{y}_n), \quad \text{(A4)}$$

$$6\pi\eta a^3 M^{\Omega S,c}_{ijn,\alpha\alpha} = \left\{\left(\frac{a}{R}\right)^3[9y^2(-3+y^2)/16(-1+y^2)^3]+\left(\frac{a}{R}\right)^5\{-[9y^2(-35+7y^2\right.\right.$$

$$\left.\left.-5y^4+y^6)]/80(-1+y^2)^5\}\right\}(\delta_{ns}\hat{y}_m\hat{y}_j+\delta_{sj}\hat{y}_m\hat{y}_n)\epsilon_{ims}, \quad \text{(A5)}$$

$$6\pi\eta a^3 M^{ES,c}_{mklr,\alpha\alpha} = \left\{\left(\frac{a}{R}\right)^3[3(160+144y^2-15y^4+3y^6)/64(-1+y^2)^3]\right.$$

$$+\left(\frac{a}{R}\right)^5[9(-224-856y^2-99y^4-6y^6+y^8)/160(-1+y^2)^5]$$

$$\left.+\left(\frac{a}{R}\right)^7[9(1120+9632y^2+6651y^4+363y^6-7y^8+y^{10})/1600(-1+y^2)^7]\right\}$$

$$\times(\hat{y}_m\hat{y}_k-\frac{1}{3}\delta_{mk})(\hat{y}_l\hat{y}_r-\frac{1}{3}\delta_{li})+\left\{\left(\frac{a}{R}\right)^3[9(5+y^2)/16(-1+y^2)^3]\right.$$

$$+\left(\frac{a}{R}\right)^5[-9(21+47y^2-5y^4+y^6)/40(-1+y^2)^5]$$

$$+\left(\frac{a}{R}\right)^7[9(105+609y^2+222y^4+30y^6-7y^8+y^{10})/400(-1+y^2)^7]\Big\}$$
$$\times(\delta_{ml}\hat{y}_k\hat{y}_r+\delta_{mr}\hat{y}_k\hat{y}_l+\delta_{kl}\hat{y}_m\hat{y}_r+\delta_{kr}\hat{y}_m\hat{y}_l+-4\hat{y}_m\hat{y}_l\hat{y}_k\hat{y}_r)$$
$$+\left\{\left(\frac{a}{R}\right)^3\{-[9(-10+10y^2-5y^4+y^6)]/32(-1+y^2)^3\}\right.$$
$$+\left(\frac{a}{R}\right)^5[-9(42-20y^2+15y^4-6y^6+y^8)/80(-1+y^2)^5]$$
$$+\left(\frac{a}{R}\right)^7[9(210+210y^2+75y^4-21y^6+7y^8-y^{10})/800(-1+y^2)^7]\Big\}$$
$$\times(\delta_{ml}\delta_{kr}+\delta_{mr}\delta_{kl}-\delta_{ml}\hat{y}_k\hat{y}_r-\delta_{mr}\hat{y}_k\hat{y}_l-\delta_{kl}\hat{y}_m\hat{y}_r$$
$$-\delta_{kr}\hat{y}_m\hat{y}_l+\hat{y}_m\hat{y}_k\hat{y}_r\hat{y}_l-\delta_{lr}\delta_{km}+\delta_{km}\hat{y}_l\hat{y}_r+\delta_{lr}\hat{y}_m\hat{y}_k). \tag{A6}$$

2. Entrainment mobilities

The far-field entrainment mobilities for particles inside a spherical cavity are listed for all of the components of the grand mobility matrix (here $\zeta=y^{-1}\sqrt{1-2bxy+y^2}$, where ζ is the distance of the entrained particle to the image point of the forced particle):

$$6\pi\eta a M^{UF,c}_{ij,\beta\alpha}=M^{UF,c}_1\hat{y}_i\hat{y}_j+M^{UF,c}_2\hat{y}_i\hat{y}^{\perp}_j+M^{UF,c}_3\hat{y}^{\perp}_i\hat{y}_j+M^{UF,c}_4\hat{y}^{\perp}_i\hat{y}^{\perp}_j+M^{UF,c}_5\delta_{ij}, \tag{A7a}$$

$$M^{UF,c}_1=\left(\frac{a}{R}\right)[(3\{-6+2y^2-4bxy(-5+y^2)-(1+b^2)x^4y^2(-1+3y^2)+4bx^3y(-2+b^2$$
$$+5y^2)-x^2[-4+9y^2+y^4+b^2(2+19y^2-3y^4)]\})/8y^5\zeta^5$$
$$-(3\{4b^3x^2y^2+b^2xy[3-5y^2+x^2(-5+3y^2)]+xy[6-4y^2+3x^4y^2(-1+y^2)$$
$$+x^2(-4+9y^2-3y^4)]+b[3(-1+y^2)-9x^4y^2(-1+y^2)+x^2(3-16y^2$$
$$+9y^4)]\})/8(-1+b^2)xy^4\zeta^3+[9b(-1+x^2)(-1+y^2)(-1+2bxy$$
$$-x^2y^2)]/8(-1+b^2)xy^3\zeta^2]+\left(\frac{a}{R}\right)^3[(3\{4b^5x^4y^2[-1+2(-2+x^2)y^2+y^4]$$
$$+b^4x^3y[2+(34-7x^2)y^2+(-7-2x^2+x^4)y^4+3x^2y^6]$$
$$+2b^3x^2y^2[-14+3y^2-3x^4y^2+x^2(7-2y^2+y^4)]$$
$$-xy^3[2+x^8y^4+2x^2(-12+7y^2)+x^6y^2(5-2y^2+y^4)+x^4(14-6y^2+3y^4)]$$
$$-b^2xy[-14+5y^2+17x^6y^4+x^2(9-12y^2+14y^4)+x^4y^2(14-38y^2+21y^4)]$$
$$+b[-2+y^2+7x^8y^6+x^6y^4(33-14y^2+7y^4)+x^2(1-14y^2+15y^4)$$
$$+x^4y^2(11-50y^2+29y^4)]\})/8(-1+b^2)xy^8\zeta^7$$
$$+[3b(-2+x^2+y^2)(-1+2bxy-x^2y^2)^3]/8(-1+b^2)xy^7\zeta^6]$$
$$+\left(\frac{a}{R}\right)^5\{[-10+81x^2y^2-48x^4y^4-32b^4x^4y^4+x^6y^6-3b^2x^2y^2(21-46x^2y^2$$
$$+x^4y^4)+4bxy(5-36x^2y^2+9x^4y^4)+b^3(72x^3y^3-48x^5y^5)]/8y^9\zeta^9$$
$$+[24b^3x^4y^4+b^2(3xy-42x^3y^3-17x^5y^5)-xy(10-7x^2y^2+4x^4y^4+x^6y^6)$$
$$+b(1+21x^2y^2+11x^4y^4+7x^6y^6)]/8(-1+b^2)xy^8\zeta^7$$
$$+b(-1+2bxy-x^2y^2)^3/8(-1+b^2)xy^7\zeta^6\}, \tag{A7b}$$

$$M_2^{UF,c} = \left(\frac{a}{R}\right)[-[9(-1+x^2)(-1+y^2)]/8(1-b^2)^{1/2}xy - (3\{3(-1+y^2)$$
$$-15bxy(-1+y^2) - 15b^2x^6y^4(-1+y^2) + 3bx^7y^5(-1+y^2)$$
$$+x^2[3-(5+28b^2)y^2+30b^2y^4] + bx^5y^3[-7+12y^2-3y^4+b^2(-23+21y^2)]$$
$$+x^4y^2[4b^4-2y^2+b^2(26-43y^2+15y^4)] - bx^3y[13-28y^2+9y^4$$
$$+b^2(2-17y^2+21y^4)]\})/8(1-b^2)^{1/2}xy^6\zeta^5]$$
$$+\left(\frac{a}{R}\right)^3[-[3(-2+x^2+y^2)]/8(1-b^2)^{1/2}xy + (3\{-2+y^2$$
$$+7b^2x^8y^6 - bx^9y^7 - 7bxy(-2+y^2) - bx^7y^5(4+17b^2-2y^2+y^4)$$
$$+b^2x^6y^4(11+24b^2-14y^2+7y^4) + x^2[1+(14-56b^2)y^2+(-9+30b^2)y^4]$$
$$+bx^5y^3[14+8y^2-2y^4+b^2(-49+34y^2-19y^4)] + x^4y^2[-9-4y^2$$
$$+b^2(26-18y^2+7y^4)+4b^4(1-12y^2+7y^4)] - bx^3y[5+16y^2$$
$$-14y^4+b^2(2-86y^2+49y^4)]\})/8(1-b^2)^{1/2}xy^8\zeta^7]$$
$$+\left(\frac{a}{R}\right)^5\{-1/8(1-b^2)^{1/2}xy + [1-48x^2y^2+81x^4y^4-96b^5x^5y^5-10x^6y^6$$
$$+8b^4x^4y^4(27+2x^2y^2) - 3b^3x^3y^3(63-26x^2y^2+11x^4y^4)$$
$$+3b^2x^2y^2(28-57x^2y^2+26x^4y^4+3x^6y^6) - bxy(9-105x^2y^2+108x^4y^4$$
$$+3x^6y^6+x^8y^8)]/8(1-b^2)^{1/2}xy^{10}\zeta^9\}, \qquad \text{(A7c)}$$

$$M_3^{UF,c} = \left(\frac{a}{R}\right)[(3(1-b^2)^{1/2}x\{4b^2x^2y + bx[-2+(-7+x^2)y^2-3(-1+x^2)y^4]$$
$$+y[5-3y^2+x^2(-3+5y^2)]\})/8y^5\zeta^5]$$
$$+\left(\frac{a}{R}\right)^3[-(3x\{4b^4x^2y[-1+2(-2+x^2)y^2+y^4] - bx(2+(26-7x^2)y^2$$
$$+[-7-2x^2+x^4)y^4+3x^2y^6] + b^3x[2+(26-7x^2)y^2+(-7-2x^2+x^4)y^4$$
$$+3x^2y^6] + b^2y[-14+5y^2-13x^4y^2+x^2(9+22y^2-9y^4)] + y[14-5y^2$$
$$+5x^4y^2+x^2(-5-6y^2+5y^4)]\})/8(1-b^2)^{1/2}y^7\zeta^7]$$
$$+\left(\frac{a}{R}\right)^5(\{x[32b^5x^3y^3+24b^4x^2y^2(-3+2x^2y^2) + b^2(-35+162x^2y^2-63x^4y^4)$$
$$-3bxy(21-38x^2y^2+x^4y^4) + b^3xy(63-146x^2y^2+3x^4y^4)$$
$$+5(7-18x^2y^2+3x^4y^4)]\}/8(1-b^2)^{1/2}y^8\zeta^9), \qquad \text{(A7d)}$$

$$M_4^{UF,c} = \left(\frac{a}{R}\right)[-[9b(-1+x^2)(-1+y^2)]/4(-1+b^2)xy - (3\{4b^5x^4y^2+b^4x^3y[-2$$
$$+(21-23x^2)y^2+21(-1+x^2)y^4]+x^3y[-2+(6-8x^2)y^2-3(2-3x^2+x^4)y^4$$
$$+3x^2(-1+x^2)y^6] + b^3x^2y^2[45(-1+y^2)-15x^4y^2(-1+y^2)+x^2(37$$
$$-60y^2+15y^4)]+b[6(-1+y^2)-15x^6y^4(-1+y^2)+3x^2(2-7y^2+5y^4)$$
$$+x^4y^2(19-30y^2+15y^4)] + b^2xy[-30(-1+y^2)+3x^6y^4(-1+y^2)$$
$$+x^2(-26+63y^2-33y^4)+x^4(-29y^2+36y^4-3y^6)]\})/8(-1+b^2)xy^6\zeta^5]$$

$$
\begin{aligned}
&+\left(\frac{a}{R}\right)^3[(3\{4b^5x^4y^2[1+6(-2+x^2)y^2+7y^4]-b^4x^3y[2+(-94+49x^2)y^2\\
&+(49-34x^2+17x^4)y^4+19x^2y^6]-x^3y[2+2(-12+7x^2)y^2\\
&+(14-6x^2+3x^4)y^4+x^2(5-2x^2+x^4)y^6+x^4y^8]+b^3x^2y^2[7x^6y^4\\
&+35(-2+y^2)+x^4y^2(22-14y^2+7y^4)+x^2(27-44y^2+14y^4)]\\
&-b^2xy[x^8y^6+14(-2+y^2)+x^6y^4(22-2y^2+y^4)+x^2(10-22y^2+7y^4)\\
&+x^4y^2(7-44y^2+18y^4)]+b[7x^8y^6+2(-2+\ y^2)+x^2(2-14y^2+7y^4)\\
&+x^6y^4(24-14y^2+7y^4)+x^4y^2(11-48y^2+\ 28y^4)]\})/8(-1+b^2)xy^8\zeta^7\\
&+[3b(-2+x^2+y^2)(-1+2bxy-x^2y^2)^3]/4(-1+b^2)xy^7\zeta^6]\\
&+\left(\frac{a}{R}\right)^5\{b/(4xy-4b^2xy)+[-96b^6x^5y^5+8b^5x^4y^4(27+2x^2y^2)\\
&-3b^4x^3y^3(63-18x^2y^2+11x^4y^4)-x^3y^3(84-51x^2y^2+6x^4y^4+x^6y^6)\\
&+b^3x^2y^2(63-117x^2y^2+157x^4y^4+9x^6y^6)-b^2xy(18-105x^2y^2+261x^4y^4\\
&+33x^6y^6+x^8y^8)+b(2+9x^2y^2+153x^4y^4-5x^6y^6+9x^8y^8)]/\\
&8(-1+b^2)xy^{10}\zeta^9\}, \qquad \text{(A7e)}\\
M_5^{UF,c}=&\left(\frac{a}{R}\right)[(3\{4b^3x^2y^2+b^2xy[3-5y^2+x^2(-5+3y^2)]+xy[6-4y^2\\
&+3x^4y^2(-1+y^2)+x^2(-4+9y^2-3y^4)]+b[3(-1+y^2)-9x^4y^2(-1+y^2)\\
&+x^2(3-16y^2+9y^4)]\})/8(-1+b^2)xy^4\zeta^3-[9b(-1+x^2)\\
&\times(-1+y^2)(-1+2bxy-x^2y^2)]/8(-1+b^2)xy^3\zeta^2]\\
&+\left(\frac{a}{R}\right)^3(3b(-2+x^2+y^2)/8(-1+b^2)xy\\
&+\{8b^3x^2y^2+xy[3x^6y^4+4(-5+3y^2)+3x^4y^2(3-2y^2+y^4)\\
&+x^2(12-14y^2+9y^4)]+b^2xy[-10+3y^2+21x^4y^2+x^2(3-46y^2+21y^4)]\\
&-b[15x^6y^4+3(-2+y^2)+15x^4y^2(2-2y^2+y^4)\\
&+x^2(3-52y^2+30y^4)]\}/8(-1+b^2)xy^6\zeta^5)\\
&+\left(\frac{a}{R}\right)^5\{[-24b^3x^4y^4+b^2xy(-3+42x^2y^2+17x^4y^4)+xy(10-7x^2y^2+4x^4y^4\\
&+x^6y^6)-b(1+21x^2y^2+11x^4y^4+7x^6y^6)]/8(-1+b^2)xy^8\zeta^7\\
&-[b(-1+2bxy-x^2y^2)^3]/8(-1+b^2)xy^7\zeta^6\}, \qquad \text{(A7f)}\\
6\pi\eta a^2M_{is,\beta\alpha}^{UL,c}=&M_1^{UL,c}\hat{y}_i(\hat{y}_n\cdot\epsilon_{nsj}\cdot\hat{y}_j^{\perp})+M_2^{UL,c}\hat{y}_i^{\perp}(\hat{y}_n\cdot\epsilon_{nsj}\cdot\hat{y}_j^{\perp})\\
&+M_3^{UL,c}\epsilon_{isj}\cdot\hat{y}_j+M_4^{UL,c}\epsilon_{isj}\cdot\hat{y}_j^{\perp}, \qquad \text{(A8a)}\\
M_1^{UL,c}=&\left(\frac{a}{R}\right)^2(9(-1+x^2)/8(1-b^2)^{1/2}x+\{9(-1+x^2)[-1+x^2y^2\\
&+8b^3x^3y^3-b^2x^2y^2(11+5x^2y^2)+bxy(5+2x^2y^2+x^4y^4)]\}/8(1-b^2)^{1/2}xy^5\zeta^5)
\end{aligned}
$$

$$+\left(\frac{a}{R}\right)^4(\{3[-1+14x^2y^2-5x^4y^4-32b^4x^4y^4+8b^3x^3y^3(7+2x^2y^2)$$
$$+b^2(-35x^2y^2+2x^4y^4-7x^6y^6)+bxy(7-21x^2y^2+5x^4y^4+x^6y^6)]\}/$$
$$8(1-b^2)^{1/2}xy^7\zeta^7+[3(1-2bxy+x^2y^2)^3]/8(1-b^2)^{1/2}xy^6\zeta^6]), \tag{A8b}$$

$$M_2^{UL,c}=\left(\frac{a}{R}\right)^2(9b(-1+x^2)/4(-1+b^2)x+\{9(-1+x^2)[8b^4x^3y^3$$
$$-5b^3x^2y^2(3+x^2y^2)+x^3y^3(3+x^2y^2)+b^2xy(10+9x^2y^2+x^4y^4)$$
$$-b(2+5x^2y^2+5x^4y^4)]\}/8(-1+b^2)xy^5\zeta^5)$$
$$+\left(\frac{a}{R}\right)^4(\{3[-32b^5x^4y^4+8b^4x^3y^3(7+2x^2y^2)+x^3y^3(21+2x^2y^2+x^4y^4)$$
$$-b^3x^2y^2(35+6x^2y^2+7x^4y^4)+b^2xy(14-7x^2y^2+24x^4y^4+x^6y^6)$$
$$-b(2+7x^2y^2+32x^4y^4+7x^6y^6)]\}/8(-1+b^2)xy^7\zeta^7$$
$$-[3b(-1+2bxy-x^2y^2)^3]/4(-1+b^2)xy^6\zeta^6), \tag{A8c}$$

$$M_3^{UL,c}=\left(\frac{a}{R}\right)^2[-(3\{2b^3x^2+b^2(4xy-6x^3y)+b[-3+9x^4y^2+x^2(1-9y^2)]$$
$$+xy[5-3x^4y^2+3x^2(-1+y^2)]\})/8(-1+b^2)xy^3\zeta^3$$
$$-[9b(-1+x^2)(-1+2bxy-x^2y^2)]/8(-1+b^2)xy^2\zeta^2]$$
$$+\left(\frac{a}{R}\right)^4(3b/8(-1+b^2)x+\{3[8b^2x^3y^3+xy(5+2x^2y^2+x^4y^4)$$
$$-b(1+10x^2y^2+5x^4y^4)]\}/8(-1+b^2)xy^5\zeta^5), \tag{A8d}$$

$$M_4^{UL,c}=\left(\frac{a}{R}\right)^2\{-[3(1-b^2)^{1/2}x]/4y^3\zeta^3\}+\left(\frac{a}{R}\right)^4[0], \tag{A8e}$$

$$6\pi\eta a^3M_{ij,\beta\alpha}^{\Omega L,c}=M_1^{\Omega L,c}\hat{y}_i\hat{y}_j+M_2^{\Omega L,c}\hat{y}_i\hat{y}_j^{\perp}+M_3^{\Omega L,c}\hat{y}_i^{\perp}\hat{y}_j+M_4^{\Omega L,c}\hat{y}_i^{\perp}\hat{y}_j^{\perp}+M_5^{\Omega L,c}\delta_{ij}, \tag{A9a}$$

$$M_1^{\Omega L,c}=\left(\frac{a}{R}\right)^3(9/8(-1+b^2)-\{9[1-2x^2y^2+b^4x^2y^2+b^2x^2y^2(11+5x^2y^2)$$
$$-2b^3(xy+4x^3y^3)-bxy(3+2x^2y^2+x^4y^4)]\}/8(-1+b^2)y^5\zeta^5), \tag{A9b}$$

$$M_2^{\Omega L,c}=\left(\frac{a}{R}\right)^3(9b/8(1-b^2)^{1/2}-\{9[b+7bx^2y^2+3b^3x^2y^2+5bx^4y^4$$
$$-b^2xy(4+7x^2y^2)-xy(1+3x^2y^2+x^4y^4)]\}/8(1-b^2)^{1/2}y^5\zeta^5), \tag{A9c}$$

$$M_3^{\Omega L,c}=\left(\frac{a}{R}\right)^2\{-[9(1-b^2)^{1/2}x(-1+bxy)]/8y^4\zeta^5\}, \tag{A9d}$$

$$M_4^{\Omega L,c}=\left(\frac{a}{R}\right)^2(9(1+b^2)/8(-1+b^2)-\{9[1-2x^2y^2+3b^4x^2y^2-5b^3(xy+3x^3y^3)$$
$$-bxy(5+5x^2y^2+2x^4y^4)+b^2(1+19x^2y^2+10x^4y^4)]\}/8(-1+b^2)y^5\zeta^5), \tag{A9e}$$

$$M_5^{\Omega L,c} = \left(\frac{a}{R}\right)^3 (9/(8-8b^2) - \{3[-5+7x^2y^2+2b^3(xy+12x^3y^3) + b^2(2-37x^2y^2-15x^4y^4)+bxy(13+6x^2y^2+3x^4y^4)]\}/8(-1+b^2)y^5\zeta^5), \tag{A9f}$$

$$6\pi\eta a^3 \boldsymbol{M}_{inj,\beta\alpha}^{US,c} = M_1^{US,c}\hat{y}_i\left(\hat{y}_n\hat{y}_j - \tfrac{1}{3}\delta_{nj}\right) + M_2^{US,c}\hat{y}_i^{\perp}\left(\hat{y}_n\hat{y}_j - \tfrac{1}{3}\delta_{ij}\right) + M_3^{US,c}\hat{y}_i\left(\hat{y}_n^{\perp}\hat{y}_j^{\perp} - \tfrac{1}{3}\delta_{ij}\right) + M_4^{US,c}\hat{y}_i^{\perp}\left(\hat{y}_n^{\perp}\hat{y}_j^{\perp} - \tfrac{1}{3}\delta_{ij}\right) + M_5^{US,c}\left(\hat{y}_i\hat{y}_n\hat{y}_j^{\perp} + \hat{y}_i\hat{y}_n^{\perp}\hat{y}_j\right) + M_6^{US,c}\left(\hat{y}_i^{\perp}\hat{y}_n\hat{y}_j^{\perp} + \hat{y}_i\hat{y}_n^{\perp}\hat{y}_j\right) + M_7^{US,c}\left(\delta_{in}\hat{y}_j^{\perp} + \delta_{ij}\hat{y}_n^{\perp} - \tfrac{2}{3}\delta_{jn}\hat{y}_i^{\perp}\right) + M_8^{US,c}\left(\delta_{in}\hat{y}_j + \delta_{ij}\hat{y}_n - \tfrac{2}{3}\delta_{jn}\hat{y}_i^{\perp}\right), \tag{A10a}$$

$$\begin{aligned}
M_1^{US,c} = {} & \left(\frac{a}{R}\right)^2 [(9\{4b^6x^5y^3 + b^5x^4y^2[-2+(-25+11x^2)y^2 - 13(-1+x^2)y^4] \\
& + b^4x^3y^3[70-36y^2+19x^4y^2(-1+y^2)+x^2(-68+73y^2-19y^4)] + x^3y^5[2 \\
& + x^6y^2(-3+y^2) - 4x^2(-1+y^2) - x^4(8-5y^2+y^4)] + b[-7x^8y^6(-3+y^2) \\
& + 2(-2+y^2) + 2x^2(2-8y^2+3y^4) + 2x^4y^2(7-15y^2+5y^4) + x^6y^4(30-21y^2 \\
& + 7y^4)] + b^3x^2y^2[-70+36y^2-7x^6y^4(-1+y^2)+x^4y^2(99-64y^2+7y^4) + x^2(72 \\
& - 127y^2+47y^4)] + b^2xy[-14(-2+y^2) + x^8y^6(-1+y^2) - x^6y^4(57-22y^2 \\
& + y^4) - 4x^2(7-21y^2+9y^4) + x^4(-76y^2+77y^4-19y^6)]\})/8(-1 \\
& + b^2)xy^9\zeta^7 - [9b(-1+x^2)(-2+y^2)(-1+2bxy-x^2y^2)^3]/4(-1+b^2)xy^8\zeta^6] \\
& + \left(\frac{a}{R}\right)^4 [3b(-16+6x^2+5y^2)/20(-1+b^2)xy^2 + (3\{4b^6x^5y^3[-15+18(-8 \\
& + 3x^2)y^2+65y^4] + b^5x^4y^2[30+(1496-351x^2)y^2+(-585+776x^2-291x^4)y^4 \\
& - 435x^2y^6] + x^3y^5[-70+9x^8y^4+x^2(-624+290y^2)+x^6y^2(63-24y^2 \\
& + 5y^4) + x^4(264-88y^2+15y^4)] + b^2xy[-288+90y^2+3x^{10}y^8 \\
& + x^8y^6(288-8y^2+5y^4) - 3x^4y^2(-168+360y^2+5y^4) + 2x^2(54-552y^2 \\
& + 185y^4) + x^6y^4(645-848y^2+210y^4)] - b[-32+10y^2+81x^{10}y^8 + 4x^2(3-36y^2 \\
& + 5y^4) + 3x^8y^6(187-72y^2+15y^4) + 6x^4y^2(9-152y^2+30y^4) + x^6y^4(432 \\
& - 1096y^2+365y^4)] - b^3x^2y^2[27x^8y^6 + 4(-252+85y^2) + 3x^6y^4(52-24y^2 \\
& + 15y^4) + x^4y^2(729-816y^2+40y^4) + x^2(408-1624y^2+495y^4)] \\
& + b^4x^3y^3[81x^6y^4 + 36(-44+15y^2) + 9x^4y^2(43-24y^2+15y^4) \\
& + x^2(564-1752y^2+725y^4)]\})/40(-1+b^2)xy^{11}\zeta^9] \\
& + \left(\frac{a}{R}\right)^6 (\{3[-288b^7x^6y^6 + 8b^6x^5y^5(99+34x^2y^2) + b^5x^4y^4(-891-454x^2y^2 \\
& + 161x^4y^4) + 3x^5y^5(286-127x^2y^2+8x^4y^4+x^6y^6) + 3b^4x^3y^3(126 \\
& + 77x^2y^2 - 104x^4y^4 + 21x^6y^6) - b^3x^2y^2(198-363x^2y^2+39x^4y^4 \\
& + 915x^6y^6 + 11x^8y^8) + b^2xy(44+282x^2y^2-33x^4y^4+1741x^6y^6 \\
& + 133x^8y^8 + x^{10}y^{10}) - b(4+22x^2y^2+792x^4y^4+1067x^6y^6-94x^8y^8 \\
& + 33x^{10}y^{10})]\}/40(-1+b^2)xy^{13}\zeta^{11} - [3b(-1+2bxy \\
& - x^2y^2)^5]/10(-1+b^2)xy^{12}\zeta^{10}),
\end{aligned} \tag{A10b}$$

$$
\begin{aligned}
M_2^{US,c} = \left(\frac{a}{R}\right)^2 & [9b^2(-1+x^2)(-1+y^2)/4(1-b^2)^{3/2}xy^2 + (3(1-b^2)^{1/2}x\{5-9y^2 \\
& + 3bx^5y^3(-1+y^2) + bx(y+15y^3) + bx^3y(3+12b^2+4y^2 \\
& - 3y^4) + x^4y^2[12-10y^2+3b^2(-5+3y^2)] - x^2[3+5y^2-6y^4+b^2(6+7y^2 \\
& + 9y^4)]\})/8y^7\zeta^7 + (3\{x^2y^2[-5+3y^2+x^2(3-5y^2)] + 4b^5x^3y^3[7-6y^2+6x^2(-1 \\
& + y^2)] + b^3xy[-30(-1+y^2) + 3x^6y^4(-1+y^2) + x^2(-30+49y^2-27y^4) \\
& - 3x^4y^2(9-10y^2+y^4)] + bx^3y^3[13-9y^2+3x^4y^2(-1+y^2) - 3x^2(3-4y^2 \\
& + y^4)] + b^4x^2y^2[-50+48y^2-15x^4y^2(-1+y^2) + x^2(48-65y^2+15y^4)] \\
& + b^2[6(-1+y^2) - 15x^6y^4(-1+y^2) + x^2(6-11y^2+9y^4) + x^4y^2(9-20y^2 \\
& + 15y^4)]\})/8(1-b^2)^{3/2}xy^7\zeta^5] \\
& + \left(\frac{a}{R}\right)^4 [3b^2(-8+3x^2+5y^2)/20(1-b^2)^{3/2}xy^2 \\
& + (3\{4b^7x^5y^3[-15+18(-8+3x^2)y^2+65y^4] \\
& + b^6x^4y^2[30+(1336-351x^2)y^2+(-585+776x^2-291x^4)y^4-435x^2y^6] \\
& + 5x^2y^4[10+15x^6y^2+x^2(88-45y^2)+3x^4(-9-8y^2+5y^4)] \\
& - b^4x^2y^2[-504+265y^2+27x^8y^6+2x^4y^2(189+80y^2)+9x^6y^4(-10 \\
& - 8y^2+5y^4)+3x^2(83-96y^2+210y^4)] + bx^3y^3[141x^4y^2+3x^8y^6 \\
& + 8(-48+5y^2)+x^6y^6(-8+5y^2)+x^2(84-696y^2+335y^4)] \\
& + b^5x^3y^3[(-1224+565y^2+81x^6y^4+3x^4y^2(92-72y^2+45y^4) \\
& + x^2(519-1056y^2+760y^4)] + b^3xy[3x^{10}y^8+18(-8+5y^2) \\
& + x^8y^6(135-8y^2+5y^4)+3x^6y^4(41-120y^2+75y^4) \\
& + x^2(54+264y^2+235y^4)+x^4(-39y^2+312y^4-95y^6)] + b^2[16-10y^2 \\
& - 27x^{10}y^8+x^2(-6+72y^2-145y^4)-9x^8y^6(42-8y^2+5y^4) \\
& + 3x^4(y^2-16y^4+60y^6)+x^6(108y^4+848y^6-480y^8)]\})/40(1-b^2)^{3/2}xy^{11}\zeta^9] \\
& + \left(\frac{a}{R}\right)^6 (3b^2/20(1-b^2)^{3/2}xy^2 - \{3(1-b^2)^{1/2}x[-35+550x^2y^2 \\
& - 615x^4y^4+32b^4x^4y^4+60x^6y^6-8b^3x^3y^3(11+26x^2y^2)+b^2(99x^2y^2 \\
& + 558x^4y^4-201x^6y^6)-bxy(119+627x^2y^2-603x^4y^4+9x^6y^6)]\}/ \\
& 40y^{11}\zeta^{11} + \{3[128b^7x^5y^5+32b^6x^4y^4(-9+x^2y^2)-5x^2y^2(7-18x^2y^2 \\
& + 3x^4y^4)+4b^5x^3y^3(63-58x^2y^2+9x^4y^4)+bx^3y^3(147-165x^2y^2 \\
& + 9x^4y^4+x^6y^6)-b^4x^2y^2(98-351x^2y^2+268x^4y^4+9x^6y^6) \\
& + b^2(-2+61x^2y^2-405x^4y^4+83x^6y^6-9x^8y^8)+b^3xy(18-231x^2y^2 \\
& + 521x^4y^4+27x^6y^6+x^8y^8)]\}/40(1-b^2)^{3/2}xy^{11}\zeta^9), \qquad \text{(A10c)}
\end{aligned}
$$

$$
\begin{aligned}
M_3^{US,c} = \left(\frac{a}{R}\right)^2 & [-(9\{4b^6x^5y^3+b^5x^4y^2[-2+(31-37x^2)y^2+35(-1+x^2)y^4]+x^3y^3[-8 \\
& + 10y^2-2x^6y^4(-1+y^2)+x^4y^2(7-9y^2+2y^4)+x^2(10-15y^2+7y^4)]
\end{aligned}
$$

$$
\begin{aligned}
&+b^4x^3y^3[-78+80y^2-35x^4y^2(-1+y^2)+x^2(72-113y^2+35y^4)]\\
&+2b^3x^2y^2[-35(-1+y^2)+7x^6y^4(-1+y^2)+x^2(-33+74y^2-35y^4)\\
&+x^4(-33y^2+42y^4-7y^6)]+b[4-4y^2+14x^8y^6(-1+y^2)-2x^2(2-9y^2+7y^4)\\
&+x^4(-16y^2+45y^4-35y^6)+x^6(-37y^4+49y^6-14y^8)]+2b^2xy[14(-1+y^2)\\
&+x^6y^4(21-22y^2+y^4)+3x^4y^2(9-16y^2+7y^4)+x^2(14-41y^2+25y^4)\\
&+x^8(y^6-y^8)]\})/8(-1+b^2)xy^9\zeta^7-[9b(-1+x^2)(-1+y^2)(-1+2bxy\\
&-x^2y^2)^3]/2(-1+b^2)xy^8\zeta^6]\\
&+\left(\frac{a}{R}\right)^4[3b(-8+3x^2+5y^2)/10(-1+b^2)xy^2+(3\{20b^6x^5y^3[3+6(-8+3x^2)y^2\\
&+35y^4]-5b^5x^4y^2[6+3(-152+63x^2)y^2+(315-152x^2+57x^4)y^4\\
&+105x^2y^6]+x^3y^3[-480+350y^2+6x^8y^6+x^6y^4(27-16y^2+10y^4)\\
&+3x^4y^2(7-24y^2+15y^4)+x^2(210+24y^2+35y^4)]-b[54x^{10}y^8\\
&+4(-8+5y^2)+6x^2(2-24y^2+15y^4)+3x^8y^6(53-48y^2+30y^4)\\
&+3x^4y^2(28-424y^2+315y^4)+x^6y^4(567-424y^2+315y^4)]+2b^2xy[3x^{10}y^8\\
&+18(-8+5y^2)+x^2(54-24y^2-35y^4)+x^8y^6(108-8y^2+5y^4)\\
&+12x^6y^4(29-24y^2+15y^4)+9x^4(y^2-112y^4+70y^6)]+b^4x^3y^3[189x^6y^4\\
&+40(-54+35y^2)+15x^2(48-72y^2+35y^4)+x^4(435y^2-504y^4+315y^6)]\\
&-2b^3x^2y^2[27x^8y^6+63(-8+5y^2)-3x^2(-53+80y^2)\\
&+3x^6y^4(94-24y^2+15y^4)+x^4(-752y^4+420y^6)]\})/40(-1+b^2)xy^{11}\zeta^9]\\
&+\left(\frac{a}{R}\right)^6(-\{3[480b^7x^6y^6+40b^6x^5y^5(-33+2x^2y^2)\\
&+b^5x^4y^4(1485-790x^2y^2+281x^4y^4)-b^4x^3y^3(882-1485x^2y^2\\
&+1504x^4y^4+99x^6y^6)-x^3y^3(420-693x^2y^2+156x^4y^4+11x^6y^6+2x^8y^8)\\
&+2b^3x^2y^2(99-561x^2y^2+1456x^4y^4+115x^6y^6+11x^8y^8)\\
&-2b^2xy(22-321x^2y^2+1353x^4y^4-130x^6y^6+55x^8y^8+x^{10}y^{10})\\
&+b(4+22x^2y^2+957x^4y^4-754x^6y^6+149x^8y^8+22x^{10}y^{10})]\}/\\
&40(-1+b^2)xy^{13}\zeta^{11}-[3b(-1+2bxy-x^2y^2)^5]/10(-1+b^2)xy^{12}\zeta^{10}), \quad \text{(A10d)}
\end{aligned}
$$

$$
\begin{aligned}
M_4^{US,c}=&\left(\frac{a}{R}\right)^2[-(9\{2-2y^2+4b^7x^5y^3+2x^6y^4+x^4y^2(-5+7y^2)+x^2(-2+9y^2-7y^4)\\
&+b^6x^4y^2[-2+(35-37x^2)y^2+35(-1+x^2)y^4]+b^4x^2y^2[-105(-1+y^2)\\
&+14x^6y^4(-1+y^2)+x^2(-99+245y^2-140y^4)-2x^4y^2(67-77y^2+7y^4)]\\
&+bxy[14(-1+y^2)-6x^8y^6(-1+y^2)+3x^6y^4(7-9y^2+2y^4)+7x^2(2-7y^2\\
&+5y^4)+x^4y^2(31-56y^2+21y^4)]-2b^3xy[-21(-1+y^2)+x^8y^6(-1+y^2)\\
&-x^6y^4(56-57y^2+y^4)-7x^2(3-13y^2+10y^4)-2x^4y^2(38-63y^2\\
&+28y^4)]+b^5x^3y^3[105(-1+y^2)-35x^4y^2(-1+y^2)+x^2(93-140y^2+35y^4)]\\
&+b^2[6-6y^2+42x^8y^6(-1+y^2)+x^2(-6+62y^2-56y^4)
\end{aligned}
$$

$$
\begin{aligned}
&- 3x^6y^4(37-49y^2+14y^4)+x^4(-62y^2+161y^4-105y^6)]\})/8(1-b^2)^{3/2}xy^9\zeta^7\\
&-[9(1+3b^2)(-1+x^2)(-1+y^2)(-1+2bxy-x^2y^2)^3]/4(1-b^2)^{3/2}xy^8\zeta^6]\\
&+\left(\frac{a}{R}\right)^4[3(1+3b^2)(-8+3x^2+5y^2)/20(1-b^2)^{3/2}xy^2\\
&+(3\{16-10y^2-30x^8y^6+x^6y^4(189+80y^2)+x^2(-6+72y^2-45y^4)\\
&+20b^7x^5y^3[3+6(-8+3x^2)y^2+35y^4]+x^4y^2(3-424y^2+315y^4)\\
&-5b^6x^4y^2[6+(-488+189x^2)y^2+(315-152x^2+57x^4)y^4+105x^2y^6]\\
&+3b^5x^3y^3[63x^6y^4+105(-8+5y^2)+3x^4y^2(90-56y^2+35y^4)\\
&+5x^2(51-144y^2+70y^4)]+2b^3xy[3x^{10}y^8+27(-8+5y^2)\\
&+x^8y^6(297-8y^2+5y^4)+9x^6y^4(102-88y^2+55y^4)+3x^2(27\\
&-392y^2+245y^4)+3x^4y^2(177-816y^2+560y^4)]-3b^4x^2y^2[18x^8y^6+63(-8\\
&+5y^2)+6x^6y^4(68-8y^2+5y^4)+x^2(159-920y^2+525y^4)+x^4y^2(315\\
&-1088y^2+630y^4)]-3b^2[54x^{10}y^8+2(-8+5y^2)+6x^2(1-40y^2+25y^4)\\
&+3x^8y^6(53-48y^2+30y^4)+x^6y^4(441-424y^2+315y^4)\\
&+x^4y^2(120-1096y^2+735y^4)]+bxy[18x^{10}y^8+18(-8+5y^2)\\
&+3x^8y^6(27-16y^2+10y^4)+9x^6y^4(2-24y^2+15y^4)+9x^2(6-56y^2+35y^4)\\
&+x^4(129y^2-48y^4-70y^6)]\})/40(1-b^2)^{3/2}xy^{11}\zeta^9]\\
&+\left(\frac{a}{R}\right)^6(-\{3[2+11x^2y^2-594x^4y^4+607x^6y^6+480b^8x^6y^6-50x^8y^8\\
&+40b^7x^5y^5(-33+2x^2y^2)+b^6x^4y^4(1485-430x^2y^2+281x^4y^4)\\
&-3b^5x^3y^3(231-165x^2y^2+773x^4y^4+33x^6y^6)+b^4x^2y^2(297-528x^2y^2\\
&+4647x^4y^4+642x^6y^6+22x^8y^8)-2b^3xy(33+264x^2y^2+1749x^4y^4\\
&-21x^6y^6+154x^8y^8+x^{10}y^{10})-bxy(22+99x^2y^2-627x^4y^4+443x^6y^6\\
&+33x^8y^8+6x^{10}y^{10})+3b^2(2+44x^2y^2+759x^4y^4-536x^6y^6\\
&+149x^8y^8+22x^{10}y^{10})]\}/40(1-b^2)^{3/2}xy^{13}\zeta^{11}\\
&-3(1+3b^2)(-1+2bxy-x^2y^2)^5/20(1-b^2)^{3/2}xy^{12}\zeta^{10}), \qquad \text{(A10e)}
\end{aligned}
$$

$$
\begin{aligned}
M_5^{US,c}=&\left(\frac{a}{R}\right)^2[9(-1+x^2)[-2+(1+b^2)y^2]/8(1-b^2)^{3/2}xy^2+(9\{-2+(1+b^2)y^2\\
&-7b^2x^8y^6(-3+b^2+2y^2)+bx^9y^7(-3+b^2+2y^2)-7bxy[-2+(1+b^2)y^2]\\
&-2bx^3y[7+(-19-25b^2+2b^4)y^2+(9+17b^2+9b^4)y^4]+x^2[2-4(2\\
&+9b^2)y^2+(5+18b^2+19b^4)y^4]+2bx^7y^5[-5+9b^4+5y^2-y^4+b^2(-25\\
&+17y^2)]+bx^5y^3[-27+4b^6+36y^2+8b^4y^2-7y^4+b^2(-47+68y^2-35y^4)]\\
&-x^6y^4[y^2+b^6(13+5y^2)+b^4(-26+19y^2)+b^2(-57+59y^2-14y^4)]\\
&+x^4y^2[7-7y^2-y^4+b^6(-2+3y^2+5y^4)+b^4(4-27y^2+24y^4)\\
&+b^2(33-81y^2+42y^4)]\})/8(1-b^2)^{3/2}xy^9\zeta^7]
\end{aligned}
$$

$$+\left(\frac{a}{R}\right)^4[3[-16+6x^2+5(1+b^2)y^2]/40(1-b^2)^{3/2}xy^2-(3\{-16+5(1+b^2)y^2$$
$$-27b^2(-3+b^2)x^{10}y^8+3b(-3+b^2)x^{11}y^9-9bxy[-16+5(1+b^2)y^2]$$
$$+3x^2[2-24(1+7b^2)y^2+5(4+7b^2+13b^4)y^4]-bx^3y[54+24(-9-59b^2$$
$$+12b^4)y^2+5(29+89b^2+50b^4)y^4]+bx^9y^7[-45+90b^4+24y^2-10y^4$$
$$-b^2(261+8y^2)]+3b^2x^8y^6[68-79b^4-72y^2+30y^4+b^2(179+24y^2)]$$
$$+3bx^7y^5[79+24b^6+40y^2-15y^4+b^4(94-80y^2)$$
$$+b^2(-449+232y^2-105y^4)]+x^4y^2[27+424y^2-270y^4$$
$$+3b^4(20-288y^2+75y^4)+b^6(-30+392y^2+225y^4)+3b^2(53$$
$$-656y^2+360y^4)]+x^6y^4[-189-80y^2+25y^4+b^6(-297+632y^2$$
$$-125y^4)+4b^2(162-96y^2+35y^4)+2b^4(297-756y^2+400y^4)]-bx^5y^3(21$$
$$+312y^2-265y^4-6b^4(8-72y^2+25y^4)+4b^6(-15+48y^2+25y^4)$$
$$+3b^2(197-984y^2+525y^4)]\})/40(1-b^2)^{3/2}xy^{11}\zeta^9]$$
$$+\left(\frac{a}{R}\right)^6(\{3[-2-11x^2y^2+594x^4y^4-607x^6y^6+96b^8x^6y^6$$
$$+50x^8y^8-8b^7x^5y^5(33+58x^2y^2)-18b^5x^3y^3(14+11x^2y^2-80x^4y^4$$
$$+3x^6y^6)+b^4x^4y^4(-264-2961x^2y^2+54x^4y^4+11x^6y^6)+b^6(297x^4y^4$$
$$+802x^6y^6-35x^8y^8)+b^3x^3y^3(735+2112x^2y^2-894x^4y^4+152x^6y^6-x^8y^8)$$
$$-3b^2x^2y^2(33+429x^2y^2-582x^4y^4+133x^6y^6+11x^8y^8)$$
$$+bxy(22-153x^2y^2-726x^4y^4+578x^6y^6+12x^8y^8+3x^{10}y^{10})]\}/$$
$$40(1-b^2)^{3/2}xy^{13}\zeta^{11}+3(1-2bxy+x^2y^2)^5/20(1-b^2)^{3/2}xy^{12}\zeta^{10}), \qquad \text{(A10f)}$$

$$M_6^{US,c}=\left(\frac{a}{R}\right)^2[-(9(4b^6x^5y^3+b^5x^4y^2(-2+(7-13x^2)y^2-5(-1+x^2)y^4)$$
$$+b^4x^3y^3(-31-5y^2+18x^4y^2+x^2(25-11y^2))+x^3y^3(4-5y^2+x^6y^4$$
$$-x^4y^2(-4+y^2)+x^2(-2+3y^2))+b^3x^2y^2(35-7x^6y^4+x^4y^2(-44+17y^2)$$
$$+x^2(-31+56y^2-10y^4))+b(2-7x^8y^6+x^6y^4(-13+2y^2)+x^2(-2+7y^2)$$
$$+x^4y^2(-9+7y^2+5y^4))+b^2xy(-14+x^8y^6-x^6y^4(-20+y^2)+x^4(43y^2$$
$$-34y^4)+x^2(14-43y^2+10y^4))))/(8(-1+b^2)xy^9\zeta^7)$$
$$+(9b(-1+x^2)(-1+2bxy-x^2y^2)^3)/(4(-1+b^2)xy^8\zeta^6)]$$
$$+\left(\frac{a}{R}\right)^4[(3b(-8+3x^2))/(20(-1+b^2)xy^2)+(3(4b^6x^5y^3(15+6(-8+3x^2)y^2$$
$$-25y^4)+b^5x^4y^2(-30+(552-297x^2)y^2+(225+632x^2-237x^4)y^4$$
$$-125x^2y^6)+b^4x^3y^3(-648-175y^2+90x^6y^4+x^4(597y^2-240y^4)$$
$$+3x^2(51-504y^2+125y^4))+x^3y^3(192-175y^2+3x^8y^6-6x^4y^2(-29+4y^2)$$
$$+x^2(-42-384y^2+175y^4)+x^6(9y^4-8y^6))+b^3x^2y^2(504-27x^8y^6$$
$$-3x^2(43-472y^2+150y^4)+x^4y^2(-351+248y^2+250y^4)$$

$$+x^6(-93y^4+72y^6))+b(16-27x^{10}y^8+6x^8y^6(-29+12y^2)+x^2(-6+72y^2)$$
$$+3x^4y^2(-19+16y^2+75y^4)+x^6(-108y^4+464y^6-125y^8))$$
$$+b^2xy(-144+3x^{10}y^8-3x^6y^4(29+104y^2)-9x^4y^2(-37-8y^2+50y^4)$$
$$+x^2(54-888y^2+350y^4)+x^8(117y^6-8y^8))))/(40(-1+b^2)xy^{11}\zeta^9)]$$
$$+\left(\frac{a}{R}\right)^6(\{3[-96b^7x^6y^6+8b^6x^5y^5(33+58x^2y^2)+b^5x^4y^4(-297-1162x^2y^2$$
$$+35x^4y^4)+b^4x^3y^3(63+1188x^2y^2-625x^4y^4+54x^6y^6)+x^3y^3(-168$$
$$+792x^2y^2-291x^4y^4+10x^6y^6+x^8y^8)-b^3x^2y^2(99+330x^2y^2$$
$$-1226x^4y^4+466x^6y^6+11x^8y^8)+b^2xy(22+435x^2y^2-1320x^4y^4$$
$$+1112x^6y^6+46x^8y^8+x^{10}y^{10})-b(2+11x^2y^2+33x^4y^4+892x^6y^6$$
$$-101x^8y^8+11x^{10}y^{10})]\}/40(-1+b^2)xy^{13}\zeta^{11}-3b(-1$$
$$+2bxy-x^2y^2)^5/20(-1+b^2)xy^{12}\zeta^{10}), \tag{A10g}$$

$$M_7^{US,c}=\left(\frac{a}{R}\right)^2(-[9(1+b^2)(-1+x^2)(-1+y^2)]/8(1-b^2)^{3/2}xy^2+\{9(-1+x^2)(-1$$
$$+y^2)[1+5b^4x^2y^2-5b^3(xy+3x^3y^3)-bxy(5+5x^2y^2+2x^4y^4)$$
$$+b^2(1+15x^2y^2+10x^4y^4)]\}/8(1-b^2)^{3/2}xy^7\zeta^5)$$
$$+\left(\frac{a}{R}\right)^4[(3\{-8+5y^2+32b^5x^3y^3-x^4y^2(27+16y^2)+x^2(3+56y^2-45y^4)$$
$$-bxy[6x^8y^6+x^2(21-32y^2)+7(-8+5y^2)+7x^4y^4(-8+5y^2)+x^6y^4(21$$
$$-16y^2+10y^4)]+b^4x^2y^2[-56+25y^2+105x^4y^2+x^2(15-296y^2+175y^4)]$$
$$+b^2[-8+5y^2+42x^8y^6+7x^6y^4(15-16y^2+10y^4)+x^4y^2(138-248y^2$$
$$+175y^4)+x^2(3-336y^2+230y^4)]-b^3xy[105x^6y^4+7(-8+5y^2)$$
$$+35x^4y^2(6-8y^2+5y^4)+x^2(21-496y^2+350y^4)]\})/40(1-b^2)^{3/2}xy^9\zeta^7$$
$$+3(1+b^2)(-8+3x^2+5y^2)(-1+2bxy-x^2y^2)^3/40(1-b^2)^{3/2}xy^8\zeta^6]$$
$$+\left(\frac{a}{R}\right)^6(-[3(1+b^2)]/40(1-b^2)^{3/2}xy^2-\{3[-1+48x^2y^2-81x^4y^4$$
$$+120b^5x^5y^5+10x^6y^6+b^4(21x^2y^2-270x^4y^4-95x^6y^6)+3b^3xy(3$$
$$+63x^2y^2+25x^4y^4+21x^6y^6)+bxy(9-21x^2y^2+57x^4y^4+9x^6y^6+2x^8y^8)$$
$$-b^2(1+141x^2y^2-99x^4y^4+83x^6y^6+18x^8y^8)]\}/40(1-b^2)^{3/2}xy^{11}\zeta^9), \tag{A10h}$$

$$M_8^{US,c}=\left(\frac{a}{R}\right)^2[(9b(-1+x^2))/(8(-1+b^2)xy^2)+(9(-1+x^2)(b^3x^2y^2(-5+y^2)$$
$$+xy^3(1+2x^2+x^4y^2)+b^2xy(5+(-1+8x^2)y^2)-b(1+5x^4y^4$$
$$+x^2y^2(5+y^2))))/(8(-1+b^2)xy^7\zeta^5)]$$
$$+\left(\frac{a}{R}\right)^4[(3(32b^4x^3y^3+xy^3(15-3x^8y^4+x^2(96-35y^2)$$

$$
\begin{aligned}
&+6x^4(-7+4y^2)+x^6y^2(-15+8y^2))+b^3x^2y^2(-56+5y^2+21x^4y^2\\
&+x^2(15-104y^2-25y^4))+b^2xy(56-15y^2-48x^6y^4+9x^4y^2(-7+16y^2)\\
&+x^2(-21+152y^2+35y^4))+b(-8+21x^8y^6+x^2(3-112y^2-5y^4)\\
&+x^4y^2(48-176y^2+25y^4)+x^6(84y^4-56y^6))))/(40(-1+b^2)xy^9\zeta^7)\\
&+(3b(-8+3x^2)(-1+2bxy-x^2y^2)^3)/(40(-1+b^2)xy^8\zeta^6)]\\
&+\left(\frac{a}{R}\right)^6(-3b/40(-1+b^2)xy^2-\{3[24b^4x^5y^5\\
&+b^3(21x^2y^2-54x^4y^4-79x^6y^6)+x^3y^3(84-51x^2y^2+6x^4y^4+x^6y^6)\\
&+3b^2xy(3+51x^4y^4+10x^6y^6)-b(1+57x^2y^2+72x^4y^4+5x^6y^6\\
&+9x^8y^8)]\}/40(-1+b^2)xy^{11}\zeta^9),
\end{aligned}
\tag{A10i}
$$

$$
\begin{aligned}
6\pi\eta a^3 M^{OS,c}_{sjn,\beta\alpha} = \big\{&M_1^{OS,c}\hat{y}_m^{\perp}\hat{y}_i\big(\hat{y}_n\hat{y}_j-\tfrac{1}{3}\delta_{nj}\big)+M_2^{OS,c}(\hat{y}_m^{\perp}\hat{y}_i\hat{y}_n^{\perp}\hat{y}_j+\hat{y}_m^{\perp}\hat{y}_i\hat{y}_n\hat{y}_j^{\perp})\\
&+M_3^{OS,c}\hat{y}_m^{\perp}\hat{y}_i\big(\hat{y}_n^{\perp}\hat{y}_j^{\perp}-\tfrac{1}{3}\delta_{nj}\big)+M_4^{OS,c}(\delta_{in}\hat{y}_m\hat{y}_j+\delta_{ij}\hat{y}_m\hat{y}_n)\\
&+M_5^{OS,c}\big[\delta_{in}\hat{y}_m^{\perp}\hat{y}_j+\delta_{ij}\hat{y}_m^{\perp}\hat{y}_n-\tfrac{1}{3}\delta_{jn}(\hat{y}_m^{\perp}\hat{y}_i+\hat{y}_m\hat{y}_i^{\perp})\big]\\
&+M_6^{OS,c}\big[\delta_{in}\hat{y}_m\hat{y}_j^{\perp}+\delta_{ij}\hat{y}_m\hat{y}_n^{\perp}-\tfrac{1}{3}\delta_{jn}(\hat{y}_m^{\perp}\hat{y}_i+\hat{y}_m\hat{y}_i^{\perp})\big]\\
&+M_7^{OS,c}(\delta_{in}\hat{y}_m^{\perp}\hat{y}_j^{\perp}+\delta_{ij}\hat{y}_m^{\perp}\hat{y}_n^{\perp})\big\}\epsilon_{smi},
\end{aligned}
\tag{A11a}
$$

$$
\begin{aligned}
M_1^{OS,c} = &\left(\frac{a}{R}\right)^3[(9\{4b^6x^3y^3(-5+y^2)+b^5x^2y^2[35+(-7+25x^2)y^2\\
&+11x^2y^4]-b^2xy[-28+(14-85x^2)y^2+(43x^2-44x^4)y^4+x^4(18+x^2)y^6+x^6y^8]\\
&+b[-4+(2-14x^2)y^2-45x^4y^4+(11x^4-21x^6)y^6+7x^6y^8]\\
&+x^3y^5[6+x^2(13-5y^2)-x^4y^2(-3+y^2)]-b^4xy[14+x^4y^4(15+19y^2)\\
&+x^2y^2(-5+37y^2)]+b^3(2+7x^2y^2(-9+7y^2)+x^4(-50y^4+48y^6)+7x^6(y^6\\
&+y^8)]\})/8(1-b^2)^{3/2}y^9\zeta^7+9b(-2+b^2+y^2)(-1+2bxy-x^2y^2)^3/4(1-b^2)^{3/2}y^8\zeta^6]\\
&+\left(\frac{a}{R}\right)^5(9b(-2+b^2)/20(1-b^2)^{3/2}y^2-\{9[40b^6x^5y^5+x^5y^5(143\\
&+6x^2y^2+3x^4y^4)+b^5(63x^2y^2-90x^4y^4-5x^6y^6)-3b^4xy(6+21x^2y^2\\
&+13x^6y^6)+b^3(2-117x^2y^2+117x^4y^4-11x^6y^6+9x^8y^8)-b(4+18x^2y^2\\
&+279x^4y^4+152x^6y^6+27x^8y^8)+b^2(36xy+231x^3y^3+69x^5y^5\\
&+105x^7y^7-x^9y^9)]\}/40(1-b^2)^{3/2}y^{11}\zeta^9),
\end{aligned}
\tag{A11b}
$$

$$
\begin{aligned}
M_2^{OS,c} = &\left(\frac{a}{R}\right)^3[-(9\{2+(-1+7x^2)y^2-x^2(7+5x^2)y^4+4x^4y^6+4b^5x^3y^3(-5+3y^2)\\
&+b^4x^2y^2[35+(-21+65x^2)y^2-31x^2y^4]+b^3xy[-14+(7-100x^2)y^2\\
&+(46x^2-70x^4)y^4+35x^4y^6]+bxy[-14+(7-20x^2)y^2-2x^2(-6+7x^2)y^4\\
&+(7x^4-4x^6)y^6+2x^6y^8]-b^2[-2+(1-42x^2)y^2+(14x^2-80x^4)y^4
\end{aligned}
$$

$$+ (43x^4 - 28x^6)y^6 + 14x^6y^8]\})/8(-1+b^2)y^9\zeta^7 + 9(1+b^2)(-2+y^2)(-1$$
$$+ 2bxy - x^2y^2)^3/8(-1+b^2)y^8\zeta^6]$$
$$+ \left(\frac{a}{R}\right)^5 (-[9(1+b^2)]/20(-1+b^2)y^2 - \{9[-2 - 9x^2y^2 + 108x^4y^4$$
$$+ 120b^5x^5y^5 - 25x^6y^6 - b^4x^2y^2(63 + 270x^2y^2 + 235x^4y^4) + 6b^3xy(3$$
$$+ 63x^2y^2 + 65x^4y^4 + 21x^6y^6) + 2bxy(9 - 21x^2y^2 - 3x^4y^4 + 9x^6y^6 + 2x^8y^8)$$
$$- 2b^2(1 + 36x^2y^2 + 171x^4y^4 + 38x^6y^6 + 18x^8y^8)]\}/40(-1+b^2)y^{11}\zeta^9), \quad \text{(A11c)}$$

$$M_3^{OS,c} = \left(\frac{a}{R}\right)^3 (\{9(-1+y^2)[20b^6x^3y^3 + x^3y^3(15 + 7x^2y^2 + 2x^4y^4) - 35b^5(x^2y^2 + 3x^4y^4)$$
$$+ b^4xy(14 + 185x^2y^2 + 105x^4y^4) - b(6 + 21x^2y^2 + 35x^4y^4 + 14x^6y^6)$$
$$- 2b^3(1 + 56x^2y^2 + 70x^4y^4 + 21x^6y^6) + b^2(42xy + 60x^3y^3 + 56x^5y^5 + 6x^7y^7)]\}/$$
$$8(1-b^2)^{3/2}y^9\zeta^7 - 9b(3+b^2)(-1+y^2)(-1+2bxy - x^2y^2)^3/4(1-b^2)^{3/2}y^8\zeta^6)$$
$$+ \left(\frac{a}{R}\right)^5 (-[9b(3+b^2)]/20(1-b^2)^{3/2}y^2 - \{9[280b^6x^5y^5$$
$$+ x^3y^3(105 - 28x^2y^2 + 9x^4y^4 + 2x^6y^6) - 63b^5(x^2y^2 + 10x^4y^4 + 5x^6y^6)$$
$$+ 3b^4xy(6 + 231x^2y^2 + 140x^4y^4 + 63x^6y^6) + 6b^2xy(9 - 21x^2y^2 + 56x^4y^4$$
$$+ 15x^6y^6 + x^8y^8) - 3b(2 + 9x^2y^2 + 42x^4y^4 + 21x^6y^6 + 6x^8y^8) - 2b^3(1 + 99x^2y^2$$
$$+ 126x^4y^4 + 147x^6y^6 + 27x^8y^8)]\}/40(1-b^2)^{3/2}y^{11}\zeta^9), \quad \text{(A11d)}$$

$$M_4^{OS,c} = \left(\frac{a}{R}\right)^3 [9b^2/8(-1+b^2)y^2 + (9\{-x^2y^4 + b^4x^2y^2(-4+y^2) + bxy^3(2 + 3x^2 + x^4y^2)$$
$$+ b^3xy[5 + (-2 + 7x^2)y^2] - b^2(1 + 6x^2y^2 + 5x^4y^4)\})/8(-1+b^2)y^7\zeta^5]$$
$$+ \left(\frac{a}{R}\right)^5 (\{9b[8b^3x^4y^4 - x^3y^3(21 + 2x^2y^2 + x^4y^4) - b^2xy(7 + 14x^2y^2$$
$$+ 19x^4y^4) + b(1 + 21x^2y^2 + 27x^4y^4 + 7x^6y^6)]\}/40(-1+b^2)y^9\zeta^7$$
$$+ 9b^2(-1 + 2bxy - x^2y^2)^3/40(-1+b^2)y^8\zeta^6), \quad \text{(A11e)}$$

$$M_5^{OS,c} = \left(\frac{a}{R}\right)^3 [-9b/8(1-b^2)^{1/2}y^2 - (9\{b^3x^2y^2(-4+y^2) + xy^3(1 + 3x^2$$
$$+ x^4y^2) + b^2xy[5 + (-1 + 7x^2)y^2] - b[1 + 5x^4y^4$$
$$+ x^2y^2(6 + y^2)]\})/8(1-b^2)^{1/2}y^7\zeta^5]$$
$$+ \left(\frac{a}{R}\right)^5 (\{9[-8b^3x^4y^4 + x^3y^3(21 + 2x^2y^2 + x^4y^4) + b^2xy(7 + 14x^2y^2$$
$$+ 19x^4y^4) - b(1 + 21x^2y^2 + 27x^4y^4 + 7x^6y^6)]\}/40(1-b^2)^{1/2}y^9\zeta^7$$
$$- 9b(-1 + 2bxy - x^2y^2)^3/40(1-b^2)^{1/2}y^8\zeta^6), \quad \text{(A11f)}$$

$$M_6^{OS,c} = \left(\frac{a}{R}\right)^3 [- [9b(1+b^2)(-1+y^2)]/8(1-b^2)^{3/2}y^2 + (9\{-xy^3 + b^5x^2y^2(-4 + 5y^2) + b[-1+(1+x^2)y^2] + b^4xy[5+3(-2+5x^2)y^2 - 15x^2y^4] + b^2xy[5+(-3+5x^2)y^2 + x^2(-5+2x^2)y^4 - 2x^4y^6] + b^3[-1+(1-17x^2)y^2 - 5x^2(-3+2x^2)y^4 + 10x^4y^6)]\}/8(1-b^2)^{3/2}y^7\zeta^5] + \left(\frac{a}{R}\right)^5 (\{9b[1-14x^2y^2+5x^4y^4+40b^4x^4y^4 - 7b^3(xy+10x^3y^3+5x^5y^5) - bxy(7+7x^4y^4+2x^6y^6) + b^2(1+56x^2y^2+25x^4y^4 + 14x^6y^6)]\}/40(1-b^2)^{3/2}y^9\zeta^7 + 9b(1+b^2)(-1 + 2bxy - x^2y^2)^3/40(1-b^2)^{3/2}y^8\zeta^6), \tag{A11g}$$

$$M_7^{OS,c} = \left(\frac{a}{R}\right)^3 [9(1+b^2)(-1+y^2)/8(-1+b^2)y^2 + (9\{1-(1+x^2)y^2 + b^4x^2y^2(4-5y^2) + 5b^3xy(-1+y^2)(1+3x^2y^2) + bxy(-1+y^2)(5+5x^2y^2+2x^4y^4) - b^2[-1+(1-17x^2)y^2 - 5x^2(-3+2x^2)y^4 + 10x^4y^6]\})/8(-1+b^2)y^7\zeta^5] + \left(\frac{a}{R}\right)^5 (\{9[-1+14x^2y^2 - 5x^4y^4 - 40b^4x^4y^4 + 7b^3(xy+10x^3y^3+5x^5y^5) + bxy(7+7x^4y^4+2x^6y^6) - b^2(1+56x^2y^2+25x^4y^4+14x^6y^6)]\}/ 40(-1+b^2)y^9\zeta^7 - [9(1+b^2)(-1+2bxy-x^2y^2)^3]/40(-1+b^2)y^8\zeta^6), \tag{A11h}$$

$$\begin{aligned} 6\pi\eta a^3 M_{minj,\beta\alpha}^{ES,c} = {} & M_1^{ES,c}\big(\hat{y}_m\hat{y}_i - \tfrac{1}{3}\delta_{mi}\big)\big(\hat{y}_n\hat{y}_j - \tfrac{1}{3}\delta_{nj}\big) + M_2^{ES,c}\big(\hat{y}_n\hat{y}_j - \tfrac{1}{3}\delta_{nj}\big)(\hat{y}_m^\perp\hat{y}_i + \hat{y}_m\hat{y}_i^\perp) \\ & + M_3^{ES,c}\big(\hat{y}_m\hat{y}_i - \tfrac{1}{3}\delta_{mi}\big)(\hat{y}_n^\perp\hat{y}_j + \hat{y}_n\hat{y}_j^\perp) + M_4^{ES,c}(\hat{y}_m^\perp\hat{y}_i\hat{y}_n^\perp\hat{y}_j + \hat{y}_m^\perp\hat{y}_i\hat{y}_n\hat{y}_j^\perp \\ & + \hat{y}_m\hat{y}_i^\perp\hat{y}_n^\perp\hat{y}_j + \hat{y}_m\hat{y}_i^\perp\hat{y}_n\hat{y}_j^\perp) + M_5^{ES,c}\big(\hat{y}_m^\perp\hat{y}_i^\perp - \tfrac{1}{3}\delta_{mi}\big)\big(\hat{y}_n\hat{y}_j - \tfrac{1}{3}\delta_{nj}\big) \\ & + M_6^{ES,c}\big(\hat{y}_m\hat{y}_i - \tfrac{1}{3}\delta_{mi}\big)\big(\hat{y}_n^\perp\hat{y}_j^\perp - \tfrac{1}{3}\delta_{nj}\big) + M_7^{ES,c}\big(\hat{y}_m^\perp\hat{y}_i^\perp - \tfrac{1}{3}\delta_{mi}\big)(\hat{y}_n^\perp\hat{y}_j + \hat{y}_n\hat{y}_j^\perp) \\ & + M_8^{ES,c}\big(\hat{y}_n^\perp\hat{y}_j^\perp - \tfrac{1}{3}\delta_{nj}\big)(\hat{y}_m^\perp\hat{y}_i + \hat{y}_m\hat{y}_i^\perp) + M_9^{ES,c}\big(\hat{y}_m^\perp\hat{y}_i^\perp - \tfrac{1}{3}\delta_{mi}\big)\big(\hat{y}_n^\perp\hat{y}_j^\perp - \tfrac{1}{3}\delta_{nj}\big) \\ & + M_{10}^{ES,c}\big(\delta_{mn}\hat{y}_i\hat{y}_j + \delta_{mj}\hat{y}_i\hat{y}_n + \delta_{in}\hat{y}_m\hat{y}_j + \delta_{ij}\hat{y}_m\hat{y}_n - \tfrac{4}{3}\delta_{nj}\hat{y}_i\hat{y}_m - \tfrac{4}{3}\delta_{im}\hat{y}_n\hat{y}_j \\ & + \tfrac{4}{9}\delta_{im}\delta_{nj}\big) + M_{11}^{ES,c}\big[\delta_{mn}\hat{y}_i^\perp\hat{y}_j + \delta_{mj}\hat{y}_i^\perp\hat{y}_n + \delta_{in}\hat{y}_m^\perp\hat{y}_j + \delta_{ij}\hat{y}_m^\perp\hat{y}_n \\ & - \tfrac{2}{3}\delta_{nj}(\hat{y}_i\hat{y}_m^\perp + \hat{y}_i^\perp\hat{y}_m) - \tfrac{2}{3}\delta_{mi}(\hat{y}_n\hat{y}_j^\perp + \hat{y}_n^\perp\hat{y}_j)\big] + M_{12}^{ES,c}\big[\delta_{mn}\hat{y}_i\hat{y}_j^\perp + \delta_{mj}\hat{y}_i\hat{y}_n^\perp \\ & + \delta_{in}\hat{y}_m\hat{y}_j^\perp + \delta_{ij}\hat{y}_m\hat{y}_n^\perp - \tfrac{2}{3}\delta_{nj}(\hat{y}_i\hat{y}_m^\perp + \hat{y}_i^\perp\hat{y}_m) - \tfrac{2}{3}\delta_{mi}(\hat{y}_n\hat{y}_j^\perp + \hat{y}_n^\perp\hat{y}_j)\big] \\ & + M_{13}^{ES,c}\big(\delta_{mn}\hat{y}_i^\perp\hat{y}_j^\perp + \delta_{mj}\hat{y}_i^\perp\hat{y}_n^\perp + \delta_{in}\hat{y}_m^\perp\hat{y}_j^\perp + \delta_{ij}\hat{y}_m^\perp\hat{y}_n^\perp - \tfrac{4}{3}\delta_{nj}\hat{y}_i^\perp\hat{y}_m^\perp \\ & - \tfrac{4}{3}\delta_{im}\hat{y}_n^\perp\hat{y}_j^\perp + \tfrac{4}{9}\delta_{im}\delta_{nj}\big) + M_{14}^{ES,c}\big(\delta_{mn}\delta_{ij} + \delta_{mj}\delta_{ni} - \tfrac{2}{3}\delta_{nj}\delta_{im}\big), \end{aligned} \tag{A12a}$$

$$M_1^{ES,c} = \left(\frac{a}{R}\right)^3 [(9\{2b^4x^2(-2+y^2) - 2(-1+x^2)(-2+y^2) + b^2[1+y^2-3x^2(-1 + y^2)]\})/4(-1+b^2)^2x^2y^2 + (9\{8-4y^2+4b^9x^7y^5(-18+13y^2) - 2x^2(4$$

$$
\begin{aligned}
&-20y^2+9y^4)+x^6y^4(-63+49y^2+10y^4)+b^8x^6y^4[312+(-143+97x^2)y^2\\
&-3(5+29x^2)y^4]+x^4(-36y^2+81y^4-39y^6)+b^7x^5y^3(-418+(209\\
&-507x^2)y^2+(33+164x^2-27x^4)y^4+3x^2(13+9x^2)y^6)\\
&-b^6x^4y^2[-252-6(-35+66x^2)y^2+(78+163x^2-455x^4)y^4\\
&+(17x^2+50x^4-9x^6)y^6+9(x^4+x^6)y^8]-b^4x^2[-8\\
&+(67+153x^2)y^2+(63-339x^2+720x^4)y^4+4x^2(81-159x^2+106x^4)y^6\\
&+(142x^4-211x^6-99x^8)y^8+27x^6(-1+x^2)y^{10}]+b^5x^3y[-72+(141\\
&+59x^2)y^2+(107-23x^2+54x^4)y^4-18x^2(-8+5x^2+20x^4)y^6\\
&-x^4(108-107x^2+x^4)y^8+(x^6+x^8)y^{10}]+bxy[36(-2+y^2)\\
&-2x^{10}y^8(-9+5y^2)+x^8y^6(81-57y^2+8y^4)+8x^2(9-36y^2+16y^4)\\
&+x^6y^4(273-254y^2+33y^4)+x^4y^2(252-403y^2+147y^4)]\\
&+b^3xy[18(1+y^2)+x^{10}y^8(-11+3y^2)+x^8y^6(522-299y^2-3y^4)\\
&+4x^6y^4(252-211y^2+63y^4)+x^2(54-411y^2+269y^4)\\
&+x^4y^2(611-1043y^2+432y^4)]+b^2[-2(1+y^2)+18x^{10}y^8(-9+5y^2)\\
&-4x^8y^6(158-121y^2+18y^4)-3x^2(2-83y^2+45y^4)-3x^4y^2(93\\
&-254y^2+105y^4)+x^6(-681y^4+881y^6-340y^8)]\}/8(-1+b^2)^2x^2y^{11}\zeta^9]\\
&+\left(\frac{a}{R}\right)^5[-(9\{288b^{10}x^8y^6-4(-4+y^2)+x^8y^6(567+140y^2-50y^4)\\
&+x^2(-8+88y^2-22y^4)-8b^9x^7y^5[99+(65+34x^2)y^2-15y^4]\\
&+x^6y^4(-99-994y^2+481y^4)+x^4(-44y^2+198y^4-117y^6)\\
&+b^8x^6y^4[1136+(890+481x^2)y^2+(-327+926x^2-161x^4)y^4-393x^2y^6]\\
&-b^7x^5y^3[910+(150+979x^2)y^2+(-363-556x^2+496x^4)y^4\\
&+x^2(-490+54x^2+63x^4)y^6-27x^4y^8]+b^6x^4y^2[396+(-660+524x^2)y^2\\
&+(-274-3218x^2+2135x^4)y^4+x^2(-95-3728x^2+2198x^4)y^6\\
&+x^4(1228+22x^2+11x^4)y^8-11x^6y^{10}]+b^5x^3y[-88+(462+269x^2)y^2\\
&+(245+1698x^2-55x^4)y^4+(407x^2+3312x^4-2386x^6)y^6\\
&+(-1492x^4+562x^6-523x^8)y^8-x^6(89+2x^2+x^4)y^{10}+x^8y^{12}]\\
&+b^4x^2[8-11(18+23x^2)y^2+(-99+1782x^2-2047x^4)y^4\\
&+(-1021x^2+3696x^4-3064x^6)y^6+(-658x^4+4554x^6-2461x^8)y^8\\
&+x^6(-1855-154x^2+121x^4)y^{10}+33x^8y^{12}]-b^2[198x^{12}y^{10}\\
&+2(2+y^2)+x^8y^6(3179-88y^2-80y^4)+2x^{10}y^8(283-132y^2+44y^4)\\
&+x^2(6-770y^2+209y^4)+x^4y^2(429-2640y^2+568y^4)\\
&+x^6y^4(1494-5170y^2+2173y^4)]+b^3xy[-11x^{12}y^{10}\\
&+22(2+y^2)+x^{10}y^8(817+14y^2-3y^4)+x^8y^6(5830-1006y^2+339y^4)\\
&+x^2(66-1650y^2+533y^4)+x^4y^2(1235-6642y^2+1793y^4)+x^6y^4(4367\\
&-8456y^2+3476y^4)]+bxy[18x^{12}y^{10}+44(-4+y^2)+x^{10}y^8(99-24y^2
\end{aligned}
$$

$$
\begin{aligned}
&+8y^4)+4x^2(22-198y^2+53y^4)+x^8y^6(-696-162y^2+53y^4)\\
&+x^4y^2(396-450y^2+209y^4)+x^6(231y^4+1148y^6-614y^8)]\}/40(-1\\
&+b^2)^2x^2y^{13}\zeta^{11}-\{9(-1+2bxy-x^2y^2)^5[4b^4x^2-2(-4+2x^2+y^2)\\
&-b^2(2+3x^2+y^2)]\}/20(-1+b^2)^2x^2y^{12}\zeta^{10})]\\
&+\left(\frac{a}{R}\right)^7[-[9(-4+b^2)(-1+2bxy-x^2y^2)^7]/100(-1+b^2)^2x^2y^{16}\zeta^{14}\\
&+\{9[8+52x^2y^2+143x^4y^4-7748x^6y^6+5663x^8y^8+2080b^{10}x^8y^8\\
&-350x^{10}y^{10}-8b^9x^7y^7(710+467x^2y^2)+b^8x^6y^6(5785\\
&+1642x^2y^2-1883x^4y^4)+b^7x^5y^5(-2145+11431x^2y^2+19909x^4y^4\\
&-139x^6y^6)+b^6x^4y^4(-1122-16627x^2y^2-30455x^4y^4+5055x^6y^6\\
&+13x^8y^8)+b^4x^2y^2(-143+3102x^2y^2+12441x^4y^4+55901x^6y^6\\
&-4954x^8y^8-91x^{10}y^{10})+b^5x^3y^3(429+9438x^2y^2+8109x^4y^4-33577x^6y^6\\
&+674x^8y^8-x^{10}y^{10})+b^3xy(26-1573x^2y^2-18876x^4y^4-37229x^6y^6\\
&+19511x^8y^8-970x^{10}y^{10}+7x^{12}y^{12})-bxy(104+572x^2y^2\\
&-3861x^4y^4-13073x^6y^6+6397x^8y^8+33x^{10}y^{10}+12x^{12}y^{12})\\
&+b^2(-2+559x^2y^2+2167x^4y^4+16445x^6y^6-27109x^8y^8+3848x^{10}y^{10}\\
&+156x^{12}y^{12})]\}/200(-1+b^2)^2x^2y^{15}\zeta^{13}], \qquad \text{(A12b)}
\end{aligned}
$$

$$
\begin{aligned}
M_2^{ES,c}=&\left(\frac{a}{R}\right)^3[(9b\{4-2y^2+x^2[-2+y^2+b^2(-3+2y^2)]\})/4(1-b^2)^{3/2}x^2y^2\\
&+(9\{4b^8x^7y^5(-18+13y^2)+b^7x^6y^4[252+(-135+97x^2)y^2-3(5\\
&+29x^2)y^4]+b^6x^5y^3[-318+(246-422x^2)y^2+(-26+241x^2-27x^4)y^4\\
&+3x^2(13+9x^2)y^6]+b^5x^4y^2[189+9(-47+64x^2)y^2+3(52-180x^2\\
&+125x^4)y^4+x^2(62-178x^2+9x^4)y^6-9(x^4+x^6)y^8]\\
&+b^3x^2[6+(-256+153x^2)y^2+9(14-83x^2+47x^4)y^4\\
&+6x^2(53-120x^2+68x^4)y^6+x^4(299-322x^2+81x^4)y^8\\
&-9x^6(-4+5x^2)y^{10}]+b^4x^3y[-54+(456-393x^2)y^2+(-214\\
&+893x^2-606x^4)y^4-3x^2(100-174x^2+99x^4)y^6-x^4(138-170x^2\\
&+x^4)y^8+(x^6+x^8)y^{10}]-x^3y^5[4+x^2(22-26y^2)+x^6y^4(-3+y^2)\\
&+x^4(-35+19y^2+6y^4)]+b^2xy[-4x^8y^6(-3+y^2)^2\\
&-36(-2+y^2)+x^{10}y^8(-9+5y^2)-2x^2(18-135y^2\\
&+59y^4)+x^4(-129y^2+395y^4-204y^6)+x^6(-195y^4+248y^6-39y^8)]\\
&+b[4(-2+y^2)+6x^4y^2(3-9y^2+5y^4)+2x^2(2-19y^2+9y^4)\\
&+x^8y^6(-40+11y^2+9y^4)+x^6(9y^4-33y^6-10y^8)]\})/8(1-b^2)^{3/2}x^2y^{11}\zeta^9]\\
&+\left(\frac{a}{R}\right)^5[\{9b[(2+3b^2)x^2+2(-4+y^2)]\}/20(1-b^2)^{3/2}x^2y^2-(9\{288b^9x^8y^6\\
&-8b^8x^7y^5[99+(65+34x^2)y^2-15y^4]+b^7x^6y^4[996+(650+681x^2)y^2
\end{aligned}
$$

$$
\begin{aligned}
&+(-91+926x^2-161x^4)y^4-393x^2y^6]-b^6x^5y^3[714+8(-90+143x^2)y^2\\
&+(286-366x^2+451x^4)y^4+x^2(-271+54x^2+63x^4)y^6-27x^4y^8]\\
&+b^5x^4y^2[297+165(-12+7x^2)y^2+(548-4248x^2+2115x^4)y^4+2x^2(301\\
&-1581x^2+921x^4)y^6+x^4(1193+22x^2+11x^4)y^8-11x^6y^{10}]-b^4x^3y[66\\
&+3(-616+239x^2)y^2+(490-5328x^2+2343x^4)y^4+x^2(946-6228x^2\\
&+3477x^4)y^6+(2362x^4-478x^6+424x^8)y^8+x^6(143+2x^2+x^4)y^{10}\\
&-x^8y^{12}]+b^3x^2[6+33(-24+7x^2)y^2+6(33-572x^2+217x^4)y^4\\
&+x^2(752-4542x^2+2277x^4)y^6-7x^4(-263-54x^2+33x^4)y^8\\
&+x^6(-415-132x^2+99x^4)y^{10}+44x^8y^{12}]-x^3y^5[28\\
&+x^2(624-330y^2)+x^8y^6(-6+y^2)+x^6y^2(245-18y^2\\
&+y^4)+x^4(-385-648y^2+272y^4)]-b^2xy[9x^{12}y^{10}+44(-4+y^2)\\
&+x^{10}y^8(63-12y^2+4y^4)+2x^2(22-396y^2+71y^4)\\
&+x^8y^6(-1145-438y^2+103y^4)+x^4y^2(219-1968y^2+946y^4)\\
&+x^6(726y^4+1442y^6-923y^8)]+b[4(-4+y^2)+2x^4y^2(11\\
&+66y^2+10y^4)+x^{10}y^8(200-66y^2+11y^4)+x^2(4-88y^2\\
&+22y^4)+x^8y^6(-741-782y^2+275y^4)+x^6(-153y^4\\
&+748y^6-504y^8)]\})/40(1-b^2)^{3/2}x^2y^{13}\zeta^{11}]\\
&+\left(\frac{a}{R}\right)^7(-[9b(-1+2bxy-x^2y^2)^7]/25(1-b^2)^{3/2}x^2y^{16}\zeta^{14}\\
&+\{9[2080b^9x^8y^8-8b^8x^7y^7(650+467x^2y^2)+b^7x^6y^6(4225+3482x^2y^2\\
&-1883x^4y^4)+b^6x^7y^7(7281+17178x^2y^2-139x^4y^4)+3x^5y^5(-1144\\
&+2764x^2y^2-699x^4y^4+14x^6y^6+x^8y^8)+b^5x^4y^4(-1518-14742x^2y^2\\
&-32673x^4y^4+4312x^6y^6+13x^8y^8)+b^4x^3y^3(1716+8580x^2y^2\\
&+26490x^4y^4-19525x^6y^6+580x^8y^8-x^{10}y^{10})-b^3x^2y^2(572\\
&+5544x^2y^2+7215x^4y^4-29420x^6y^6+5835x^8y^8+78x^{10}y^{10})+b(-8\\
&-52x^2y^2+1342x^4y^4+4004x^6y^6-12605x^8y^8+1118x^{10}y^{10}-39x^{12}y^{12})\\
&+b^2xy(104+572x^2y^2+5148x^4y^4-23135x^6y^6+13900x^8y^8\\
&+141x^{10}y^{10}+6x^{12}y^{12})]\}/200(1-b^2)^{3/2}x^2y^{15}\zeta^{13}), \qquad \text{(A12c)}
\end{aligned}
$$

$$
\begin{aligned}
M_3^{ES,c}=&\left(\frac{a}{R}\right)^3[(9b\{5-4y^2+x^2[-7+(5+b^2)y^2]\})/4(1-b^2)^{3/2}x^2y^2\\
&+(9\{4b^8x^7y^5(6+5y^2)+b^7x^6y^4[-24-(63+79x^2)y^2+5(-7+5x^2)y^4]\\
&+b^6x^5y^3[6+(213-151x^2)y^2+(-55+197x^2+30x^4)y^4]\\
&+b^4x^3y^3[543-415y^2+x^8y^6+23x^6y^4(-12+11y^2)+x^2(-747+1358y^2\\
&-690y^4)-3x^4y^2(383-376y^2+42y^4)]+b[-10+8y^2+18x^{10}y^8(3-2y^2)\\
&+21x^4y^2(3-7y^2+3y^4)+x^8y^6(199-182y^2+36y^4)\\
&+x^2(14-55y^2+36y^4)+x^6y^4(129-228y^2+136y^4)]
\end{aligned}
$$

$$+b^3x^2y^2[-317+252y^2-9x^8y^6(-9+8y^2)+4x^6y^4(138-115y^2$$
$$+9y^4)+3x^2(147-355y^2+210y^4)+x^4y^2(1041-1224y^2+281y^4)]$$
$$+b^5x^4y^4[-480+315y^2-9x^6y^4+x^4(504y^2-481y^4)$$
$$+x^2(618-837y^2+290y^4)]+b^2xy[90-72y^2+x^{10}y^8(-9+8y^2)$$
$$+x^2(-126+405y^2-262y^4)+x^8y^6(-231+165y^2-4y^4)-2x^6y^4(216$$
$$-233y^2+72y^4)+x^4(-435y^2+656y^4-219y^6)]+x^3y^5[5+x^2(41$$
$$-44y^2)+x^4(-56+61y^2-18y^4)+x^6(-27y^2+24y^4-4y^6)$$
$$+x^8(-6y^4+4y^6)]\})/8(1-b^2)^{3/2}x^2y^{11}\zeta^9]$$
$$+\left(\frac{a}{R}\right)^5[(9\{96b^9x^8y^6-8b^8x^7y^5[33+(-25+58x^2)y^2+35y^4]+b^7x^6y^4[192$$
$$+(470+207x^2)y^2+(235+626x^2-35x^4)y^4-175x^2y^6]+b^6x^5y^3[-42$$
$$+(-2370+1727x^2)y^2+(605-3714x^2+2525x^4)y^4-3x^2(-645+28x^2$$
$$+18x^4)y^6]+x^3y^5[-35+6x^{10}y^6+7x^2(-156+77y^2)+x^4(616+114y^2$$
$$-38y^4)+x^8y^4(33-12y^2+4y^4)+x^6y^2(13-66y^2+22y^4)]+b^5x^4y^4[3300$$
$$-1175y^2+11x^8y^6+x^6y^4(-639+22y^2)+x^2(-2574+6612y^2-3695y^4)$$
$$-2x^4y^2(2793+99y^2+31y^4)]-b[-20+8y^2+66x^{12}y^{10}+2x^2(7-55y^2$$
$$+22y^4)+x^{10}y^8(247-132y^2+44y^4)+2x^8y^6(825-197y^2+74y^4)$$
$$+x^4y^2(77-660y^2+119y^4)+x^6y^4(342-2932y^2+1377y^4)]$$
$$-b^3x^2y^2[99x^{10}y^8+198(-5+2y^2)+x^8y^6(1389-66y^2+44y^4)$$
$$+x^6y^4(-465-2478y^2+935y^4)+x^2(693-2640y^2+1346y^4)$$
$$+x^4(1896y^2+774y^4-1141y^6)]+b^2xy[9x^{12}y^{10}+44(-5$$
$$+2y^2)+2x^{10}y^8(171-3y^2+2y^4)+x^8y^6(2033-612y^2+220y^4)$$
$$+2x^2(77-495y^2+233y^4)+x^6y^4(-33-4202y^2+1715y^4)+x^4(651y^2$$
$$-186y^4-473y^6)]+b^4x^3y^3[-2310+889y^2-x^{10}y^8+x^6y^4(513-338y^2$$
$$+198y^4)+x^2(1701-5592y^2+3025y^4)+x^4(4422y^2+1002y^4-692y^6)$$
$$+x^8(449y^6-2y^8)]\})/40(1-b^2)^{3/2}x^2y^{13}\zeta^{11}-[9b(-10+7x^2$$
$$+4y^2)(-1+2bxy-x^2y^2)^5]/20(1-b^2)^{3/2}x^2y^{12}\zeta^{10}]$$
$$+\left(\frac{a}{R}\right)^7(-[9b(-1+2bxy-x^2y^2)^7]/20(1-b^2)^{3/2}x^2y^{16}\zeta^{14}$$
$$+\{9[800b^9x^8y^8+8b^8x^7y^7(-70+557x^2y^2)+b^7x^6y^6(-3055$$
$$-18062x^2y^2+893x^4y^4)+b^6x^5y^5(6435+28044x^2y^2-13389x^4y^4$$
$$+94x^6y^6)+3x^5y^5(2002-2287x^2y^2+342x^4y^4+13x^6y^6+2x^8y^8)$$
$$-b^5x^4y^4(5610+21528x^2y^2-35445x^4y^4+3430x^6y^6+13x^8y^8)$$
$$+b^3x^2y^2(-715+495x^2y^2+22191x^4y^4-41354x^6y^6+606x^8y^8-39x^{10}y^{10})$$
$$+b^4x^3y^3(2145+8151x^2y^2-39819x^4y^4+21586x^6y^6+176x^8y^8+x^{10}y^{10})$$
$$+b^2xy(130+715x^2y^2-7722x^4y^4+36356x^6y^6-6529x^8y^8$$

$$+471x^{10}y^{10}+3x^{12}y^{12})-b(10+65x^2y^2+2035x^4y^4+14768x^6y^6$$
$$-10301x^8y^8+929x^{10}y^{10}+78x^{12}y^{12})]\}/200(1-b^2)^{3/2}x^2y^{15}\zeta^{13}), \qquad \text{(A12d)}$$

$$M_4^{ES,c}=\left(\frac{a}{R}\right)^3[-(9\{(-2+x^2)(-2+y^2)+b^4x^2(2+y^2)+b^2[5-7y^2+x^2(-9$$
$$+7y^2)]\})/8(-1+b^2)^2x^2y^2-(3\{x^8y^6(-27+y^2)+12(-2+y^2)$$
$$+24b^9x^7y^5(6+5y^2)-3x^6y^4(-76+73y^2+9y^4)$$
$$+x^2(12-119y^2+57y^4)+3x^4y^2(19-105y^2+76y^4)$$
$$+6b^8x^6y^4[-84-(39+79x^2)y^2+5(-7+5x^2)y^4]$$
$$+4b^7x^5y^3[159+(139+141x^2)y^2+3(-13+37x^2+15x^4)y^4]$$
$$-6b^6x^4y^2[63+(227-200x^2)y^2+(-263+452x^2-184x^4)y^4$$
$$+x^2(-241+321x^2+9x^4)y^6]+2b^5x^3y[54+(831-1248x^2)y^2$$
$$+(-1113+2537x^2-2193x^4)y^4-3x^2(668-773x^2+70x^4)y^6$$
$$+3x^4(-79+143x^2+x^4)y^8]+b^4x^2[-12+2(-478+825x^2)y^2$$
$$+3(442-1591x^2+1607x^4)y^4+3x^2(1355-1895x^2+758x^4)y^6$$
$$+x^4(1806-1727x^2+135x^4)y^8-27x^6(-5+9x^2)y^{10}]$$
$$+b^2[-81x^{10}y^8(-5+3y^2)+6(-5+7y^2)+3x^4y^2(205-766y^2$$
$$+311y^4)+x^8y^6(1659-1520y^2+351y^4)+3x^6y^4(353$$
$$-830y^2+507y^4)+x^2(54-923y^2+561y^4)]+b^3xy[54(5-7y^2)$$
$$+3x^{10}y^8(-5+9y^2)-3x^8y^6(503-320y^2+5y^4)-3x^6y^4(793-876y^2$$
$$+431y^4)-3x^2(162-839y^2+637y^4)+x^4(-2271y^2+4438y^4-1911y^6)]$$
$$+3bxy[-36(-2+y^2)+3x^{10}y^8(-5+3y^2)+x^2(-36+281y^2-133y^4)$$
$$+x^8y^6(-65+60y^2-13y^4)+x^4(-135y^2+424y^4-243y^6)$$
$$+x^6(-249y^4+306y^6-59y^8)]\})/16(-1+b^2)^2x^2y^{11}\zeta^9]$$
$$+\left(\frac{a}{R}\right)^5(9\{-192b^{10}x^8y^6+45x^{10}y^8+4(-4+y^2)+x^2(4-102y^2+27y^4)$$
$$+16b^9x^7y^5[33+(-25+58x^2)y^2+35y^4]+x^8y^6(-801-194y^2+45y^4)$$
$$+x^4y^2(27-770y^2+437y^4)+2b^8x^6y^4[-332+(122-647x^2)y^2+(-351$$
$$-626x^2+35x^4)y^4+175x^2y^6]+4b^7x^5y^3[119+(344-66x^2)y^2+(-143$$
$$+1238x^2-840x^4)y^4+3x^2(-291+14x^2+9x^4)y^6]+x^6(437y^4$$
$$+1642y^6-801y^8)-2b^6x^4y^2[99+(1320-955x^2)y^2$$
$$+(-883+4262x^2-3516x^4)y^4+x^2(-3438-1524x^2+233x^4)y^6$$
$$+x^4(257+22x^2+11x^4)y^8]+2b^5x^3y[22+(1208-982x^2)y^2$$
$$+(-829+4378x^2-3465x^4)y^4+3x^2(-1089-818x^2+345x^4)y^6$$
$$+(1083x^4-94x^6-131x^8)y^8+x^6(-123+2x^2+x^4)y^{10}]$$
$$+b^4x^2[-4+2(-502+437x^2)y^2+(698-6842x^2+4285x^4)y^4$$
$$+(3901x^2+402x^4-1437x^6)y^6+x^4(-1821-7022x^2+3011x^4)y^8$$

$$
\begin{aligned}
&+x^6(2927+66x^2+55x^4)y^{10}+55x^8y^{12}]-bxy[15x^{12}y^{10}\\
&+44(-4+y^2)+2x^6y^4(627+808y^2-444y^4)+x^{10}y^8(90\\
&-38y^2+13y^4)+2x^8y^6(-420-118y^2+35y^4)+x^2(44-898y^2+239y^4)\\
&+x^4y^2(253-2268y^2+1210y^4)]-b^3xy[5x^{12}y^{10}+22(-10+7y^2)\\
&+x^4(1229y^2-4232y^4)+x^{10}y^8(746+6y^2+5y^4)+2x^8y^6(3209\\
&-882y^2+337y^4)+x^2(198-2626y^2+1073y^4)+2x^6y^4(198\\
&-6926y^2+3031y^4)]+b^2[-20+14y^2+165x^{12}y^{10}\\
&+2x^8y^6(2504-260y^2+81y^4)+x^{10}y^8(310-418y^2+143y^4)\\
&+x^2(18-874y^2+265y^4)+4x^6y^4(-7-2599y^2+1191y^4)\\
&+x^4(287y^2-1628y^4-164y^6)]\})/80(-1+b^2)^2x^2y^{13}\zeta^{11}\\
&-\{9(-1+2bxy-x^2y^2)^5[2b^4x^2+b^2(10-9x^2-7y^2)-2(-4+x^2\\
&+y^2)]\}/40(-1+b^2)^2x^2y^{12}\zeta^{10}]\\
&+\left(\frac{a}{R}\right)^7(-[9(4+5b^2)]/200(-1+b^2)^2x^2y^2+\{9[-8-87x^2y^2-2598x^4y^4\\
&+15678x^6y^6-9038x^8y^8+1600b^{10}x^8y^8+485x^{10}y^{10}\\
&+16b^9x^7y^7(-218+557x^2y^2)+2b^8x^6y^6(793-15774x^2y^2+893x^4y^4)\\
&+4b^7x^5y^5(572+11655x^2y^2-8506x^4y^4+47x^6y^6)-2b^6x^4y^4(1108\\
&+19123x^2y^2-41949x^4y^4+3289x^6y^6+13x^8y^8)+2b^5x^3y^3(1216\\
&+8177x^2y^2-42886x^4y^4+28762x^6y^6-166x^8y^8+x^{10}y^{10})+b^4x^2y^2(-750\\
&-11751x^2y^2+47086x^4y^4-116904x^6y^6+4136x^8y^8+39x^{10}y^{10})\\
&+bxy(104+859x^2y^2+4199x^4y^4-27878x^6y^6+9062x^8y^8+83x^{10}y^{10}\\
&+19x^{12}y^{12})-b^2(10+567x^2y^2-3695x^4y^4+56992x^6y^6-48826x^8y^8\\
&+4977x^{10}y^{10}+247x^{12}y^{12})+b^3(130xy+1857x^3y^3+325x^5y^5\\
&+101406x^7y^7-28604x^9y^9+1465x^{11}y^{11}-3x^{13}y^{13})]\zeta\}/\\
&400(-1+b^2)^2x^2y(-1+2bxy-x^2y^2)^7), \qquad \text{(A12e)}
\end{aligned}
$$

$$
\begin{aligned}
M_5^{ES,c}=&\left(\frac{a}{R}\right)^3[-\{9b^2[-3+(1+2b^2)x^2](-1+y^2)\}/4(-1+b^2)^2x^2y^2\\
&+(3\{12b^9x^7y^5(18-13y^2)+3b^8x^6y^4[-192+(127-97x^2)y^2+3(5\\
&+29x^2)y^4]+b^7x^5y^3[654+(-677+699x^2)y^2+3(53-234x^2+27x^4)y^4\\
&-9x^2(13+9x^2)y^6]+3b^6x^4y^2[-126+(347-293x^2)y^2\\
&+(-239+529x^2-146x^4)y^4+(-104x^2+167x^4-9x^6)y^6\\
&+9(x^4+x^6)y^8]+b^4x^2[-12+(574-240x^2)y^2-3(188\\
&-569x^2+265x^4)y^4-3x^2(445-577x^2+334x^4)y^6+(-1254x^4+1045x^6\\
&-135x^8)y^8+135x^6(-1+x^2)y^{10}]+b^5x^3y[108+60(-17+10x^2)y^2\\
&+2(462-1126x^2+507x^4)y^4+3x^2(428-509x^2+175x^4)y^6\\
&+3x^4(175-174x^2+x^4)y^8-3(x^6+x^8)y^{10}]+3bx^3y^3[11-7y^2
\end{aligned}
$$

$$+x^2(-15+16y^2-33y^4)+2x^6y^4(2-3y^2+y^4)+x^4y^2(-51+19y^2$$
$$+16y^4)]+b^3xy[162(-1+y^2)-15x^{10}y^8(-1+y^2)+15x^8y^6(2-3y^2+y^4)$$
$$+12x^6y^4(41-49y^2+16y^4)+x^2(54-687y^2+609y^4)$$
$$+x^4y^2(303-899y^2+924y^4)]+x^2y^2[-5+3y^2+x^2(3-45y^2$$
$$+66y^4)+x^4(66y^2-42y^6)+x^6(-42y^4+40y^6)]-b^2[18(-1+y^2)$$
$$+x^8y^6(-261+173y^2+54y^4)+x^2(6-97y^2+87y^4)+3x^4y^2(11-71y^2$$
$$+94y^4)+x^6(84y^4-81y^6-51y^8)]]\})/8(-1+b^2)^2x^2y^{11}\zeta^9]$$
$$+\left(\frac{a}{R}\right)^5[(9\{288b^{10}x^8y^6-8b^9x^7y^5[99+(65+34x^2)y^2-15y^4]$$
$$+b^8x^6y^4[856+(666+465x^2)y^2+(17+926x^2-161x^4)y^4-393x^2y^6]$$
$$+b^7x^5y^3[-518+(574-165x^2)y^2+(-583+312x^2+58x^4)y^4+(124x^2$$
$$-54x^4-63x^6)y^6+27x^4y^8]+b^6x^4y^2[198+(-1650+199x^2)y^2+(919$$
$$-3738x^2+613x^4)y^4+x^2(913-3274x^2+1523x^4)y^6+x^4(1427+22x^2$$
$$+11x^4)y^8-11x^6y^{10}]-b^5x^3y[44+20(-64+11x^2)y^2$$
$$+2(326-2168x^2+759x^4)y^4+3x^2(440-1974x^2+977x^4)y^6$$
$$+x^4(2973-352x^2+214x^4)y^8+x^6(176+2x^2+x^4)y^{10}-x^8y^{12}]$$
$$+b^4x^2[4+116(-5+x^2)y^2+(292-2002x^2+941x^4)y^4+x^2(749$$
$$-3726x^2+2613x^4)y^6+(2661x^4+1538x^6-785x^8)y^8+x^6(-557-110x^2$$
$$+55x^4)y^{10}+55x^8y^{12}]+bx^3y^3[-106+41y^2-2x^8y^6(-6-2y^2+y^4)$$
$$+x^6y^4(-529-20y^2+10y^4)+x^2(97-60y^2+286y^4)+x^4(396y^2$$
$$+1422y^4-583y^6)]-x^2y^2[-14+5y^2+70x^8y^6$$
$$+2x^6y^4(-190-72y^2+35y^4)+x^2(5-242y^2+185y^4)$$
$$+x^4(185y^2+888y^4-380y^6)]-b^3xy[5x^{12}y^{10}+66(-2+y^2)$$
$$+5x^{10}y^8(13-2y^2+y^4)+x^8y^6(-1694-382y^2+191y^4)+x^2(22-806y^2$$
$$+379y^4)+x^4y^2(349-694y^2+1155y^4)+x^6(693y^4+3176y^6-1332y^8)]$$
$$+b^2[6(-2+y^2)+x^{10}y^8(483-44y^2+22y^4)+x^2(2-94y^2+43y^4)$$
$$+x^4y^2(21-550y^2+497y^4)+x^8y^6(-1587-1314y^2+583y^4)+x^6(169y^4$$
$$+2142y^6-1199y^8)]\})/40(-1+b^2)^2x^2y^{13}\zeta^{11}+9b^2(-6+x^2+2b^2x^2$$
$$+3y^2)(-1+2bxy-x^2y^2)^5/20(-1+b^2)^2x^2y^{12}\zeta^{10}]$$
$$+\left(\frac{a}{R}\right)^7(27b^2(-1+2bxy-x^2y^2)^7/100(-1+b^2)^2x^2y^{16}\zeta^{14}$$
$$-\{9[2080b^{10}x^8y^8-8b^9x^7y^7(654+467x^2y^2)+b^8x^6y^6(4329$$
$$+3626x^2y^2-1883x^4y^4)+b^7x^5y^5(-143+6659x^2y^2+18039x^4y^4$$
$$-139x^6y^6)+5x^2y^2(7+194x^2y^2-1469x^4y^4+1044x^6y^6-72x^8y^8)$$
$$+b^6x^4y^4(-2305-13572x^2y^2-34696x^4y^4+5600x^6y^6+13x^8y^8)$$
$$+b^5x^3y^3(1000+10244x^2y^2+28019x^4y^4-26611x^6y^6+549x^8y^8-x^{10}y^{10})$$

$$+bx^3y^3(-287+949x^2y^2+12771x^4y^4-6031x^6y^6+76x^8y^8+2x^{10}y^{10})$$
$$-b^4x^2y^2(394+855x^2y^2+11206x^4y^4-42544x^6y^6+8056x^8y^8+65x^{10}y^{10})$$
$$+b^3xy(78+1003x^2y^2-3328x^4y^4-31921x^6y^6+22629x^8y^8$$
$$-18x^{10}y^{10}+5x^{12}y^{12})-b^2(6+109x^2y^2+2100x^4y^4-17498x^6y^6$$
$$+26496x^8y^8-2983x^{10}y^{10}+26x^{12}y^{12})]\}/200(-1+b^2)^2x^2y^{15}\zeta^{13}), \qquad \text{(A12f)}$$

$$M_6^{ES,c}=\left(\frac{a}{R}\right)^3[\{9[3+(-3-4b^2+4b^4)x^2](-1+y^2)\}/4(-1+b^2)^2x^2y^2+\{3[-18(-1$$
$$+y^2)+162bxy(-1+y^2)-27b^2(-15+7b^2+2b^4)x^{10}y^8(-1+y^2)$$
$$+3b(-15+7b^2+2b^4)x^{11}y^9(-1+y^2)+3bx^9y^7(67-78y^2+11y^4$$
$$+63b^6(-1+y^2)+b^2(442-435y^2-7y^4)+2b^4(-115+114y^2+y^4)]$$
$$+x^2[-18+94y^2-78y^4+b^2(-24+601y^2-573y^4)$$
$$+b^4(24-29y^2+3y^4)]-3bx^3y[-54+232y^2-182y^4$$
$$+b^2(-72+409y^2-329y^4)+b^4(72-83y^2+7y^4)]+3bx^7y^5[90-155y^2$$
$$+49y^4+20b^8(-6+7y^2)+b^4(-193+409y^2-212y^4)+b^6(-277+174y^2$$
$$+63y^4)+4b^2(314-385y^2+79y^4)]+x^8y^6[3-5y^2+b^8(285-315y^2)$$
$$+b^2(-1395+1726y^2-297y^4)-6b^6(-230+206y^2+9y^4)$$
$$+b^4(-1785+1504y^2+189y^4)]-3x^6y^4[-16+9y^2-y^4$$
$$+5b^8(-72+61y^2+21y^4)-4b^6(34-77y^2+76y^4)+b^2(751-1116y^2$$
$$+349y^4)+b^4(517-766y^2+355y^4)]-3x^4y^2[-2(-13+9y^2+8y^4)$$
$$+b^6(-252+226y^2+44y^4)+b^4(215-344y^2+85y^4)+b^2(227-836y^2$$
$$+643y^4)]+bx^5y^3[b^4(573+286y^2-1227y^4)+6(96-145y^2+33y^4)$$
$$+b^6(-1290+997y^2+429y^4)+b^2(1653-4193y^2$$
$$+2868y^4)]\})/8(-1+b^2)^2x^2y^{11}\zeta^9]$$
$$+\left(\frac{a}{R}\right)^5[\{9[6+(-3-4b^2+4b^4)x^2-3y^2]\}/20(-1+b^2)^2x^2y^2$$
$$-\{9[11b^2(-15+7b^2+2b^4)x^{12}y^{10}+b(15-7b^2-2b^4)x^{13}y^{11}-6(-2+y^2)$$
$$+66bxy(-2+y^2)+bx^{11}y^9[84-99b^6-22y^2+11y^4$$
$$+b^2(701+14y^2-7y^4)+2b^4(-178-2y^2+y^4)]$$
$$+x^2[-6+52y^2-28y^4+b^2(-8+622y^2-307y^4)+b^4(8-14y^2+5y^4)]$$
$$+x^{10}y^8[-5+281b^8+b^2(-774+242y^2-121y^4)+b^6(766+44y^2-22y^4)$$
$$+b^4(-1258-154y^2+77y^4)]+x^8y^6[-131+480b^{10}+6y^2-5y^4$$
$$+b^2(354+1200y^2-526y^4)+b^8(-897+322y^2-231y^4)$$
$$+2b^6(2764-508y^2+359y^4)-2b^4(4053-734y^2+473y^4)]$$
$$+bx^9y^7[367+80b^8-124y^2+62y^4+b^4(2661+668y^2-334y^4)$$
$$+b^6(-2686-198y^2+99y^4)+b^2(1558-1006y^2+503y^4)]$$
$$+x^6y^4[482+390y^2-131y^4+b^4(346+13752y^2-7674y^4)$$

$$+b^8(1520+3174y^2-1937y^4)+2b^2(-1520-858y^2+493y^4)$$
$$+8b^6(-161-1257y^2+748y^4)]+bx^3y[66-488y^2+256y^4+b^4(-88$$
$$+106y^2-41y^4)+b^2(88-1598y^2+775y^4)]+bx^7y^5[-1122-786y^2$$
$$+265y^4+b^6(1683+4416y^2-2488y^4)+40b^8(-33-35y^2+21y^4)$$
$$+b^2(7755-1168y^2+840y^4)+3b^4(-1408-1674y^2+841y^4)]$$
$$-x^4y^2[28+836y^2-482y^4+b^4(347+572y^2-538y^4)+4b^6(-99-165y^2$$
$$+106y^4)+b^2(351-4708y^2+2576y^4)]+bx^5y^3[326+2040y^2-1276y^4$$
$$+b^4(697+7148y^2-4422y^4)+b^6(-994-2554y^2+1573y^4)$$
$$+b^2(961-12178y^2+6897y^4))]\}/40(-1+b^2)^2x^2y^{13}\zeta^{11}]$$
$$+\left(\frac{a}{R}\right)^7(27(-1+2bxy-x^2y^2)^7/100(-1+b^2)^2x^2y^{16}\zeta^{14}$$
$$+\{9[6+4x^2y^2-4204x^4y^4+7969x^6y^6-1704x^8y^8+5600b^{10}x^8y^8$$
$$-15x^{10}y^{10}+8b^9x^7y^7(-2106+371x^2y^2)+b^8x^6y^6(20631-29210x^2y^2$$
$$+779x^4y^4)-b^7x^5y^5(12727-67279x^2y^2+11241x^4y^4+143x^6y^6)$$
$$+2b^6x^4y^4(1697-34827x^2y^2+28352x^4y^4-1171x^6y^6+13x^8y^8)$$
$$+b^5x^3y^3(287+37375x^2y^2-104483x^4y^4+15115x^6y^6+492x^8y^8$$
$$-2x^{10}y^{10})+b^3x^3y^3(-1861-45578x^2y^2+61651x^4y^4-12669x^6y^6$$
$$-750x^8y^8+7x^{10}y^{10})-b^4x^2y^2(35+8847x^2y^2-93106x^4y^4+44734x^6y^6$$
$$-2761x^8y^8+91x^{10}y^{10})+b^2x^2y^2(499+13947x^2y^2-41756x^4y^4$$
$$+21066x^6y^6+533x^8y^8+143x^{10}y^{10})-bxy(78+142x^2y^2-13208x^4y^4$$
$$+17895x^6y^6-1537x^8y^8+67x^{10}y^{10}+11x^{12}y^{12})]\}/$$
$$200(-1+b^2)^2x^2y^{15}\zeta^{13}), \tag{A12g}$$

$$M_7^{ES,c}=\left(\frac{a}{R}\right)^3[-\{9b[-2+(1+b^2)x^2]\}/2(1-b^2)^{3/2}x^2y^2-(9\{4b^8x^7y^5(6+5y^2)$$
$$+b^7x^6y^4[-144-(15+79x^2)y^2+5(-7+5x^2)y^4]+b^6x^5y^3[206+5(-17$$
$$+79x^2)y^2+(35-61x^2+30x^4)y^4]+x^5y^3[4+(22-26x^2)y^2+(-35+19x^2$$
$$+6x^4)y^4+x^4(-3+x^2)y^6]-3b^5x^4y^2[42+3(-35+57x^2)y^2+x^2(-57$$
$$+89x^2)y^4+x^2(-35+28x^2+3x^4)y^6]-b^3x^2[4+36(-7+4x^2)y^2$$
$$+18x^2(-35+17x^2)y^4+(-459x^4+321x^6)y^6+3x^4(35-43x^2+18x^4)y^8]$$
$$+b^4x^3y[36+12(-35+29x^2)y^2+12x^2(-47+31x^2)y^4$$
$$+3x^2(-35-9x^2+66x^4)y^6+(x^6+x^8)y^8]$$
$$+b[8-9x^{10}y^8+x^8y^6(-5+2y^2)+9x^4y^2(-2+7y^2)+4x^2(-1+9y^2)$$
$$+x^6y^4(-45+57y^2+35y^4)]+b^2xy[-72+6x^{10}y^8-6x^8y^6(-9+y^2)$$
$$-36x^2(-1+7y^2)+3x^4y^2(38-127y^2+35y^4)$$
$$+x^6(243y^4-239y^6)]\})/8(1-b^2)^{3/2}x^2y^{11}\zeta^9]$$

$$+\left(\frac{a}{R}\right)^5[9b[-4+(1+b^2)x^2]/10(1-b^2)^{3/2}x^2y^2-(9\{96b^9x^8y^6$$
$$-8b^8x^7y^5[33+(-25+58x^2)y^2+35y^4]+b^7x^6y^4[472+(-970$$
$$+1311x^2)y^2+(595+626x^2-35x^4)y^4-175x^2y^6]-b^6x^5y^3[434+3(-670$$
$$+693x^2)y^2+(385+654x^2-179x^4)y^4+x^2(-1085+84x^2+54x^4)y^6]$$
$$-x^5y^3[28+(624-330x^2)y^2+(-385-648x^2+272x^4)y^4$$
$$+x^2(245-18x^2+x^4)y^6+x^6(-6+x^2)y^8]+b^5x^4y^2[198+3(-770$$
$$+529x^2)y^2+6x^2(-208+57x^2)y^4+3x^2(-595-824x^2+398x^4)y^6$$
$$+x^4(525+22x^2+11x^4)y^8]-b^4x^3y[44+24(-77+31x^2)y^2$$
$$+12x^2(-229+22x^2)y^4+3x^2(-385-2036x^2+978x^4)y^6+x^4(1575$$
$$-538x^2+289x^4)y^8+x^8(2+x^2)y^{10}]+b^3x^2[4+44(-18+5x^2)y^2$$
$$+6x^2(-462+71x^2)y^4+3x^4(-1894+797x^2)y^6$$
$$-3x^4(-595+34x^2+13x^4)y^8+3x^6(-175-44x^2+22x^4)y^{10}]$$
$$+b^2xy[176-6x^{12}y^{10}+12x^{10}y^8(-8+y^2)$$
$$+44x^2(-1+18y^2)+x^8y^6(851+408y^2)-3x^4y^2(38-1086y^2+385y^4)$$
$$+x^6y^4(-1419-1022y^2+1015y^4)]+b[-16+11x^{12}y^{10}+x^2(4-88y^2)$$
$$-22x^4y^2(-1+9y^2)+x^8y^6(-444-692y^2+175y^4)+x^6(155y^4+508y^6$$
$$-595y^8)+x^{10}(200y^8-66y^{10})]\})/40(1-b^2)^{3/2}x^2y^{13}\zeta^{11}]$$
$$+\left(\frac{a}{R}\right)^7(9b/25(1-b^2)^{3/2}x^2y^2-\{9[800b^9x^8y^8+8b^8x^7y^7(-430$$
$$+557x^2y^2)+b^7x^6y^6(6305-12302x^2y^2+893x^4y^4)+b^6x^5y^5(-6435$$
$$+13464x^2y^2-16323x^4y^4+94x^6y^6)+b^5x^4y^4(3003-6903x^2y^2$$
$$+39828x^4y^4-2107x^6y^6-13x^8y^8)-3x^5y^5(-1144+2764x^2y^2-699x^4y^4$$
$$+14x^6y^6+x^8y^8)+b^4x^3y^3(-1716+4290x^2y^2-42060x^4y^4+15655x^6y^6$$
$$-490x^8y^8+x^{10}y^{10})+b^3x^2y^2(572+2574x^2y^2+18915x^4y^4$$
$$-28790x^6y^6+4395x^8y^8+78x^{10}y^{10})-b^2xy(104+572x^2y^2+11583x^4y^4$$
$$-26600x^6y^6+11605x^8y^8+186x^{10}y^{10}+6x^{12}y^{12})$$
$$+b(8+52x^2y^2+143x^4y^4-4589x^6y^6+10760x^8y^8-893x^{10}y^{10}$$
$$+39x^{12}y^{12})]\}/200(1-b^2)^{3/2}x^2y^{15}\zeta^{13}), \tag{A12h}$$

$$M_8^{ES,c}=\left(\frac{a}{R}\right)^3[9b[-8+(7+5b^2)x^2](-1+y^2)/4(1-b^2)^{3/2}x^2y^2$$
$$+(9\{20b^8x^7y^5(-6+7y^2)-5b^7x^6y^4[-84+(69-19x^2)y^2+21(1+x^2)y^4]$$
$$+b^6x^5y^3[-530+(610-730x^2)y^2+(-70+617x^2-63x^4)y^4+63(x^2$$
$$+x^4)y^6]-3b^5x^4y^2[-105-105(-3+4x^2)y^2+(-210+579x^2-346x^4)y^4$$
$$-3x^2(63-110x^2+2x^4)y^6+6(x^4+x^6)y^8]+x^5y^3[5+(41-44x^2)y^2$$
$$+(-56+61x^2-18x^4)y^4+(-27x^2+24x^4-4x^6)y^6$$

$$+(-6x^4+4x^6)y^8]+b^3x^2[10+(-514+486x^2)y^2$$
$$+18(28-97x^2+70x^4)y^4+9x^2(140-227x^2+83x^4)y^6+3x^4(231-295x^2$$
$$+54x^4)y^8-54x^6(-2+3x^2)y^{10}]+b^4x^3y[-90-15(-62+69x^2)y^2-3(280$$
$$-811x^2+584x^4)y^4-3x^2(476-717x^2+192x^4)y^6$$
$$+(-369x^4+574x^6-2x^8)y^8+2(x^6+x^8)y^{10}]$$
$$+b[16(-1+y^2)-36x^{10}y^8(-1+y^2)+2x^8y^6(68-90y^2+27y^4)$$
$$+2x^2(7-43y^2+36y^4)+3x^6y^4(28-81y^2+63y^4)+63x^4(y^2-3y^4$$
$$+2y^6)]+b^2xy[-144(-1+y^2)+18x^{10}y^8(-1+y^2)-3x^8y^6(69-73y^2$$
$$+4y^4)-126x^2(1-5y^2+4y^4)-6x^4y^2(76-158y^2+77y^4)+x^6(-378y^4$$
$$+631y^6-243y^8)]\})/8(1-b^2)^{3/2}x^2y^{11}\zeta^9]$$
$$+\left(\frac{a}{R}\right)^5[9b[(7+5b^2)x^2+8(-2+y^2)]/20(1-b^2)^{3/2}x^2y^2-(9\{480b^9x^8y^6$$
$$+40b^8x^7y^5[-33+(-35+2x^2)y^2+21y^4]+b^7x^6y^4[1660+125(14$$
$$+3x^2)y^2+(-1085+322x^2+281x^4)y^4-231x^2y^6]-b^6x^5y^3[1190$$
$$+40(-42+55x^2)y^2+(770-5502x^2+4139x^4)y^4+x^2(3101+198x^2$$
$$+99x^4)y^6-99x^4y^8]+b^5x^4y^2[495+15(-308+207x^2)y^2+6(385-2261x^2$$
$$+1527x^4)y^4+3x^2(2471-718x^2+676x^4)y^6+11x^4(117+4x^2$$
$$+2x^4)y^8-22x^6y^{10}]-x^5y^3[-35+7(-156+77x^2)y^2$$
$$+(616+114x^2-38x^4)y^4+x^2(13-66x^2+22x^4)y^6+x^4(33-12x^2$$
$$+4x^4)y^8+6x^6y^{10}]-b^4x^3y[110+3(-1232+669x^2)y^2+3(616-4172x^2$$
$$+2629x^4)y^4+6x^2(1078-431x^2+392x^4)y^6+x^4(1083-1166x^2$$
$$+902x^4)y^8+x^6(583+4x^2+2x^4)y^{10}-2x^8y^{12}]+b^3x^2[10+44(-36$$
$$+17x^2)y^2+6(132-924x^2+533x^4)y^4-3x^2(-924+98x^2+39x^4)y^6$$
$$+3x^4(-161-998x^2+501x^4)y^8+33x^6(39-8x^2+6x^4)y^{10}+132x^8y^{12}]$$
$$+b[44x^{12}y^{10}+16(-2+y^2)+11x^4y^2(7-36y^2+18y^4)+2x^{10}y^8(74-66y^2$$
$$+33y^4)+2x^2(7-88y^2+44y^4)+x^8y^6(1188-454y^2+297y^4)$$
$$+x^6y^4(-43-2674y^2+1547y^4)]-b^2xy[18x^{12}y^{10}+176(-2+y^2)$$
$$+42x^4y^2(19+12y^2-11y^4)+3x^{10}y^8(99-8y^2+4y^4)$$
$$+22x^2(7-72y^2+36y^4)+x^8y^6(1547-726y^2+363y^4)+x^6y^4(-858$$
$$-3986y^2+1923y^4)]\})/40(1-b^2)^{3/2}x^2y^{13}\zeta^{11}]$$
$$+\left(\frac{a}{R}\right)^7(18b/25(1-b^2)^{3/2}x^2y^2+\{9[5600b^9x^8y^8+56b^8x^7y^7(-250$$
$$+53x^2y^2)+b^6x^7y^7(59157-8214x^2y^2-143x^4y^4)+b^7x^6y^6(11375$$
$$-27146x^2y^2+779x^4y^4)+3x^5y^5(2002-2287x^2y^2+342x^4y^4$$
$$+13x^6y^6+2x^8y^8)+b^5x^4y^4(-6006-58149x^2y^2+32394x^4y^4-3481x^6y^6$$
$$+26x^8y^8)+b^4x^3y^3(3432+30030x^2y^2-48855x^4y^4+19990x^6y^6$$

$$+845x^8y^8-2x^{10}y^{10})-b^3x^2y^2(1144+5148x^2y^2-34125x^4y^4+40070x^6y^6$$
$$+1095x^8y^8+156x^{10}y^{10})+b^2xy(208+1144x^2y^2-15444x^4y^4$$
$$+38015x^6y^6-4330x^8y^8+507x^{10}y^{10}+12x^{12}y^{12})-b(16+104x^2y^2$$
$$+286x^4y^4+14807x^6y^6-8630x^8y^8+779x^{10}y^{10}$$
$$+78x^{12}y^{12})]\}/200(1-b^2)^{3/2}x^2y^{15}\zeta^{13}), \tag{A12i}$$

$$M_9^{ES,c}=\left(\frac{a}{R}\right)^3[-\{9[-2+x^2+3b^4x^2+2b^2(-5+4x^2)](-1+y^2)\}/2(-1+b^2)^2x^2y^2$$
$$-(9\{-10x^8y^6+8(-1+y^2)+20b^9x^7y^5(-6+7y^2)+9x^4y^2(2-9y^2$$
$$+7y^4)+4x^2(1-10y^2+9y^4)-5b^8x^6y^4[-96+(77-19x^2)y^2$$
$$+21(1+x^2)y^4]+x^6(39y^4-49y^6)+b^7x^5y^3[-630-15(-63+73x^2)y^2$$
$$-7(45-136x^2+9x^4)y^4+63(x^2+x^4)y^6]+b^6x^4y^2[378$$
$$+3(-651+725x^2)y^2+(1575-3122x^2+1573x^4)y^4+3x^2(329$$
$$-505x^2+6x^4)y^6-18(x^4+x^6)y^8]-3b^4x^2[-4+(424-354x^2)y^2$$
$$-3(140-503x^2+313x^4)y^4+(-1155x^2+1694x^4-589x^6)y^6$$
$$+(-735x^4+669x^6-84x^8)y^8+12x^6(-5+7x^2)y^{10}]+b^5x^3y[-108$$
$$-6(-368+343x^2)y^2-3(700-1757x^2+1059x^4)y^4+(-3213x^2+3918x^4$$
$$-891x^6)y^6+(-621x^4+889x^6-2x^8)y^8+2(x^6+x^8)y^{10}]+b^2[40(-1+y^2)$$
$$-162x^{10}y^8(-1+y^2)+135x^4y^2(2-9y^2+7y^4)+16x^2(2-29y^2$$
$$+27y^4)+x^8y^6(607-837y^2+270y^4)+x^6y^4(537-1442y^2+945y^4)]$$
$$+b^3xy[-360(-1+y^2)+28x^{10}y^8(-1+y^2)+x^8y^6(-693$$
$$+713y^2-20y^4)-48x^2(6-41y^2+35y^4)-21x^4y^2(58$$
$$-163y^2+105y^4)+x^6(-1473y^4+2428y^6-1035y^8)]+bxy[-72(-1+y^2)$$
$$+18x^{10}y^8(-1+y^2)-63x^4y^2(2-7y^2+5y^4)-36x^2(1-8y^2+7y^4)$$
$$-3x^8y^6(27-37y^2+10y^4)+x^6(-183y^4+338y^6$$
$$-135y^8)]\})/8(-1+b^2)^2x^2y^{11}\zeta^9]$$
$$+\left(\frac{a}{R}\right)^5[(9\{480b^{10}x^8y^6+50x^{10}y^8+8(-2+y^2)-x^8y^6(481+140y^2)$$
$$+11x^4y^2(2-18y^2+9y^4)+40b^9x^7y^5[-33+(-35+2x^2)y^2+21y^4]$$
$$+x^2(4-88y^2+44y^4)+b^8x^6y^4[1800+35(2+37x^2)y^2+(-105+322x^2$$
$$+281x^4)y^4-231x^2y^6]+x^6(117y^4+994y^6-567y^8)$$
$$-b^7x^5y^3[1386+165(-42+31x^2)y^2+(3465-8372x^2$$
$$+5864x^4)y^4+3x^2(1582+66x^2+33x^4)y^6-99x^4y^8]+b^6x^4y^2[594$$
$$+3(-3850+2143x^2)y^2+(5775-22456x^2+13582x^4)y^4+x^2(11508$$
$$-3862x^2+3133x^4)y^6+11x^4(201+4x^2+2x^4)y^8-22x^6y^{10}]$$
$$-b^5x^3y[132+330(-28+13x^2)y^2+33(140-742x^2+373x^4)y^4+3x^2(4081$$
$$-3536x^2+1754x^4)y^6+x^4(4464-1958x^2+1397x^4)y^8+x^6(979+4x^2$$

$$
\begin{aligned}
&+2x^4)y^{10}-2x^8y^{12}]+b^4x^2[12+330(-12+5x^2)y^2+15(132-1078x^2\\
&+445x^4)y^4+15x^2(539-896x^2+234x^4)y^6+15x^4(420-650x^2\\
&+251x^4)y^8+11x^6(405-40x^2+28x^4)y^{10}+220x^8y^{12}]\\
&+b^2[198x^{12}y^{10}+40(-2+y^2)+8x^2(4-154y^2+77y^4)\\
&+11x^4y^2(34-342y^2+171y^4)+5x^8y^6(758-482y^2+297y^4)\\
&+x^{10}y^8(691-660y^2+330y^4)+7x^6y^4(117-1360y^2\\
&+720y^4)]-b^3xy[28x^{12}y^{10}+440(-2+y^2)+5x^{10}y^8(209-8y^2+4y^4)\\
&+88x^2(4-66y^2+33y^4)+33x^4y^2(62-350y^2+175y^4)+5x^8y^6(988\\
&-638y^2+319y^4)+5x^6y^4(561-2836y^2+1530y^4)]-bxy[18x^{12}y^{10}\\
&+88(-2+y^2)+99x^4y^2(2-14y^2+7y^4)+44x^2(1-18y^2+9y^4)\\
&+3x^{10}y^8(33-20y^2+10y^4)+x^8y^6(-146-330y^2+165y^4)+x^6(627y^4\\
&+80y^6-180y^8)]\})/40(-1+b^2)^2x^2y^{13}\zeta^{11}+9(-1+2bxy-x^2y^2)^5(-4+x^2\\
&+3b^4x^2+2y^2+2b^2[4x^2+5(-2+y^2)]\}/10(-1+b^2)^2x^2y^{12}\zeta^{10}]\\
&+\left(\frac{a}{R}\right)^7(9(1+5b^2)(-1+2bxy-x^2y^2)^7/25(-1+b^2)^2x^2y^{16}\zeta^{14}\\
&-\{9[-8-52x^2y^2-143x^4y^4+7748x^6y^6-5663x^8y^8+5600b^{10}x^8y^8\\
&+350x^{10}y^{10}+56b^9x^7y^7(-190+53x^2y^2)+b^8x^6y^6(455-31066x^2y^2\\
&+779x^4y^4)+b^7x^5y^5(15015+69587x^2y^2-8011x^4y^4-143x^6y^6)\\
&+b^6x^4y^4(-15015-70889x^2y^2+25793x^4y^4-5547x^6y^6+26x^8y^8)\\
&+b^5x^3y^3(8580+33033x^2y^2-28233x^4y^4+39973x^6y^6+1417x^8y^8\\
&-2x^{10}y^{10})-b^4x^2y^2(2860+15873x^2y^2-17745x^4y^4+79115x^6y^6\\
&+5765x^8y^8+260x^{10}y^{10})+b^3xy(520+4576x^2y^2+12441x^4y^4\\
&+61865x^6y^6-4865x^8y^8+2275x^{10}y^{10}+20x^{12}y^{12})+bxy(104+572x^2y^2\\
&+1287x^4y^4-10211x^6y^6+4255x^8y^8+195x^{10}y^{10}+30x^{12}y^{12})-b^2(40\\
&+832x^2y^2+3289x^4y^4+37427x^6y^6-22675x^8y^8+3545x^{10}y^{10}\\
&+390x^{12}y^{12})]\}/200(-1+b^2)^2x^2y^{15}\zeta^{13}), \qquad \text{(A12j)}
\end{aligned}
$$

$$
\begin{aligned}
M_{10}^{ES,c}=\left(\frac{a}{R}\right)^3[&-(3\{12b^7x^5y^3(-6+y^2)-6(-2+y^2)+x^6y^4(-3+5y^2)+x^2(-12\\
&+53y^2-33y^4)+x^4y^2(-45+46y^2+3y^4)+2b^6x^4y^2[48+(4+69x^2)y^2\\
&+(-39+36x^2)y^4]-2b^5x^3y[21+(46-12x^2)y^2+(-114+115x^2\\
&+78x^4)y^4+27x^2(-1+x^2)y^6]+b^4x^2[6-2(-55+87x^2)y^2\\
&-3(74-143x^2+93x^4)y^4+x^2(-261+260x^2+63x^4)y^6\\
&+21x^4(-1+x^2)y^8]+bxy[42(-2+y^2)-3x^8y^6(-9+5y^2)\\
&+3x^6y^4(32-25y^2+5y^4)+x^4y^2(195-227y^2+54y^4)+x^2(84-239y^2\\
&+123y^4)]+b^3xy[-42+84y^2-3x^8y^6(3+y^2)+3x^6y^4(146-89y^2+y^4)\\
&+x^4y^2(483-563y^2+270y^4)+x^2(84-425y^2+279y^4)]
\end{aligned}
$$

$$
\begin{aligned}
&+b^2[6-12y^2+21x^8y^6(-9+5y^2)+x^2(-12+233y^2-123y^4)\\
&-3x^4y^2(85-175y^2+98y^4)+x^6(-486y^4+419y^6-105y^8)]\}/\\
&16(-1+b^2)^2x^2y^9\zeta^7-(9(-1+2bxy-x^2y^2)^3\{b^4x^2+(-1+x^2)(-2+y^2)\\
&+b^2[1-2y^2+2x^2(-1+y^2)]\})/8(-1+b^2)^2x^2y^8\zeta^6]\\
&+\left(\frac{a}{R}\right)^5[-\{9[4-2x^2+b^4x^2-y^2-2b^2(-1+x^2+y^2)]\}/40(-1+b^2)^2x^2y^2\\
&-(9\{-5x^8y^6+2(-4+y^2)+8b^7x^5y^3[5+2(2+x^2)y^2-13y^4]\\
&+x^6y^4(-126-34y^2+5y^4)+x^2(4-50y^2+29y^4)+x^4(23y^2+204y^4\\
&-108y^6)-2b^6x^4y^2[24+9(6+7x^2)y^2+(-117-94x^2+93x^4)y^4-7x^2y^6]\\
&+2b^5x^3y[9+(72+11x^2)y^2+2(-59-13x^2+64x^4)y^4\\
&+x^2(-7-30x^2+48x^4)y^6-15x^4y^8]+b^4x^2[-2+4(-35+23x^2)y^2\\
&+(146-462x^2+315x^4)y^4+x^2(117-872x^2+430x^4)y^6\\
&+(376x^4+18x^6-27x^8)y^8+9x^6y^{10}]+b^2[81x^{10}y^8+4(-1+y^2)\\
&+x^2(4-242y^2+41y^4)+x^8y^6(265-126y^2+45y^4)+x^6y^4(693-290y^2\\
&+109y^4)+x^4y^2(149-1146y^2+513y^4)]-bxy[9x^{10}y^8+18(-4+y^2)\\
&+x^8y^6(39-14y^2+5y^4)+3x^6y^4(-33-22y^2+7y^4)+x^2(36-186y^2\\
&+89y^4)+x^4(87y^2+114y^4-93y^6)]+b^3xy[3x^{10}y^8-36(-1+y^2)+x^2(-36\\
&+678y^2-179y^4)-x^8y^6(273+2y^2+y^4)+x^4(-479y^2+1646y^4-731y^6)\\
&+x^6(-1127y^4+426y^6-165y^8)]\})/80(-1+b^2)^2x^2y^{11}\zeta^9]\\
&+\left(\frac{a}{R}\right)^7(-\{9[4+57x^2y^2-1243x^4y^4+1139x^6y^6+64b^8x^6y^6-85x^8y^8\\
&+16b^7x^5y^5(-11+54x^2y^2)+2b^6x^4y^4(99-906x^2y^2+55x^4y^4)\\
&+2b^5x^3y^3(28+539x^2y^2-1610x^4y^4+27x^6y^6)+b^4x^2y^2(134-187x^2y^2\\
&+6881x^4y^4+223x^6y^6-11x^8y^8)+b^3xy(-22-1135x^2y^2-5324x^4y^4\\
&+1406x^6y^6-350x^8y^8+x^{10}y^{10})-bxy(44-89x^2y^2-1650x^4y^4\\
&+1030x^6y^6+34x^8y^8+7x^{10}y^{10})+b^2(2+139x^2y^2+3212x^4y^4\\
&-3500x^6y^6+742x^8y^8+77x^{10}y^{10})]\}/400(-1+b^2)^2x^2y^{13}\zeta^{11}\\
&-9(2+b^2)(-1+2bxy-x^2y^2)^5/200(-1+b^2)^2x^2y^{12}\zeta^{10}),
\end{aligned}
\tag{A12k}
$$

$$
\begin{aligned}
M_{11}^{ES,c}=&\left(\frac{a}{R}\right)^3[9b[-2+(1+b^2)x^2]/8(1-b^2)^{3/2}x^2y^2-(9\{2b^6x^5y^3(-6+y^2)\\
&+b^5x^4y^2[16+(-10+31x^2)y^2+(-5+4x^2)y^4]+b^4x^3y[-7+(32-41x^2)y^2\\
&+(5+8x^2-35x^4)y^4]+b^3x^2[1+(-35+24x^2)y^2+x^2(-50+43x^2)y^4\\
&+x^2(10-15x^2+14x^4)y^6]+x^3y^3[-3+5y^2+x^4y^4+x^2(5-2y^2)]\\
&-b[2+x^6y^4(4+3y^2)+x^2(-1+7y^2)+x^4y^2(-2+10y^2+5y^4)]\\
&+b^2xy[14-2x^8y^6+x^6y^4(-7+y^2)+x^2(-7+41y^2-10y^4)\\
&+x^4(-22y^2+34y^4)]\})/8(1-b^2)^{3/2}x^2y^9\zeta^7]
\end{aligned}
$$

$$+\left(\frac{a}{R}\right)^5[-\{9b[-4+(1+b^2)x^2]\}/40(1-b^2)^{3/2}x^2y^2-(9\{4b^6x^5y^3[5$$
$$+2(-6+5x^2)y^2-5y^4]+b^5x^4y^2[-24-3(-46+45x^2)y^2+(45+158x^2$$
$$-125x^4)y^4-25x^2y^6]+b^4x^3y[9+6(-27+19x^2)y^2+(-35-378x^2$$
$$+270x^4)y^4+(75x^2-60x^4+63x^6)y^6]-b^3x^2[1+3(-42+17x^2)y^2$$
$$+3x^2(-118+57x^2)y^4+x^2(90-62x^2+23x^4)y^6+2x^4(-25-9x^2+9x^4)y^8]$$
$$-x^3y^3[-48+35y^2+2x^6y^6+x^4y^2(-35+6y^2)+x^2(35+96y^2-35y^4)]$$
$$+b[4+2x^8y^6(-10+9y^2)+x^2(-1+18y^2)+3x^4(y^2+4y^4+15y^6)$$
$$+x^6(54y^4+116y^6-25y^8)]+b^2xy[-36+2x^{10}y^8$$
$$-3x^6y^4(31+26y^2)+x^2(9-222y^2+70y^4)+x^4(69y^2+18y^4$$
$$-90y^6)+x^8(9y^6-2y^8)]\})/40(1-b^2)^{3/2}x^2y^{11}\zeta^9]$$
$$+\left(\frac{a}{R}\right)^7(\{9[96b^7x^6y^6-8b^6x^5y^5(33+58x^2y^2)-b^4x^3y^3(63+1188x^2y^2$$
$$-625x^4y^4+54x^6y^6)+b^5(297x^4y^4+1162x^6y^6-35x^8y^8)-x^3y^3(-168$$
$$+792x^2y^2-291x^4y^4+10x^6y^6+x^8y^8)+b^3x^2y^2(99+330x^2y^2$$
$$-1226x^4y^4+466x^6y^6+11x^8y^8)-b^2xy(22+435x^2y^2-1320x^4y^4$$
$$+1112x^6y^6+46x^8y^8+x^{10}y^{10})+b(2+11x^2y^2+33x^4y^4+892x^6y^6$$
$$-101x^8y^8+11x^{10}y^{10})]\}/200(1-b^2)^{3/2}x^2y^{13}\zeta^{11}$$
$$+9b(-1+2bxy-x^2y^2)^5/100(1-b^2)^{3/2}x^2y^{12}\zeta^{10}), \tag{A12l}$$

$$M_{12}^{ES,c}=\left(\frac{a}{R}\right)^3[-\{9b[-4+(5+b^2)x^2](-1+y^2)\}/8(1-b^2)^{3/2}x^2y^2$$
$$-(9\{2b^6x^5y^3(-6+5y^2)+b^5x^4y^2[16+(-48+71x^2)y^2$$
$$+(35-70x^2)y^4]+b^4x^3y[-7+(86-126x^2)y^2-2(40-82x^2+35x^4)y^4$$
$$+35x^2(-1+2x^2)y^6]+b^3x^2[1+(-71+94x^2)y^2+(70-170x^2$$
$$+103x^4)y^4+7x^2(10-17x^2+4x^4)y^6+(14x^4-28x^6)y^8]$$
$$+b[4(-1+y^2)-14x^8y^6(-1+y^2)+x^6y^4(36-49y^2+14y^4)$$
$$+x^2(5-19y^2+14y^4)+x^4y^2(16-48y^2+35y^4)]+x^3y^3[9-10y^2$$
$$+2x^6y^4(-1+y^2)+x^2(-10+16y^2-7y^4)+x^4(-7y^2+9y^4-2y^6)]$$
$$+b^2xy[-28(-1+y^2)+4x^8y^6(-1+y^2)+x^2(-35+87y^2-50y^4)$$
$$-2x^4y^2(31-52y^2+21y^4)+x^6(-49y^4+51y^6$$
$$-2y^8)]\})/8(1-b^2)^{3/2}x^2y^9\zeta^7]$$
$$+\left(\frac{a}{R}\right)^5[-\{9b[(5+b^2)x^2+4(-2+y^2)]\}/40(1-b^2)^{3/2}x^2y^2$$
$$-(9\{20b^6x^5y^3[1+2(-6+5x^2)y^2+7y^4]-b^5x^4y^2[24+15(-38+33x^2)y^2$$
$$+5(63-38x^2+41x^4)y^4+105x^2y^6]+b^4x^3y[9+(-540+429x^2)y^2$$
$$+10(28-27x^2+30x^4)y^4+21x^2(5-6x^2+6x^4)y^6+63x^4y^8]$$

$$
\begin{aligned}
&- b^3x^2[1 + 3(-84 + 59x^2)y^2 + 3(42 - 40x^2 + 27x^4)y^4 \\
&+ x^4(-376 + 241x^2)y^6 + 12x^4(14 - 3x^2 + 3x^4)y^8 + 18x^6y^{10}] \\
&+ x^3y^3[-120 + 70y^2 + 2x^8y^6 + x^6y^4(9 - 4y^2 + 2y^4) + x^2(70 + 6y^2 + 7y^4) \\
&+ x^4y^2(7 - 18y^2 + 9y^4)] - b[18x^{10}y^8 + 4(-2 + y^2) + 2x^8y^6(29 - 18y^2 \\
&+ 9y^4) + x^2(5 - 36y^2 + 18y^4) + 3x^4y^2(5 - 106y^2 + 63y^4) + x^6y^4(180 \\
&- 106y^2 + 63y^4)] + b^2xy[4x^{10}y^8 + 36(-2 + y^2) + x^2(45 - 12y^2 - 14y^4) \\
&+ x^8y^6(81 - 4y^2 + 2y^4) + 3x^6y^4(83 - 48y^2 + 24y^4) + 3x^4y^2(-5 - 168y^2 \\
&+ 84y^4)]\})/40(1 - b^2)^{3/2}x^2y^{11}\zeta^9] \\
&+ \left(\frac{a}{R}\right)^7(\{9[480b^7x^6y^6 + 40b^6x^5y^5(-33 + 2x^2y^2) + b^5x^4y^4(1485 - 790x^2y^2 \\
&+ 281x^4y^4) - b^4x^3y^3(882 - 1485x^2y^2 + 1504x^4y^4 + 99x^6y^6) \\
&- x^3y^3(420 - 693x^2y^2 + 156x^4y^4 + 11x^6y^6 + 2x^8y^8) + 2b^3x^2y^2(99 \\
&- 561x^2y^2 + 1456x^4y^4 + 115x^6y^6 + 11x^8y^8) - 2b^2xy(22 - 321x^2y^2 \\
&+ 1353x^4y^4 - 130x^6y^6 + 55x^8y^8 + x^{10}y^{10}) + b(4 + 22x^2y^2 + 957x^4y^4 \\
&- 754x^6y^6 + 149x^8y^8 + 22x^{10}y^{10})]\}/200(1 - b^2)^{3/2}x^2y^{13}\zeta^{11} \\
&+ 9b(-1 + 2bxy - x^2y^2)^5/50(1 - b^2)^{3/2}x^2y^{12}\zeta^{10}), \qquad \text{(A12m)}
\end{aligned}
$$

$$
\begin{aligned}
M_{13}^{ES,c} = &\left(\frac{a}{R}\right)^3[9[-2 + x^2 + b^4x^2 + 7b^2(-1 + x^2)](-1 + y^2)/8(-1 + b^2)^2x^2y^2 \\
&+ (3\{12(-1 + y^2) + 12b^7x^5y^3(-6 + 5y^2) - x^6y^4(3 + 5y^2) + x^4y^2(33 - 46y^2 \\
&+ 3y^4) + x^2(6 - 53y^2 + 45y^4) + 2b^6x^4y^2[48 + (-178 + 237x^2)y^2 - 3(-43 \\
&+ 78x^2)y^4] + 2b^5x^3y[-21 + (400 - 477x^2)y^2 + (-375 + 631x^2 - 237x^4)y^4 \\
&+ 3x^2(-44 + 79x^2)y^6] + b^4x^2[6 + (-746 + 786x^2)y^2 + 3(246 - 583x^2 \\
&+ 313x^4)y^4 + x^2(957 - 1064x^2 + 189x^4)y^6 - 21x^4(-5 + 9x^2)y^8] \\
&+ b^2[42(-1 + y^2) - 189x^8y^6(-1 + y^2) + 3x^4y^2(73 - 291y^2 \\
&+ 224y^4) + x^6y^4(480 - 731y^2 + 273y^4) + x^2(42 - 389y^2 \\
&+ 351y^4)] + b^3xy[-294(-1 + y^2) + 27x^8y^6(-1 + y^2) + x^2(-294 \\
&+ 1193y^2 - 915y^4) - 3x^6y^4(188 - 193y^2 + 5y^4) + x^4(-711y^2 \\
&+ 1391y^4 - 732y^6)] + bxy[-84(-1 + y^2) + 27x^8y^6(-1 + y^2) \\
&+ x^2(-42 + 275y^2 - 225y^4) - 3x^6y^4(32 - 45y^2 + 13y^4) + x^4(-153y^2 \\
&+ 311y^4 - 138y^6)]\})/16(-1 + b^2)^2x^2y^9\zeta^7] \\
&+ \left(\frac{a}{R}\right)^5[9[-4 + x^2 + b^4x^2 + 2y^2 + 7b^2(-2 + x^2 + y^2)]/40(-1 + b^2)^2x^2y^2 \\
&+ (9\{8 - 4y^2 - 5x^8y^6 + x^2(-2 + 50y^2 - 23y^4) + x^6y^4(108 + 34y^2 + 5y^4) \\
&+ 8b^7x^5y^3[5 + (-76 + 58x^2)y^2 + 43y^4] + x^4y^2(-29 - 204y^2 + 126y^4) \\
&- 2b^6x^4y^2[24 + (-762 + 567x^2)y^2 + (387 - 254x^2 + 237x^4)y^4 + 137x^2y^6] \\
&+ 2b^5x^3y[9 + (-774 + 512x^2)y^2 + (383 - 622x^2 + 382x^4)y^4
\end{aligned}
$$

$$+x^2(247-156x^2+141x^4)y^6+78x^4y^8]-b^4x^2[2+(-896+500x^2)y^2$$
$$+(446-1410x^2+459x^4)y^4+x^2(657-1748x^2+758x^4)y^6$$
$$+x^4(812-90x^2+81x^4)y^8+45x^6y^{10}]+bxy[9x^{10}y^8$$
$$+36(-2+y^2)+13x^8y^6(3-2y^2+y^4)-3x^4y^2(-53+22y^2+5y^4)$$
$$+3x^6y^4(-3-38y^2+19y^4)+x^2(18-330y^2+157y^4)]+b^3xy[9x^{10}y^8$$
$$+126(-2+y^2)+x^8y^6(327-10y^2+5y^4)+17x^4y^2(17-154y^2$$
$$+85y^4)+x^6y^4(1049-870y^2+435y^4)+x^2(126-1146y^2$$
$$+589y^4)]-b^2[81x^{10}y^8+14(-2+y^2)+x^8y^6(275-234y^2$$
$$+117y^4)+x^2(14-350y^2+179y^4)+x^6y^4(783-734y^2$$
$$+431y^4)+x^4y^2(71-1806y^2+963y^4)]\})/80(-1+b^2)^2x^2y^{11}\zeta^9]$$
$$+\left(\frac{a}{R}\right)^7(9(2+7b^2)/200(-1+b^2)^2x^2y^2-\{9[4+57x^2y^2-1243x^4y^4$$
$$+1139x^6y^6+1216b^8x^6y^6-85x^8y^8+16b^7x^5y^5(-209+6x^2y^2)$$
$$+2b^6x^4y^4(1881-534x^2y^2+301x^4y^4)-2b^5x^3y^3(917-836x^2y^2$$
$$+2489x^4y^4+126x^6y^6)+b^4x^2y^2(728-1771x^2y^2+10253x^4y^4+1615x^6y^6$$
$$+55x^8y^8)-b^3xy(154+721x^2y^2+8096x^4y^4+298x^6y^6+662x^8y^8$$
$$+5x^{10}y^{10})-bxy(44+415x^2y^2-1452x^4y^4+760x^6y^6+76x^8y^8+13x^{10}y^{10})$$
$$+b^2(14+205x^2y^2+5192x^4y^4-3224x^6y^6+838x^8y^8$$
$$+143x^{10}y^{10})]\}/400(-1+b^2)^2x^2y^{13}\zeta^{11}), \qquad \text{(A12n)}$$

$$M_{14}^{ES,c}=\left(\frac{a}{R}\right)^3[-[9(1+2b^2)(-1+x^2)(-1+y^2)]/8(-1+b^2)^2x^2y^2+(3\{6-6y^2$$
$$+x^4y^2(-3+5y^2)+x^2(-6+11y^2-3y^4)-4b^5x^3y^3[7-6y^2+6x^2(-1$$
$$+y^2)]+b^4x^2y^2[80-78y^2+15x^4y^2(-1+y^2)+x^2(-78+95y^2-15y^4)]$$
$$+bxy[30(-1+y^2)-15x^6y^4(-1+y^2)+3x^4y^2(13-18y^2+5y^4)$$
$$+x^2(30-73y^2+39y^4)]+b^3xy[60(-1+y^2)-3x^6y^4(-1+y^2)$$
$$+3x^4y^2(39-40y^2+y^4)+x^2(60-169y^2+117y^4)]$$
$$+b^2[-12(-1+y^2)+75x^6y^4(-1+y^2)+x^2(-12+107y^2$$
$$-99y^4)+x^4(-99y^2+170y^4-75y^6)]\})/16(-1+b^2)^2x^2y^7\zeta^5]$$
$$+\left(\frac{a}{R}\right)^5[(9\{-5x^6y^4+2(-2+y^2)+32b^6x^4y^4(-2+x^2+y^2)+x^2(2$$
$$+14y^2-13y^4)-x^4y^2(13+2y^2+5y^4)-8b^5x^3y^3[-17+7y^2+2x^4y^2$$
$$+x^2(7-4y^2+2y^4)]-bxy[5x^8y^6+14(-2+y^2)+x^6y^4(16-10y^2+5y^4)$$
$$+x^4y^2(21-32y^2+16y^4)+x^2(14-66y^2+21y^4)]$$
$$+b^4x^2y^2[-112+50y^2+7x^6y^4+x^4y^2(71-14y^2+7y^4)$$
$$+x^2(50-154y^2+71y^4)]+b^2[35x^8y^6+4(-2+y^2)+7x^6y^4(16$$
$$-10y^2+5y^4)+x^2(4-154y^2+89y^4)+x^4y^2(89-200y^2+112y^4)]$$

$$
\begin{aligned}
&- b^3xy[x^8y^6 + 28(-2+y^2) + x^6y^4(94 - 2y^2 + y^4) + x^4y^2(133 - 188y^2 \\
&+ 94y^4) + x^2(28 - 218y^2 + 133y^4)]\}/80(-1+b^2)^2x^2y^9\zeta^7 + 9(1+2b^2)(-2 \\
&+ x^2 + y^2)(-1 + 2bxy - x^2y^2)^3/40(-1+b^2)^2x^2y^8\zeta^6] \\
&+ \left(\frac{a}{R}\right)^7 (9(1+2b^2)(-1+2bxy - x^2y^2)^5/200(-1+b^2)^2x^2y^{12}\zeta^{10} \\
&- \{9[-2 + 61x^2y^2 - 72x^4y^4 + 128b^7x^5y^5 + 5x^6y^6 + 32b^6x^4y^4(-9 + x^2y^2) \\
&+ 4b^5x^3y^3(63 + 2x^2y^2 + 9x^4y^4) - b^4x^2y^2(56 + 189x^2y^2 + 458x^4y^4 \\
&+ 9x^6y^6) + b^3xy(36 + 147x^2y^2 + 671x^4y^4 + 153x^6y^6 + x^8y^8) \\
&+ bxy(18 + 105x^2y^2 - 51x^4y^4 + 27x^6y^6 + 5x^8y^8) - b^2(4 + 221x^2y^2 \\
&+ 207x^4y^4 + 83x^6y^6 + 45x^8y^8)]\}/400(-1+b^2)^2x^2y^{11}\zeta^9). \qquad \text{(A12o)}
\end{aligned}
$$

[1] C. P. Brangwynne, G. H. Koenderink, F. C. MacKintosh, and D. A. Weitz, Intracellular transport by active diffusion, Trends Cell Biol. **19**, 423 (2009).

[2] A. Wodarz, Establishing cell polarity in development, Nat. Cell Biol. **4**, 39 (2002).

[3] A. Golden, Cytoplasmic flow and the establishment of polarity in C. elegans 1-cell embryos, Curr. Opin. Genet. Dev. **10**, 414 (2000).

[4] P. Gönczy and L. S. Rose, *Asymmetric cell division and axis formation in the embryo*, WormBook, 2005, available at http://www.wormbook.org/chapters/www_asymcelldiv/asymcelldiv.html

[5] J. C. Crocker and B. D. Hoffman, Multiple-particle tracking and two-point microrheology in cells, Methods Cell Biol. **83**, 141 (2007).

[6] A. S. Verkman, Solute and macromolecule diffusion in cellular aqueous compartments, Trends Biochem. Sci. **27**, 27 (2002).

[7] G. K. Batchelor, Brownian diffusion of particles with hydrodynamic interaction, J. Fluid Mech. **74**, 1 (1976).

[8] J. Bergenholtz, J. F. Brady, and M. Vicic, The non-Newtonian rheology of dilute colloidal suspensions, J. Fluid Mech. **456**, 239 (2002).

[9] T. M. Squires and J. F. Brady, A simple paradigm for active and nonlinear microrheology, Phys. Fluids **17**, 073101 (2005).

[10] A. S. Khair and J. F. Brady, Single particle motion in colloidal dispersions: A simple model for active and nonlinear microrheology, J. Fluid Mech. **557**, 73 (2006).

[11] R. N. Zia and J. F. Brady, Stress development, relaxation, and memory in colloidal dispersions: Transient nonlinear microrheology, J. Rheol. **57**, 457 (2013).

[12] J. F. Brady and G. Bossis, The rheology of concentrated suspensions of spheres in simple shear flow by numerical simulation, J. Fluid Mech. **155**, 105 (1985).

[13] N. J. Wagner and J. F. Brady, Shear thickening in colloidal dispersions, Phys. Today **62**(10), 27 (2009).

[14] J. W. Swan and R. N. Zia, Active microrheology: Fixed-velocity versus fixed-force, Phys. Fluids **25**, 083303 (2013).

[15] D. Leighton and A. Acrivos, The shear-induced migration of particles in concentrated suspensions, J. Fluid Mech. **181**, 415 (1987).

[16] J. F. Brady and J. F. Morris, Microstructure of strongly sheared suspensions and its impact on rheology and diffusion, J. Fluid Mech. **348**, 103 (1997).

[17] R. N. Zia and J. F. Brady, Single-particle motion in colloids: Force-induced diffusion, J. Fluid Mech. **658**, 188 (2010).

[18] N. J. Hoh and R. N. Zia, Hydrodynamic diffusion in active microrheology of non-colloidal suspensions: the role of interparticle forces, J. Fluid Mech. **785**, 189 (2015).
[19] N. J. Hoh and R. N. Zia, Force-induced diffusion in suspensions of hydrodynamically interacting colloids, J. Fluid Mech. **795**, 739 (2016).
[20] J. F. Brady and M. Vicic, Normal stresses in colloidal suspensions, J. Rheol. **39**, 545 (1995).
[21] D. R. Foss and J. F. Brady, Structure, diffusion and rheology of Brownian suspensions by Stokesian dynamics simulation, J. Fluid Mech. **407**, 167 (2000).
[22] R. N. Zia and J. F. Brady, Microviscosity, microdiffusivity, and normal stresses in colloidal dispersions, J. Rheol. **56**, 1175 (2012).
[23] H. C. W. Chu and R. N. Zia, Normal stresses and energy storage in suspensions of hydrodynamically interacting colloids via active microrheology (unpublished).
[24] H. C. W. Chu and R. N. Zia, The non-Newtonian rheology of hydrodynamically interacting colloids via active, nonlinear microrheology (unpublished).
[25] R. A. Lionberger and W. B. Russel, High frequency modulus of hard sphere colloids, J. Rheol. **38**, 1885 (1994).
[26] R. A. Lionberger and W. B. Russel, Effectiveness of nonequilibrium closures for the many body forces in concentrated colloidal dispersions, J. Chem. Phys. **106**, 402 (1997).
[27] R. A. Lionberger and W. B. Russel, A Smoluchowski theory with simple approximations for hydrodynamic interactions in concentrated dispersions, J. Rheol. **41**, 399 (1997).
[28] R. N. Zia, J. W. Swan, and Y. Su, Pair mobility functions for rigid spheres in concentrated colloidal dispersions: Force, torque, translation, and rotation, J. Chem. Phys. **143**, 224901 (2015).
[29] P. J. Hoogerbrugge and J. M. V. A. Koelman, Simulating microscopic hydrodynamic phenomena with dissipative particle dynamics, Europhys. Lett. **19**, 155 (2007).
[30] S. Chen and G. D. Doolen, Lattice Boltzmann method for fluid flows, Annu. Rev. Fluid Mech. **30**, 329 (1998).
[31] J. F. Brady and G. Bossis, Stokesian dynamics, Annu. Rev. Fluid Mech. **20**, 111 (1988).
[32] P. Habdas and E. R. Weeks, Video microscopy of colloidal suspensions and colloidal crystals, Curr. Opin. Colloid Interface Sci. **7**, 196 (2002).
[33] X. Cheng, J. H. McCoy, J. N. Israelachvili, and I. Cohen, Imaging the microscopic structure of shear thinning and thickening colloidal suspensions, Science **333**, 1276 (2011).
[34] G. L. Hunter, K. V. Edmond, and E. R. Weeks, Boundary Mobility Controls Glassiness in Confined Colloidal Liquids, Phys. Rev. Lett. **112**, 218302 (2014).
[35] B. Xu and J. F. Gilchrist, Microstructure of sheared monosized colloidal suspensions resulting from hydrodynamic and electrostatic interactions, J. Chem. Phys. **140**, 204903 (2014).
[36] B. J. Ackerson and N. A. Clark, Sheared colloidal suspensions, Physica A **118**, 221 (1983).
[37] N. J. Wagner and W. B. Russel, Light scattering measurements of a hard-sphere suspension under shear, Phys. Fluids A **2**, 491 (1990).
[38] J. W. Bender and N. J. Wagner, Optical measurement of the contributions of colloidal forces to the rheology of concentrated suspensions, J. Colloid Interface Sci. **172**, 171 (1995).
[39] R. Butera, M. Wolfe, J. Bender, and N. Wagner, Formation of a Highly Ordered Colloidal Microstructure Upon Flow Cessation from High Shear Rates, Phys. Rev. Lett. **77**, 2117 (1996).
[40] Y. S. Lee and N. J. Wagner, Rheological properties and small-angle neutron scattering of a shear thickening, nanoparticle dispersion at high shear rates, Ind. Eng. Chem. Res. **45**, 7015 (2006).
[41] C. Gao, S. D. Kulkarni, J. F. Morris, and J. F. Gilchrist, Direct investigation of anisotropic suspension structure in pressure-driven flow, Phys. Rev. E **81**, 041403 (2010).
[42] K. A. Gurnon and N. J. Wagner, Large amplitude oscillatory shear (LAOS) measurements to obtain constitutive equation model parameters: Giesekus model of banding and nonbanding wormlike micelles, J. Rheol. **56**, 333 (2012).
[43] M. E. Helgeson, N. J. Wagner, and L. Porcar, Investigating the structural mechanisms of shear banding using spatially-resolved flow-SANS, *Accomplishments and Opportunities*, edited by R. L. Cappelletti, NIST No. 1089 (U.S. GPO, Washington, DC, 2008), p. 42.

[44] J. R. Blake, A note on the image system for a Stokeslet in a no-slip boundary, Math. Proc. Cambridge Philos. Soc. **70**, 303 (1971).
[45] M. D. A. Cooley and M. E. O'Neill, On the slow motion generated in a viscous fluid by the approach of a sphere to a plane wall or stationary sphere, Mathematika **16**, 37 (1969).
[46] M. E. O'Neill and K. Stewartson, On the slow motion of a sphere parallel to a nearby plane wall, J. Fluid Mech. **27**, 705 (1967).
[47] J. W. Swan and J. F. Brady, Simulation of hydrodynamically interacting particles near a no-slip boundary, Phys. Fluids **19**, 113306 (2007).
[48] S. H. Lee, R. S. Chadwick, and L. G. Leal, Motion of a sphere in the presence of a plane interface. Part 1. An approximate solution by generalization of the method of Lorentz, J. Fluid Mech. **93**, 705 (1979).
[49] S. H. Lee and L. G. Leal, Motion of a sphere in the presence of a plane interface. Part 2. An exact solution in bipolar co-ordinates, J. Fluid Mech. **98**, 193 (1980).
[50] C. Berdan and L. G. Leal, Motion of a sphere in the presence of a deformable interface, J. Colloid Interface Sci. **87**, 62 (1982).
[51] A. S. Geller, S. H. Lee, and L. G. Leal, The creeping motion of a spherical particle normal to a deformable interface, J. Fluid Mech. **169**, 27 (1986).
[52] J. W. Swan and J. F. Brady, Particle motion between parallel walls: Hydrodynamics and simulation, Phys. Fluids **22**, 103301 (2010).
[53] J. W. Swan and J. F. Brady, The hydrodynamics of confined dispersions, J. Fluid Mech. **687**, 254 (2011).
[54] J. W. Swan and J. F Brady, Anisotropic diffusion in confined colloidal dispersions: The evanescent diffusivity, J. Chem. Phys. **135**, 014701 (2011).
[55] D. Goulding and J.-P. Hansen, Effective interaction between charged colloidal particles near a surface, Mol. Phys. **95**, 649 (1998).
[56] E. Yariv and H. Brenner, Near-contact electrophoretic motion of a sphere parallel to a planar wall, J. Fluid Mech. **484**, 85 (2003).
[57] V. N. Michailidou, G. Petekidis, J. W. Swan, and J. F. Brady, Dynamics of Concentrated Hard-Sphere Colloids Near a Wall, Phys. Rev. Lett. **102**, 068302 (2009).
[58] G. L. Lukacs, P. Haggie, O. Seksek, D. Lechardeur, N. Freedman, and A. S. Verkman, Size-dependent DNA mobility in cytoplasm and nucleus, J. Biol. Chem. **275**, 1625 (2000).
[59] K. Luby-Phelps, Cytoarchitecture and physical properties of cytoplasm: Volume, viscosity. diffusion, intracellular surface area, Int. Rev. Cytol. **192**, 189 (2000).
[60] C. L. Asbury, A. N. Fehr, and S. M. Block, Kinesin moves by an asymmetric hand-over-hand mechanism, Science **302**, 2130 (2003).
[61] S. M. Block, Kinesin motor mechanics: Binding, stepping, tracking, gating, and limping,, Biophys. J. **92**, 2986 (2007).
[62] C. P. Brangwynne, G. H. Koenderink, F. C. MacKintosh, and D. A. Weitz, Cytoplasmic diffusion: Molecular motors mix it up, J. Cell Biol. **183**, 583 (2008).
[63] D. Wirtz, Particle-tracking microrheology of living cells: Principles and applications, Annu. Rev. Biophys. **38**, 3282 (2009).
[64] J. A. Dix and A. S. Verkman, Crowding effects on diffusion in solutions and cells, Annu. Rev. Biophys. **37**, 247 (2008).
[65] B. R. Daniels, B. C. Masi, and D. Wirtz, Probing single-cell micromechanics in vivo: The microrheology of *C. elegans* developing embryos, Biophys. J. **90**, 4712 (2006).
[66] R. E. Goldstein, I. Tuval, and J.-W. van de Meent, Microfluidics of cytoplasmic streaming and its implications for intracellular transport, Proc. Natl. Acad. Sci. U.S.A. **105**, 3663 (2008).
[67] R. Niwayama, K. Shinohara, and A. Kimura, Hydrodynamic property of the cytoplasm is sufficient to mediate cytoplasmic streaming in the *Caenorhabiditis elegans* embryo, Proc. Natl. Acad. Sci. U.S.A. **108**, 111900 (2011).
[68] D. A. Lauffenburger and J. J. Linderman, *Receptors: Models for Binding, Trafficking, and Signalling* (Oxford University Press, Oxford, 1993).

[69] A. W. C. Lau, B. D. Hoffmann, A. Davies, J. C. Crocker, and T. C. Lubensky, Microrheology, Stress Fluctuations, and Active Behavior of Living Cells, Phys. Rev. Lett. **91**, 198101 (2003).
[70] J. Suh, D. Wirtz, and J. Hanes, Efficient active transport of gene nanocarriers to the cell nucleus, Proc. Natl. Acad. Sci. U.S.A. **100**, 3738 (2003).
[71] R. P. Kulkarni, D. D. Wu, M. E. Davis, and S. E. Fraser, Quantitating intracellular transport of polyplexes by spatiotemporal image correlation microscopy, Proc. Natl. Acad. Sci. U.S.A. **102**, 7523 (2005).
[72] J. S. H. Lee, P. Panorchan, C. M. Hale, S. B. Khatau, T. P. Kole, Y. Tseng, and D. Wirtz, Ballistic intracellular nanorheology reveals ROCK-hard cytoplasmic stiffening response to fluid flow, J. Cell Sci. **119**, 17608 (2006).
[73] A. P. Minton, The effective hard particle model provides a simple, robust and broadly applicable description of nonideal behavior in concentrated solutions of bovine serum albumin and other nonassociating proteins, J. Pharm. Sci. **96**, 3466 (2007).
[74] C. R. Cowan and A. A. Hyman, Acto-myosin reorganization and PAR polarity in C. elegans, Development **134**, 1035 (2007).
[75] *Anomalous Transport: Foundations and Applications*, edited by R. Klages, R. Günter, and I. M. Sokolov (Wiley-VCH, Weinheim, 2008).
[76] K. Lipkow and D. J. Odde, Model for protein concentration gradients in the cytoplasm, Cell. Mol. Bioeng. **1**, 84 (2008).
[77] A. G. Hendricks, B. I. Epureanu, and E. Meyhöfer, Collective dynamics of kinesin, Phys. Rev. E **79**, 031929 (2009).
[78] B. D. Hoffman and J. C. Crocker, Cell mechanics: Dissecting the physical responses of cells to force, Annu. Rev. Biomed. Eng. **11**, 259 (2009).
[79] E. Voronina, The diverse functions of germline P-granules in *Caenorhabditis elegans*, Mol. Reprod. Dev. **80**, 624 (2013).
[80] A. E. Cervantes-Martínez, A. Ramírez-Saito, R. Armenta-Calderón, M. A. Ojeda-López, and J. L. Arauz-Lara, Colloidal diffusion inside a spherical cell, Phys. Rev. E **83**, 030402 (2011).
[81] C. Kozlowski, M. Srayko, and F. Nédélec, Cortical microtubule contacts position the spindle in C. elegans embryos, Cell **129**, 499 (2007).
[82] T. Shinar, M. Mana, F. Piano, and M. J. Shelley, A model of cytoplasmically driven microtubule-based motion in the single-celled *Caenorhabditis elegans* embryo, Proc. Natl. Acad. Sci. U.S.A. **108**, 10508 (2011).
[83] A. L. Zydney, Boundary effects on the electrophoretic motion of a charged particle in a spherical cavity, J. Colloid Interface Sci. **169**, 476 (1994).
[84] N. S. Pujar and A. L. Zydney, Boundary effects on the sedimentation and hindered diffusion of charged particles, AIChE J. **42**, 2101 (1996).
[85] E. Lee, J.-W. Chu, and J.-P. Hsu, Electrophoretic mobility of a sphere in a spherical cavity, J. Colloid Interface Sci. **205**, 65 (1998).
[86] J.-P. Hsu, S.-H. Hung, and C.-Y. Kao, Electrophoresis of a sphere at an arbitrary position in a spherical cavity, Langmuir **18**, 8897 (2002).
[87] S.-H. Lou, E. Lee, and J.-P. Hsu, Dynamic electrophoresis of a sphere in a spherical cavity: Arbitrary surface potential, J. Colloid Interface Sci. **285**, 865 (2005).
[88] H. J. Keh and T. H. Hsieh, Electrophoresis of a colloidal sphere in a spherical cavity with arbitrary zeta potential distributions, Langmuir **23**, 7928 (2007).
[89] H. J. Keh and T. H. Hsieh, Electrophoresis of a colloidal sphere in a spherical cavity with arbitrary zeta potential distributions and arbitrary double-layer thickness, Langmuir **24**, 390 (2008).
[90] E. Lee, J.-W. Chu, and J.-P. Hsu, Electrophoretic mobility of a spherical particle in a spherical cavity, J. Colloid Interface Sci. **196**, 316 (1997).
[91] J.-P. Hsu, L.-H. Yeh, and Z.-S. Chen, Effect of a charged boundary on electrophoresis: A sphere at an arbitrary position in a spherical cavity, J. Colloid Interface Sci. **310**, 281 (2007).
[92] J.-P. Hsu, Z.-S. Chen, M.-H. Ku, and L.-H. Yeh, Effect of charged boundary on electrophoresis: Sphere in spherical cavity at arbitrary potential and double-layer thickness, J. Colloid Interface Sci. **314**, 256 (2007).

[93] J.-P. Hsu and Z.-S. Chen, Effects of double-layer polarization and electroosmotic flow on the electrophoresis of an ellipsoid in a spherical cavity, J. Phys. Chem. B **112**, 11270 (2008).
[94] C.-P. Tung, E. Lee, and J.-P. Hsu, Dynamic electrophoretic mobility of a sphere in a spherical cavity, J. Colloid Interface Sci. **260**, 118 (2003).
[95] T. C. Lee and H. J. Keh, Electrophoresis of a spherical particle in a spherical cavity, Microfluid. Nanofluid. **16**, 1107 (2014).
[96] E. Lee, W.-L. Min, and J.-P. Hsu, Dynamic electrophoresis of a droplet in a spherical cavity, Langmuir **22**, 3920 (2006).
[97] H. J. Keh and J. H. Chang, Boundary effects on the creeping-flow and thermophoretic motions of an aerosol particle in a spherical cavity, Chem. Eng. Sci. **53**, 2365 (1998).
[98] E. Lee, Y.-P. Tang, and J.-P. Hsu, Electrophoresis of a membrane-coated sphere in a spherical cavity, Langmuir **20**, 9415 (2004).
[99] E. Lee, T.-H. Huang, and J.-P. Hsu, Sedimentation of a composite particle in a spherical cavity, Langmuir **21**, 1729 (2005).
[100] H. J. Keh and T. C. Lee, Axisymmetric creeping motion of a slip spherical particle in a nonconcentric spherical cavity, Theor. Comput. Fluid Dyn. **24**, 497 (2010).
[101] J. P. Hsu, W. L. Hsu, and Z. S. Chen, Boundary effect on diffusiophoresis: spherical particle in a spherical cavity, Langmuir **25**, 1772 (2009).
[102] M. Wojciechowski, P. Szymczak, and M. Cieplak, The influence of hydrodynamic interactions on protein dynamics in confined and crowded spaces-assessment in simple models, Phys. Biol. **7**, 046011 (2010).
[103] G. K. Batchelor, Sedimentation in a dilute dispersion of spheres, J. Fluid Mech. **52**, 245 (1972).
[104] G. K. Batchelor and J. T. Green, The hydrodynamic interaction of two small freely-moving spheres in a linear flow field, J. Fluid Mech. **56**, 375 (1972).
[105] D. J. Jeffrey and Y. Onishi, Calculation of the resistance and mobility functions for two unequal rigid spheres in low-Reynolds-number flow, J. Fluid Mech. **139**, 261 (1984).
[106] S. Kim and S. J. Karrila, *Microhydrodynamics: Principles and Selected Applications* (Butterworth-Heinemann, Boston, 1991).
[107] D. J. Jeffrey, The calculation of the low Reynolds number resistance functions for two unequal spheres, Phys. Fluids **4**, 16 (1992).
[108] E. Cunningham, On the velocity of steady fall of spherical particles through fluid medium, Proc. R. Soc. London Ser. A **83**, 357 (1910).
[109] M. E. O'Neill and R. Majumdar, Asymmetrical slow viscous fluid motions caused by the translation or rotation of two spheres. Part I: The determination of exact solutions for any values of the ratio of radii and separation parameters, Z. Angew. Math. Phys. **21**, 164 (1970).
[110] M. E. O'Neill and S. R. Majumdar, Asymmetrical slow viscous fluid motions caused by the translation or rotation of two spheres. Part II: Asymptotic forms of the solutions when the minimum clearance, Z. Angew Math. Phys. **21**, 180 (1970).
[111] R. B. Jones, in *Theoretical Methods for Micro Scale Viscous Flows*, edited by F. Feuillebois and A. Sellier (Transworld Research Network, Kerala, 2009), Chap. 4, pp. 61–104.
[112] G. Bossis and J. F. Brady, The rheology of Brownian suspensions, J. Chem. Phys. **91**, 1866 (1989).
[113] T. M. Phung, J. F. Brady, and G. Bossis, Stokesian dynamics simulation of Brownian suspensions, J. Fluid Mech. **313**, 181 (1996).
[114] A. Sierou and J. F. Brady, Rheology and microstructure in concentrated noncolloidal suspensions, J. Rheol. **46**, 1031 (2002).
[115] C. W. Oseen, *Neuere Methoden und Ergebnisse in der Hydrodynamik* (Akademische Verlagsgesellschaft m.b.h., Leipzig, 1927), p. 337.
[116] A. Sellier, Slow viscous motion of a solid particle in a spherical cavity, Comput. Model. Eng. Sci. **25**, 165 (2008).
[117] C. Maul and S. Kim, Image systems for a Stokeslet inside a rigid spherical container, Phys. Fluids **6**, 2221 (1994).
[118] C. Maul and S. Kim, Image of a point force in a spherical container and its connection to the Lorentz reflection formula, J. Eng. Math. **30**, 119 (1996).

[119] O. A. Ladyzhenskaya, *The Mathematical Theory of Viscous Incompressible Flow*, 2nd ed. (Gordon and Breach, New York, 1969), p. 224.
[120] C. W. J. Beenakker and P. Mazur, Many-sphere hydrodynamic interactions: IV. Wall-effects inside a spherical container, Physica A **131**, 311 (1985).
[121] B. U. Felderhof and A. Sellier, Mobility matrix of a spherical particle translating and rotating in a viscous fluid confined in a spherical cell, and the rate of escape from the cell, J. Chem. Phys. **136**, 054703 (2012).
[122] C. Aponte-Rivera, Y. Su, and R. N. Zia, Equilibrium diffusion in concentrated, 3D confined suspensions (unpublished).
[123] L. Durlofsky, J. F. Brady, and G. Bossis, Dynamic simulation of hydrodynamically interacting particles, J. Fluid Mech. **180**, 21 (1987).
[124] E. Lushi, H. Wioland, and R. E. Goldstein, Fluid flows created by swimming bacteria drive self-organization in confined suspensions, Proc. Natl. Acad. Sci. U.S.A. **111**, 9733 (2014).
[125] R. E. DeWames, W. F. Hall, and M. C. Shen, On the molecular theories of polymer solutions, J. Chem. Phys. **46**, 2782 (1967).
[126] R. Zwanzig, J. Kiefer, and G. H. Weiss, On the validity of the Kirkwood-Riseman theory, Proc. Natl. Acad. Sci. U.S.A. **60**, 381 (1968).
[127] J. Rotne and S. Prager, Variational treatment of hydrodynamic interaction in polymers, J. Chem. Phys. **50**, 4831 (1969).
[128] C. P. Brangwynne, C. R. Eckmann, D. S. Courson, A. Rybarska, C. Hoege, J. Gharakhani, F. Jülicher, and A. A. Hyman, Germline P-granules are liquid droplets that localize by controlled dissolution/condensation, Science **324**, 1729 (2009).